UNIVERSITÉ DE MONTRÉAL

RELATIONSHIP BETWEEN RHEOLOGY, MORPHOLOGY AND FOAMABILITY OF THERMOPLASTIC OLEFIN (TPO) BLENDS

AMIRHOSSEIN MAANI

DÉPARTEMENT DE GÉNIE CHIMIQUE

ÉCOLE POLYTECHNIQUE DE MONTRÉAL

THÈSE PRÉSENTÉE EN VUE DE L'OBTENTION

DU DIPLÔME DE PHILOSOPHIAE DOCTOR

(GÉNIE CHIMIQUE)

JUILLET 2012

© Amirhossein Maani, 2012.

UNIVERSITÉ DE MONTRÉAL

ÉCOLE POLYTECHNIQUE DE MONTRÉAL

Cette thése intitulée:

RELATIONSHIP BETWEEN RHEOLOGY, MORPHOLOGY AND FOAMABILITY OF THERMOPLASTIC OLEFIN (TPO) BLENDS

présentée par : MAANI Amirhossein

en vue de l'obtention du diplôme de: Philosophiae Doctor

a été dûment acceptée par le jury d'examen constitué de:

M. AJJI Abdellah, Ph.D., président

M. CARREAU Pierre, Ph.D., membre et directeur de recherche

Mme HEUZEY Marie-Claude, Ph.D., membre et codirectrice de recherche

M. VIRGILIO Nick, Ph.D., membre

Mme KONTOPOULOU Marianna, Ph.D., membre

Dedication

To My Beloved Parents

Acknowledgement

I would like to express my sincere thanks to Dr. Carreau for the trust he placed in me and for all his supports throughout the period of this research. It was a rare opportunity to do a PhD under the supervision of an eminent professor with years of experience and valuable expertise. I also acknowledge all the efforts made by Dr. Heuzey for the improvement of the quality of the articles and eventually this thesis. I appreciate all her precious comments as well as her warm encouragements and supports especially during the last few months of my PhD.
I owe my sincere gratitude to Dr. Nasr Esfahany, Dr. Favis and Dr. Wood-Adams, my competent professors who granted me a fundamental perception of chemical engineering and polymer science.

I am so thankful to Dr. Nick Virgilio not only for reviewing this thesis, but also for his warm compassions and helpful discussions and especially for his precious assistance during completion of the last part of this thesis.

Many thanks to Dr. Hani Naguib for his valuable contribution in the last article and for his kind follow up on the complementary experiments performed in the University of Toronto.

I would also like to thank Bruno Blais for his great assistance in carrying out parts of this work during the period of his internship in the Chemical Engineering Department.

Many Thanks to all technical staff of the Chemical Engineering Department, particularly Mr. Jacques Beausoleil, Ms. Martine Lamarche, Mr. Gino Robin, Mr. Guillaume Lessard, Mr. Jean Huard and Ms. Claire Cerclé. An especial thank to Ms. Melina Hamdine, our brilliant research associate, for all her technical assistance and revitalizing friendly discussions we had together.

I am so grateful to Dr. Khalghollah and Mr. Hosseinloo who helped me proceed with the administrative processes for my first entry to Canada, a great favor that will never be forgotten.

I would like to deeply thank Marie Matet for her warm and quick response to my request for translating parts of this thesis to French.

Many thanks to Jaber Shabanian, Laleh Dashtban, Khalil Shahverdi and Hesamoddin Tabatabaei, my undergraduate classmates and my long-time friends who were beside me during these years and supported me in every situation.

I would like to extend my gratitude to all my friends in Montreal for their unforgettable favors and for all the memorable moments I had with them; very special thanks to Shant Shahbikian, Hesam Ghasemi, Hoda Nematollahi and Parinaz Pakniat who were always there, ready to hear me and help me.

Finally, with all my heart, I would like to express my undying gratitude to my beloved parents for the overwhelming support they provided and for scarifies they made throughout my life; there will never be a right word to express my feeling of appreciation for their unconditional love.

Résumé

Dues aux propriétés uniques des oléfines thermoplastiques (TPO), cette classe de mélange polymères a suscité un grand intérêt de la part de l'industrie de transformation des polymères. Bien que plusieurs projets de recherche ont été consacrés à l'étude de la microstructure et des propriétés diverses de ces matériaux, le comportement moussant des TPO n'a pas encore été totalement élucidé. Le but de cette étude est de contrôler le comportement moussant des TPO par la compréhension du rôle des propriétés rhéologiques et morphologiques dans la formation des structures cellulaires. Une attention particulière est accordée au phénomène de coalescence des phases qui joue un rôle majeur dans le développement de la morphologie des mélanges polymères. À cet égard, l'étendue de la coalescence causée par l'écoulement dans les TPO a été tout d'abord étudiée au moyen d'une approche rhéologique. Un modèle rhéologique en régime transitoire a été utilisé pour décrire l'évolution de la morphologie des mélanges pendant le cisaillement soumis à un champ de contraintes de cisaillement homogène. L'étude de TPO avec différentes concentrations a montré que les modèles phénoménologiques en régime transitoire peuvent être utilisés pour simuler la coalescence et pour décrire l'influence de la fréquence de collision en fonction de la fraction volumique. Il a aussi été montré que la coalescence est favorisée par une viscosité des inclusions plus faible. Cela a été attribué à l'augmentation de la mobilité interfaciale qui peut réduire le temps de drainage et faciliter la collision de deux gouttes qui s'approchent l'une de l'autre.

Pour contrôler l'extension de la coalescence des phases, dans la seconde partie de cette étude, une compatibilisation réactive a été réalisée. Un polypropylène aminé et un élastomère greffé avec de l'anhydride maléique ont été utilisés pour former des copolymères à l'interface

pendant le procédé de mélange réactif à l'état fondu. Les mesures en rhéologie dynamique ont montré que les mélanges compatibilisés se comportent comme des matériaux à l'état de transition sol-gel caractérisée par une viscosité plateau infinie et un comportement en loi de puissance du module élastique aux basses fréquences. Le comportement gélifié des mélanges compatibilisés à basse fréquence a pu être décrit en utilisant un modèle de Zener généralisé avec 3 éléments fractionnels. Les TPO compatibilisés ont aussi montré une amélioration significative de la viscosité en cisaillement transitoire aussi bien qu'un comportement de relaxation des contraintes retardé. Un tel comportement rhéologique a été attribué à la présence d'un réseau structural interconnecté dans les TPO compatibilisés, confirmé par la microscopie à force atomique.

Dans la dernière partie de ce projet de recherche, le comportement moussant des TPO a été étudié au moyen d'un bain pressurisé avec du dioxyde de carbone comme agent gonflant. La morphologie des TPO a varié avec la compatibilisation réactive, le recuit statique et la coalescence de la phase dispersée causée par le cisaillement. La structure cellulaire des TPO expansés a été caractérisée grâce à une technique microscopique capable d'identifier les positions respectives des bulles, de la phase élastomérique dispersée et de la matrice de polypropylène. Les résultats ont montré que la phase élastomérique agit en tant que site de nucléation et la morphologie cellulaire finale des TPO peut être directement corrélée à la structure initiale du mélange. Il a aussi été démontré que les propriétés élongationnelles des TPO fondus joue un rôle primordial dans le contrôle de la coalescence cellulaire. Il a été trouvé que la compatibilisation réactive était capable de modifier le pouvoir moussant à l'état fondu en augmentant le taux de nucléation et en contrôlant la phase de croissance des bulles nucléées.

Abstract

Due to the unique properties of thermoplastic olefins (TPOs), this class of polymer blends has gained a great interest in the polymer processing industry. Although several researches have been devoted to investigating the microstructure and various properties of these materials, the foaming behavior of the TPOs has not been fully understood yet. The aim of the present study is to control the foaming behavior of TPOs via the understanding of the role of rheological and morphological properties in the formation of cellular structures. A particular attention is paid to the phase coalescence phenomenon, which plays a major role in the morphology development of polymer blends. In this regard the extent of flow induced coalescence in TPOs was firstly investigated by means of a rheological approach. A transient rheological model was employed to describe the morphological evolution of the blends during shearing in a homogeneous shear flow field. Investigating TPOs with different concentrations showed that phenomenological transient models can be used to simulate the coalescence behavior and to account for the variation of collision frequency with volume fraction. It was also shown that the coalescence is favored by a decrease of the viscosity of the inclusions. This was attributed to the increased interfacial mobility, which can reduce the drainage time and facilitate the collision of two approaching drops.

To control the extent of phase coalescence, in the second part of this study, a reactive compatibilization was employed. An aminated polypropylene and a maleic anhydride grafted elastomer were used to form copolymers at the interface during a reactive melt blending process. Dynamic rheological measurements showed that the compatibilized blends behave as materials in the sol gel transition featuring infinite zero shear viscosity and power-law behavior of the

elastic moduli at low frequencies. The gel-like behavior of the compatibilized blends at low frequency could be described using a generalized Zener model with 3 fractional elements. The compatibilized TPOs also showed significant enhancements in transient shear viscosities as well as a retarded stress relaxation behavior. Such a rheological behavior was attributed to the presence of an interconnected network structure in the compatibilized TPOs as confirmed by atomic force microscopy.

In the last phase of this research, the foaming behavior of the TPOs was investigated by means of a bath setup pressurized with carbon dioxide as blowing agent. The morphology of the TPOs was varied via reactive compatibilization, static annealing and shear induced phase coalescence. The cellular structure of the TPO foams were characterized using a microscopic technique capable of positioning the respective locations of bubbles, dispersed elastomeric phase and the polypropylene matrix. The results showed that the elastomeric phase acts as the nucleating site and the final cellular morphology of the TPOs can be directly correlated to the initial blend microstructure. It was also shown that the melt elongational properties of the TPOs play a major role in controlling the extent of cell coalescence. Reactive compatibilization was found to be capable of modifying the melt foamability via increasing the nucleation rate and controlling the growth stage of the nucleated bubbles.

CONDENSÉ EN FRANÇAIS

Les oléfines thermoplastiques représentent une catégorie importante des mélanges de polymères constitués d'une phase cristalline thermoplastique rigide et d'une phase élastomérique souple. Grâce à leur excellente aptitude à la mise en œuvre et à leurs propriétés intéressantes à l'état solide, l'intérêt de cette classe de matériaux dans l'industrie s'est accru. À ce titre, les propriétés rhéologiques et morphologiques de ces mélanges ont été le sujet de plusieurs études. Toutefois le pouvoir moussant de ces matériaux et sa dépendance aux propriétés et à la microstructure des mélanges n'ont pas encore été compris. Le but de cette étude est d'améliorer le comportement des mélanges d'oléfines thermoplastiques expansées en contrôlant les propriétés morphologiques et rhéologiques. En considérant l'importance de la coalescence des phases dans le développement de la morphologie des mélanges de polymères, une approche rhéologique a d'abord été utilisée pour évaluer le comportement à la coalescence des oléfines thermoplastiques. Les mélanges d'oléfines thermoplastiques de polypropylène (PP) et de copolymères éthyléniques métallocènes catalysés (EC) ont été étudiés. La tension interfaciale entre le PP et les EC a été déterminée au moyen de mesures viscoélastiques linéaires en utilisant une version simplifiée du modèle de Palierne (1990) ainsi que l'équation de Choi et Schowalter (1975). Il a été montré que comparé à la théorie de Choi et Showalter, le modèle de Palierne donne une meilleure estimation des données à basse fréquence. Aussi, le modèle de Palierne prédit quasiment la même valeur de la tension interfaciale pour les différents mélanges, comme prévu par leur composition similaire.

La coalescence sous écoulement a été étudiée en cisaillant les échantillons à un taux de cisaillement très faible de 0.01 s^{-1}. L'évolution de la taille et l'orientation des gouttelettes

dispersées sous cisaillement ont été corrélées aux données obtenues en rhéologie en régime transitoire. La capacité du modèle Lee-Park (LP) dans la prédiction de l'étendue de la coalescence des gouttes sous cisaillement transitoire a été évaluée. Pour tenir compte de la déformation non-affine un paramètre de glissement supplémentaire (Lacroix et al. 1999) a été introduit dans le modèle LP. Le modèle LP peut prédire correctement les données de viscosité transitoire pour tous les mélanges, mais dans la plupart des cas il ne permet pas la prédiction de l'aire interfaciale, *Q*. Le modèle modifié (modèle LPL) donne une bonne prédiction de l'état morphologique de tous les mélanges conjointement avec les données rhéologiques. Pour examiner l'influence de la concentration des phases, des mélanges avec différents ratios de PP et EC (85/15, 80/20, 75/25 et 70/30 w/w) ont été étudiés. Il a été trouvé que le rapport de la taille finale sur la taille initiale des gouttelettes d_{v_f} / d_{v_0} est un faible indicateur de coalescence. Bien que la taille initiale des gouttelettes variait de manière significative avec la concentration, le rapport d_{v_f} / d_{v_0} est apparu être presque le même pour tous les mélanges. En utilisant la théorie de Smoluchowski (1917) la fréquence de collision du mélange PP/EC30 (85/15) a été estimée être presque 11 fois supérieure à la fréquence de collision du mélange PP/EC30 (70/30). En fait le rapport d_{v_f} / d_{v_0} peut refléter l'intensité de coalescence seulement quand les tailles des gouttelettes sont initialement dans la même fourchette. Cette condition est bien sûr difficile à atteindre expérimentalement. Le modèle LPL a été utilisé pour simuler le comportement morphologique en régime transitoire des mélanges pour justifier l'augmentation de la fréquence de collision avec la fraction volumique de la phase dispersée. L'exploration du comportement coalescent des mélanges avec différents ratios de viscosité a montré que la coalescence est favorisée lorsque la viscosité de la phase dispersée diminue. Bien que les mélanges avaient une morphologie initiale similaire, la taille finale des gouttelettes pour une phase dispersée de faible

viscosité (le rapport de viscosités de la phase dispersée et de la matrice était de $\eta_d/\eta_m = 0.04$) était deux fois plus grande que pour un mélange ayant des inclusions de plus haute viscosité ($\eta_d/\eta_m = 1.18$). Cela a été attribué à l'augmentation de la mobilité interfaciale dans les gouttelettes avec la plus faible viscosité. Le taux de relaxation des gouttelettes a aidé à comprendre l'augmentation de la mobilité interfaciale. Alors que le mélange avec des gouttelettes ayant une faible viscosité a révélé une morphologie sphérique après 15 min de repos (après un cisaillement à 0.3 s^{-1}), le mélange avec une phase élastomérique à haute viscosité a présenté une morphologie fibrillaire impliquant une relaxation non-complète. L'augmentation de la mobilité interfaciale dans le mélange avec les gouttelettes de faible viscosité réduit le temps de drainage et favorise la coalescence de deux gouttelettes approchantes.

La seconde partie de cette thèse a été consacrée à l'étude du rôle d'une compatibilisation réactive en contrôlant l'étendue de la coalescence des phases dans les mélanges d'oléfines thermoplastiques. Les mélanges d'oléfines thermoplastiques de PP et d'EC ont été compatibilisés de manière réactive au moyen de composés réactifs fonctionnels capables de former des copolymères à l'interface. À cette fin, des groupes d'amines fonctionnels ont d'abord été incorporés dans une solution réactionnelle de polypropylène. Le polypropylène aminé a alors été utilisé comme compatibilisant réactif lors du mélange à l'état fondu. Les mélanges composés de 70/30 w/w de PP/EC et contenant un compatibilisant selon différentes concentrations : 0 % en masse (PP70n), 5 % en masse (PP70m) et 10 % en masse (PP70h), ont été étudiés. Les mesures viscoélastiques linéaires ont montré que les mélanges compatibilisés retrouvent les caractéristiques des matériaux en l'état de transition sol-gel ; tandis que la pente du module de conservation du mélange non-compatibilisé (PP70n) dans la zone finale (au-dessus de la première décade) satisfait le critère d'un comportement liquide (*i.e.* une pente de 2), les modules

de conservations des mélanges PP70m et PP70h se conforment à la loi puissance avec de très faibles pentes respectivement de 0.2 et de 0.4. Aux hautes fréquences, par contre, les propriétés dynamiques de tous les mélanges étudiés (compatibilisés ou non) étaient identiques, cela suggère que les propriétés des deux composantes des mélanges n'ont pas été changées par la compatibilisation réactive. Le modèle d'émulsion de Palierne a échoué dans la prédiction du comportement des mélanges compatibilisés à basse fréquence, où des augmentations significatives du module de conservation ont été observées. Il a été montré qu'en appliquant une version modifiée du modèle de Palierne et aussi un modèle viscoélastique type Zener avec deux éléments fractionnés, de meilleures prédictions du module de conservation étaient obtenues; par contre ces derniers modèles n'ont pas pu prédire la tendance réelle qu'aurait l'angle de perte aux basses fréquences ; tandis que les modèles ont prédit une tendance à la baisse monotone de la tangente d'angle de perte pour les mélanges compatibilisés, les données expérimentales semblaient se stabiliser. Un modèle Zener généralisé (GZM) avec trois éléments fractionnels a permis de décrire les données de viscoélasticité linéaire sur toute la gamme des fréquences étudiées. Il a été trouvé que dans les échantillons compatibilisés, le temps de relaxation correspondant au troisième élément fractionnel (parallèle aux deux autres éléments) est plus grand que les temps de relaxation des deux autres éléments et l'exposant correspondant diminue lorsque la concentration du compatibilisant augmente ; cela est en accord avec la tendance trouvée grâce aux observations au microscope où le mélange avec la plus haute concentration de compatibilisant présentait une structure plus interconnectée.

Le modèle LPL prédit très bien le comportement rhéologique en régime transitoire et la morphologie du mélange non-compatibilisé, mais échoue dans la prédiction de la réponse transitoire des mélanges compatibilisés. Cependant, cela était attendu puisque les contraintes

supplémentaires résultant du compatibilisant réticulé ne sont pas prises en compte par le modèle LPL. Le modèle GZM a seulement prédit une partie initiale des données de la viscosité en régime transitoire des mélanges compatibilisés. Les propriétés rhéologiques des mélanges compatibilisés réactifs, incluant le comportement similaire au gel, la viscosité améliorée à faible cisaillement, la viscosité transitoire développée sur le long terme et la relaxation de contraintes retardée, suggèrent que ces mélanges présentent une structure entremêlée, liée par le copolymère compatibilisé, comme confirmé par la microscopie à force atomique.

La dépendance de la structure cellulaire à la morphologie des mélanges non-expansés et le rôle de la compatibilisation réactive dans le contrôle du comportement expansé des oléfines thermoplastiques ont été étudiés dans la dernière partie de la thèse. Un lot standard a été utilisé pour faire mousser les échantillons en utilisant du dioxyde de carbone comme agent gonflant. Deux procédés différents d'expansion ont été utilisés ; dans le premier procédé (procédé d'expansion induite par la température) les échantillons ont premièrement été saturés avec du dioxyde de carbone pendant 12 heures à température ambiante et à 45 bar. L'expansion a été effectuée en submergeant les échantillons chargés de gaz dans un bain d'huile de glycérine chauffée à 155 °C. Dans l'autre procédé d'expansion (procédé d'expansion induite par la pression) les échantillons ont d'abord été chauffés à 200 °C afin de fondre les structures cristallines. Les échantillons fondus ont ensuite été ramenés à une température de 155 °C et pressurisés par du dioxyde de carbone pendant 6 heures à une pression de 45 bar et par la suite expansé sous pression. Le pouvoir moussant du PP pur et du EC pur, ainsi que des mélanges à 60/40 w/w (PP/EC) compatibilisés à différentes concentrations en compatibilisant : 0 % en masse (PP60n), 5 % en masse (PP60m) et 10 % en masse (PP60h), a été étudié. Une méthode microscopique basée sur la technique d'imagerie à électrons rétrodiffusés a été employée pour

déterminer la localisation des bulles, des domaines élastomériques dispersés et la matrice en polypropylène. Des mesures de solubilité ont été effectuées pour déterminer la quantité relative de gaz dans les polymères pressurisés avant l'expansion.

Il a été montré que les bulles se sont préférentiellement formées dans les domaines élastomériques dispersés. Cela a été attribué au haut niveau de solubilité et de diffusabilité du gaz dans la phase élastomérique en comparaison avec sa solubilité et sa diffusabilité dans la matrice en polypropylène. Tous les échantillons expansés via la température présentent une morphologie microcellulaire ; la taille et la densité des cellules ont été mesurées comme étant respectivement 6 µm et 2.5×10^9 (cm^{-3}) pour le mélange PP60n, 3 µm et 7.6×10^9 (cm^{-3}) pour le mélange PP60m et 3 µm et 8.7×10^9 (cm^{-3}) pour le mélange PP60h. La tendance suivit par les densités de cellules est en accord avec la variation de la surface interfaciale des différents échantillons : respectivement 0.3, 0.4 et 0.7 (μm^{-1}) pour les mélanges PP60n, PP60m and PP60h.

La morphologie initiale des mélanges a aussi été altérée par une coalescence au repos aussi bien que par un cisaillement causé par la coalescence de phases et l'impact des transitions de morphologie sur la structure cellulaire des mousses obtenues a été étudiés. La surface interfaciale du mélange PP60n a varié de 0.30 μm^{-1} pour l'échantillon non traité à 0.08 μm^{-1} dans le mélange recuit et à 0.06 µm dans le mélange qui a été recuit et par la suite cisaillé à 0.01 s^{-1}. La taille et la densité des cellules ont varié respectivement de 3 µm et 2.5×10^9 (cm^{-3}) pour le mélange non-traité à 25 µm et 1.6×10^7 (cm^{-3}) pour le mélange recuit et à 42 µm et 6.0×10^6 (cm^{-3}) pour le mélange cisaillé.

L'expansé induite par la pression des mélanges non compatibilisés a entraîné la formation de bulles très grossières ; cela a été attribué à la fonte de la structure cristalline du PP dans ce

procédé en raison de laquelle la matrice de PP ne peut plus contrôler la croissance des bulles nuclées. Aussi, la morphologie cellulaire détériorée peut être en partie expliquée par la solubilité réduite du CO_2 à la haute température utilisée dans le procédé d'expansion induite par la pression. Toutefois, les mélanges compatibilisés ont présenté une morphologie cellulaire fine avec une taille et une densité de cellules respectivement de 9 µm et 3.6×10^8 (cm^{-3}) pour le mélange PP60m et de 7 µm et 9.9×10^8 (cm^{-3}) pour le mélange PP60h. En considérant que la morphologie cellulaire finale est aussi influencée par les propriétés viscoélastiques des TPO, le comportement rhéologique des matériaux soumis à un cisaillement et à un écoulement élongationnel a aussi été étudié. Il a été montré que l'addition du compatibilisant a résulté en des propriétés viscoélastiques améliorées aux basses fréquences ainsi qu'une augmentation du comportement durcisseur. Le caractère non-linéaire des TPO observé grâce aux mesures de rhéologie élongationnelle est dû à la présence de la phase élastomérique dans le système, laquelle a été montrée comme étant un polymère au comportement durcisseur. De surcroît, le caractère durcisseur du mélange peut être en partie attribué aux forces interfaciales créées pendant la déformation des domaines caoutchouteux en extension uniaxiale. Un tel durcissement interfacial était plus prononcé dans les systèmes compatibilisés, spécialement aux plus faibles taux de cisaillement où la contribution de l'interface en régime transitoire devient comparable à la contribution des composants purs. Les résultats ont montré que la compatibilisation réactive peut significativement améliorer le comportement expansé des oléfines thermoplastiques par l'augmentation du taux de nucléation et le contrôle de la phase de croissance des bulles nucléées. Cela a été attribué à une dispersion plus fine de la phase élastomérique ainsi qu'à l'amélioration des propriétés viscoélastiques des oléfines thermoplastiques compatibilisées.

TABLE OF CONTENTS

Dedication III

Acknowledgement IV

Résumé VI

Abstract VIII

CONDENSÉ EN FRANÇAIS X

TABLE OF CONTENTS XVII

LIST OF TABLES XX

LIST OF FIGURES XXI

NOMENCLATURES XXVII

LIST OF ABBREVIATIONS XXXI

CHAPTER 1: INTRODUCTION 1

CHAPTER 2: LITERATURE REVIEW 4

2.1 Development of phase morphology in immiscible polymer blends 4

2.1.1 Drop breakup 5

2.1.2 Coalescence 7

2.1.3 Role of interfacial modifications 13

2.2 Rheological models 20

2.3 Foaming behavior of polymer blends 29

2.2.1 Nucleation 30

2.2.1.1 Classical Mechanism of Heterogeneous Nucleation 30

2.2.1.1 Microvoid Nucleation Mechanism 32

2.2.2 Growth 34

2.4. Summary 36

CHAPTER 3: OBJECTIVES 39

CHAPTER 4: ORGANIZATION OF THE ARTICLES 41

CHAPTER 5: Coalescence in Thermoplastic Olefin (TPO) Blends under Shear Flow 43

Abstract 44

Introduction 45

Background 46

Experimental 49

A. Materials and Sample Preparation 49

B. Rheological/Morphological Measurements 50

Results and Discussion 51

A. Determination of interfacial tension 51

B. Morphology evolution under transient shear 59

Concluding remarks 73

Acknowledgments 73

References 74

CHAPTER 6: Rheological and Morphological Properties of Reactively Compatibilized Thermoplastic Olefin (TPO) Blends 78

Abstract 79

I. Introduction 79

II. Materials and experimental method 82

A. Materials 83

B. Compatibilization 83

C. Blend preparation 85

D. Morphology 86

E. Rheometry 87

III. Rheological models 87

IV. Results and Discussion 92

A. Initial morphology 93

B. Dynamic measurements 96

C. Transient rheological /morphological behavior 107

V. Concluding remarks 112

Acknowledgements 113

References 113

CHAPTER 7: Foaming Behavior of Microcellular Thermoplastic Olefin Blends 117

Abstract 118

I. Introduction 119

II. Experimental 122

A. Materials and preparation methods 122

B. Rheological experiments 123

C. Sorption measurements 124

D. Foaming 125

E. Microscopy 126

III. Results and discussion 127

A. Temperature-induced foaming 128

B. Pressure-induced foaming 136

IV. Conclusions 144

Acknowledgements 145

References 145

CHAPTER 8: GENERAL DISCUSSION 149

CHAPTER 9: CONCLUSIONS AND RECOMMENDATIONS 154

9.1 Conclusions 154

9.2 Original contributions 157

9.3 Recommendations 157

References 161

LIST OF TABLES

Table 5.1 Main characteristics of the neat materials..... 49

Table 5.2. Interfacial tension and relaxation time obtained by different methods for the (85/15) blends. 56

Table 5.3 Parameters used for predicting the transient shear viscosity of different blends with LP and LPL models at 0.01(s^{-1})..... 68

Table 6.1. Properties of the polymers used..... 83

Table 6.2. Fitting parameters of the fractional Zener model with two fractional elements..... 99

Table 6.3. Fitting parameters of the generalized Zener model. 103

Table 6.4. Parameters used for predicting the transient shear viscosity of the PP70n blend..... 109

Table 7.1 Diffusivity and solubility of CO2 in neat PP and EC and their 60/40 (PP/EC) blend 132

LIST OF FIGURES

Fig. 2.1. Morphological hysteresis in different sequences of increasing shear and decreasing shear rate [Minale et al. (1997)]. 9

Fig. 2.2. Transient morphology evolution of PS/HDPE 80/20 blend during shearing [Martin et al. (2000)]. 11

Fig. 2.3. Volume average equivalent diameter of the minor phase versus strain during creep experiments at different applied sheared stresses [Martin et al. (2000)]. 12

2.4 Illustration of the film drainage process during collision of two deformable drops [Lyu et al. (2002a)]. 14

Fig. 2.5. Mechanisms proposed for coalescence inhibition using copolymer compatibilizers: (a) interfacial tension gradient (Marangoni force) and (b) steric repulsion [Lyu et al. (2002b)]. 15

Fig. 2.6. Atomic force micrograph depicting the interfacial erosion in reactively compatibilized BIMSM/PA blend [Bhadane et al. (2008)]. 17

Fig. 2.7. Formation of cluster like morphology in PA6/SAN (30/70) blends compatibilized with 4.8 wt% SANMA compatibilizer [Sailer and Handge (2008)]. 18

Fig. 2.8. Morphology of compatibilized PDMS/PI (30/70) blends compatibilized by (a) premade copolymers and (b) reactive species [Deleo and Velankar (2008)]. 20

Fig. 2.9. Illustration of different relaxation mechanisms and the corresponding rate equations involved in the Lee and Park model (1994) 27

Fig. 2.10. Heterogeneous bubble nucleation $\Delta G^*_{hetero} < \Delta G^*_{homo}$ [Lee et al. (2004)]. 31

Fig. 2.11. Transmission electron micrograph (TEM) showing the presence of microvoids in PS/PB blend [Keskkula et al. (1986)]. 33

Fig. 2.12. Scanning electron micrograph of styrenic foams a) polystyrene b) nucleated polystyrene [Ramesh et al. (1994a)] 34

Fig. 2.13. Micrographs of (a) unfoamed) and (b) foamed PP/PER (50/50) blends. The dark phases represent the PER inclusions and bubbles in the unfoamed and foamed samples respectively. 36

Fig. 5.1 Storage moduli of the neat components and of the 85/15 and 70/30 (w/w) PP/EC blends at 200 ^{o}C; (a) PP/EC1, (b) PP/EC5, (c) PP/EC30. 53

Fig. 5.2. Time weighted relaxation spectrum as well as subtracted relaxation spectrum for the blends containing 15% and 30% dispersed phase. (a) PP/EC1, (b) PP/EC5, (c) PP/EC30. The solid lines indicate the window of validity based on the experimental frequency. 54

Fig. 5.3 Predictions of the storage and loss moduli of the PP/EC(85/15) blends with the Palierne and Choi-Showalter models. (a) PP/EC1(85/15), (b) PP/EC5(85/15), (c) PP/EC30(85/15). 58

Fig. 5.4 Comparison between the stress growth viscosity data and predictions of the LP and LPL models for the PP/EC (70/30) blends at T=200°C, (s^{-1}). a) PP/EC1(70/30); b)PP/EC5(70/30); c)PP/EC30(70/30). 63

Fig. 5.5 Variation of the normalized specific interfacial area with time for the PP/EC (70/30) blends at T=200°C, $\dot{\gamma} = 0.01\,(s^{-1})$. 64

Fig. 5.6. Micrographs showing coalescence after shearing. Left micrographs: initial morphology; right micrographs: after 40 min. shearing at $\dot{\gamma} = 0.01$ s^{-1}. a) PP/EC1(70/30)); b) PP/EC30(70/30). The ratio of final to initial droplet size (d_{v_f} / d_{v_0}) was measured to be 1.3 and 3 for PP/EC1(70/30) andPP/EC30(70/30) blend respectively. 65

Fig. 5.7. Stress growth viscosity and morphological data for two consecutive stress growth experiments, at $\dot{\gamma} = 0.3\,\mathrm{s}^{-1}$ and $\dot{\gamma} = 0.01\,\mathrm{s}^{-1}$. The micrographs were taken after 15 min recovery following the first stress growth. a) PP/EC1(70/30); b) PP/EC30(70/30). 67

Fig. 5.8. Comparison of stress growth viscosity data and predictions of the LP and LPL models for PP/EC30 blends at 200°C, $\dot{\gamma} = 0.01\,\mathrm{s}^{-1}$. a) PP/EC30(85/15); b) PP/EC30(80/20); c) PP/EC30(75/25). 69

Fig. 5.9. Variation of the final droplet size normalized by the initial value for the blends with different initial morphologies (□) and simulated blends with a same initial droplet size (▲). 71

Fig. 5.10. Comparison between the predictions of the PLP model and experimental data for PP/EC30(75/25) blend pre-sheared at 0.02 s^{-1} for 600 s. 72

Fig. 6.1. Schematic of the reactions involved in synthesizing the compatibilizer copolymer..... 85

Fig. 6.2. Mechanical representation of a) ordinary Zener model, b) Zener model with two fractional elements [Sailer and Handge (2007)] and c) generalized Zener model (GZM). 89

Fig. 6.3. AFM micrographs of PP70 samples quenched right after mixing in the internal mixer: a) PP70n, b) PP70m, and c) PP70h. 94

Fig. 6.4. AFM micrographs of PP70 samples after compression molding and squeezing in the gap of the cone and plate geometry at 200 °C for 30 min: a) PP70n, b) PP70m, and c) PP70h. . 95

Fig. 6.5. Variations of the storage modulus (a) and the complex viscosity (b) with frequency for the PP70 blends with different levels of compatibilizer. The insertions show the predictions of the Palierne model (data are shifted by factors shown). 97

Fig. 6.6. Predictions of the Zener model with two fractional elements (FE) and of the Palierne model with equilibrium modulus for the storage modulus of the PP70h blend (data are shifted by factors shown). The solid line in red represents the behavior of suspensions of rigid particles predicted by the Palierne model for rigid inclusions. 100

Fig. 6.7. Comparison between the experimental data (shifted by factors shown) and the predictions of the loss tangent versus frequency for the PP70 blends using the modified Palierne model, the Zener model with two FE and its fractional generalization (GZM). 102

Fig. 6.8. Morphology of the PP/EC (85/15) blends: (a) non-compatibilized (PP85n) and (b) compatibilized with 5wt% PPNH2 (PP85h). 105

Fig. 6.9. Storage modulus (a) and loss tangent (b) as functions of frequency for PP85n and PP85h blends, along with the predictions of GZM and the Palierne model. 106

Fig. 6.10. Stress growth data for the PP70n and PP70m blends at $\dot{\gamma} = 0.01$ and $\dot{\gamma} = 0.1\,\mathrm{s}^{-1}$. Solid lines represent the predictions of the LPL model for the PP70n blend. 107

Fig. 6.11. Stress growth data for the PP70h blend at $\dot{\gamma} = 0.01$, $\dot{\gamma} = 0.005$ and $\dot{\gamma} = 0.002\,\mathrm{s}^{-1}$, along with the predictions of the generalized Zener model (GZM). 108

Fig. 6.12. Stress relaxation behavior of the PP70 blends after cessation of shearing at $\dot{\gamma} = 0.01\,s^{-1}$. 110

Fig. 6.13. Morphology of blends with different compatibilizer concentrations after shearing at $\dot{\gamma} = 0.01\,s^{-1}$ for 1h: (a) PP70n, (b) PP70m and (c) PP70h. 111

Fig. 7.1. Pressurizing setup used for foaming experiments: 1) high pressure chamber, 2) covering flange, 3) gas inlet (outlet), 4) temperature sensor connection, 5) safety relief outlet. 125

Fig. 7.2. BEI micrographs of the unfoamed TPOs with different levels of compatibilizer: a) PP60n; b) PP60m; c) PP60h. 129

Fig. 7.3. BEI micrographs at two different scales of TPO foams with different levels of compatibilizer foamed by temperature-induced foaming: (a1, a2) PP60n; (b1,b2) PP60m; (c1,c2) PP60h. 130

Fig. 7.4. Stress growth viscosity data of the neat PP and neat EC and PP60n blend at 200 ^{o}C at a shear rate of 0.01 s^{-1}. 133

Fig. 7.5. BEI micrographs unfoamed PP60n blends: a) before annealing; b) annealed at 200 ^{o}C; and c) annealed and subsequently sheared at 0.01 s^{-1} and 200 ^{o}C for 20 min. 134

Fig. 7.6. Micrographs of foamed PP60n blends prepared under different shearing and thermal history: a) non annealed; b) annealed at 200 ^{o}C; and c) annealed at 200 ^{o}C and subsequently sheared at 0.01 s^{-1} for 20 min. Samples were foamed using temperature-induced foaming. 135

Fig. 7.7. Morphology of the unfoamed TPOs with different levels of compatibilizer: a) PP60n; b) PP60m; c) PP60h. The samples were firstly heated at 200 oC and annealed at 155 ^{o}C for 1 h. 137

Fig. 7.8. Micrographs at different scales of TPO foams with different levels of compatibilizer foamed by pressure-induced foaming: a) PP60n; (b1,b2) PP60m; (c1,c2) PP60h. 138

Fig. 7.9. Variations of the storage modulus and complex viscosities with frequency for TPOs with different levels of compatibilizer measured at 155 ^{o}C..... 140

Fig. 7.10 .Variations of the loss tangent with frequency for TPOs with different levels of compatibilizer. Measurements were performed at 155 ^{o}C..... 141

Fig. 7.11. Transient elongational viscosities of the neat materials (a) and the blends with different levels of compatibilizer (b) measured at 155 ^{o}C. Data have been multiplied by shown factors for clarity reasons. 143

NOMENCLATURES

English letters

A	Area of the micrographs
B	Specific interfacial perimeter
Ca	Capillary number
Ca_{crit}	Critical Capillary number
c_1	The coalescence relaxation dimensionless rate constant in the Lee and Park model
c_2	The shape relaxation dimensionless rate constant in the Lee and Park model
c_3	The break-up and shape relaxations dimensionless rate constant in the Lee and Park model
d	Droplet diameter
d_1	The degree of total relaxation in Lee and Park model
d_2	The degree of size relaxation in Lee and Park model
d_3	The degree of break-up and shape relaxations in Lee and Park model
d_n	Number averaged droplet diameter
d_v	Volume averaged droplet diameter
e_i	Unit vector normal to the interface
F	Geometrical factor of the nucleating agent in the classical heterogeneous nucleation model
h	Film thickness
h_c	critical film thickness
G	Elastic modulus
G_i	Relaxation modulus of the ith fractional element in the Zener model
G_e	Equilibrium modulus

G^*	Complex modulus
G'	Storage modulus
G''	Loss modulus
k	Ratio of the dispersed to the continuous phase viscosity
k_B	Boltzmann constant
$M(\ )$	Mittage-Leffler function
M_w	Weight averaged molecular weight
M_n	Number averaged molecular weight
N	Cell density
n	Exponent of the fractional element in the Zener model
P	Isotropic pressure
Q	Specific interfacial area
q	The anisotropy tensor
R	Droplet radius
R_v	Volume averaged droplet radius
$\langle r_0^2 \rangle$	square mean end to end distance of the molecules
S	Total interfacial area
T	Temperature
T_g	Glass transition temperature
T_m	Melting point
t	time
t_d	Drainage time
u	Average velocity
u_p	Pressure driven portion of the film velocity
u_t	Velocity at the drop interface

V	Volume
W	Weight gain of the pressurized sample during sorption experiment

Greek letters

α	Interfacial tension
β'	Interfacial dilatation modulus in the Palierne emulsion model
γ	Shear strain
$\dot{\gamma}$	Shear rate
$\dot{\gamma}_{ij}$	The components of the rate of deformation tensor
$\Gamma()$	Gamma function
δ	Phase angle
δ_{ij}	The Kronecker delta
$\dot{\varepsilon}$	Henckey strain rate
ζ	The slip parameter in the modified Lee and Park model (LPL model)
η	Steady state viscosity
η^{+}	Transient viscosity
η^{*}	Complex viscosity
κ_{ij}	The components of the velocity gradient tensor
λ	Relaxation time of the fractional elements in the Zener model
ρ	Density
σ	The stress tensor
Σ_{min}	Minimum coverage of the block copolymers at the interface

τ	Characteristic time
ϕ	Volume fraction
ω	Angular frequency

LIST OF ABBREVIATIONS

AFM	Atomic force microscopy
BEI	Back scattering electron imaging
EC	Ethylene copolymer
FE	Fractional element
HDPE	High density polyethylene
MA	Maleic anhydride
MFI	Melt flow index
PA	Polyamide
PDMS	Polydimethylsiloxane
PE	Polyethylene
PER	Polypropylene-ethylene copolymer rubber
PI	Polyisoprene
PMMA	Polymethylmethacrylate
PPE	Poly(dimethyl-phenylene ether)
PS	Polystyrene
SAN	Styrene-acrylonitrile
SAOS	Small amplitude oscillatory shear
SEM	Scanning electron microscopy
TEM	Transmission electron microscopy
TPO	Thermoplastic olefin
XPS	X-ray photoelectronic spectroscopy

CHAPTER 1
INTRODUCTION

Blending of polymers is by far one of the most efficient techniques to generate new materials with desired physical and mechanical properties while satisfying the economic aspects. On the other hand, foaming of polymeric substances is an effective way to use less material and reduce the product costs. Combination of these two techniques is a new challenging issue as the relationship between the rheological and micro-structural properties of the foamable compound and the final cellular morphology is not clarified and a fundamental study on this problematic is still lacking. Understanding the foamability of polymer blends is of great industrial importance, especially in automotive applications where a reduction of the energy consumption is sought. Benefits of reduced vehicle weight can have an important environmental impact since there is a 6-8 % improvement in fuel efficiency for every 10 % in weight reduction.

The main motivation of this study is the increasing interest of automotive industries in fabricating automotive parts using light weight materials. Thermoplastic olefins (TPOs) are widely used by automotive industry in applications such as bumper fascias, claddings and exterior trim. TPOs are also finding increased use in interior automotive applications including instrument panels and air bags. Thermoplastic Olefins (TPOs) are indeed a class of material that consists of a hard thermoplastic continuous phase and a soft elastomeric dispersed phase. These compounds exhibits good processability and very attractive solid state properties such as: excellent mechanical properties at low density, soft feel and comfort, excellent weatherability and recyclability. According to a study of Freedonia Group, Inc. (2005), the global demand for thermoplastic olefins is forecast to rise 6.3 percent per year to 936000 metric tons by 2014. Development of foaming technology for TPOs could reduce the material costs up to 25%.

As for the other types of immiscible polymer blends the properties of TPOs is relying on the extent of interfacial area and interfacial adhesion between the constituent phases. The magnitude of the interface and its function is controlled by the microstructure of the dispersed phase formed during mixing processes. Although the flow path in the mixing devices provides different combinations of intense shear and elongational stresses large enough for breaking the dispersed domains into very fine inclusions, the separated domains tend to reassociate in larger phases to minimize the thermodynamic energy of the system, a phenomenon called *coalescence*. This phenomenon becomes more important in post-mixing sequences where coalescence can occur in the absence of flow (quiescent coalescence) or in flow fields of molding processes. In the latter, phase integration is favored by the prevailing stresses which can facilitate the drainage of the matrix liquid intervening the coalescing drops.

In view of the importance of coalescence in determining the final morphology of polymer blends, the first part of this thesis is devoted to understanding the coalescence behavior of TPOs under shear flow; subsequently a reactive compatibilization is employed to stabilize the TPOs morphology against coalescence. For this purpose a surface modifier component is synthesized and used to form a copolymer compatibilizer during reactive mixing. Having obtained an understanding of how to control the extent of coalescence, the last phase of the thesis looks at the influence of reactive compatibilization and morphology control on the foaming behavior of the TPOs.

This dissertation is based on three articles that have been published or submitted to scientific journals and is organized in 9 chapters:

- Chapter 2 provides a critical literature survey considering the related issues.
- The objectives are introduced in Chapter 3.
- The organization of the articles is described in Chapter 4.
- Chapters 5, 6 and 7 include the three articles written in the scope of this study.
- Chapter 8 presents a general discussion pertaining to the results obtained in this work.
- Finally Chapter 9 presents the conclusions of this study and the recommendations for future work.

CHAPTER 2
LITERATURE REVIEW

2.1 Development of phase morphology in immiscible polymer blends

Similar to liquid-liquid mixtures the miscibility in polymer blends is also determined by the free energy of mixing (ΔG_m) which is a function of the enthalpic (ΔH_m) and entropic (ΔS_m) changes in the system:

$$\Delta G_m = \Delta H_m - T\Delta S_m \tag{2.1}$$

Since the total number of macromolecules in polymer blends is much smaller than for the low molecular weight liquids, the combinatorial entropic contribution in polymeric pairs is quite low. This often leads to positive values of the free energy of mixing as the enthalpic term is generally positive, at least for non polar polymers. While negative values of ΔG_m is necessary for a miscible systems, the thermodynamic stability of a completely miscible mixture is established when the following condition concerning the compositional dependence of the free energy is also satisfied:

$$\left(\frac{\partial^2 \Delta G_m}{\partial \phi_i^{\,2}}\right)_{T,P} > 0 \tag{2.2}$$

The latter condition indeed assures that the infinitesimal changes in composition toward the phase separated region are not thermodynamically favored and do not drive the free energy to the lower values [Paul and Newman (1978)].

For high molecular weight polymers these miscibility criteria are rarely met and hence polymer blends are generally thought to be *immiscible* resulting in multiphase structures. The

microstructure, i.e. morphology of these blends, is developed during the melt processing and includes very complex phenomena like break-up or coalescence of the dispersed phase. The morphology development is dependent on several influencing parameters such as interfacial tension, composition of the constituents, flow field, viscosity ratio, normal stresses and phase viscoelasticity. The final morphology is determined by the competition between the break-up and coalescence phenomena during mixing.

2.1.1 Drop breakup

Earlier studies on the drop deformation and breakup of a liquid drop in an emulsion go back to the Taylor's work (1934). For a mixture of Newtonian fluids, Taylor showed that the drop deformation is a function of viscosity ratio (ratio of the dispersed phase to the matrix viscosity, η_d / η_m) and the ratio of hydrodynamic to interfacial forces expressed by the Capillary (*Ca*) number:

$$Ca = \frac{\eta_m |\dot{\gamma}| R}{\alpha} \tag{2.3}$$

where η_m is the matrix viscosity, $|\dot{\gamma}|$ is the magnitude of the velocity gradient tensor, R is the drop radius and α represents the interfacial tension. Depending on the viscosity ratio, the droplet subjected to irrotational or shear flow undergoes a transient deformation and as the Ca number increases the droplet may form a highly elongated thinning thread which may eventually breaks into smaller droplets. The minimum *Ca* number beyond which the deformed droplet becomes unstable and undergoes fracture is commonly known as the critical Capillary number ($Ca_{crit.}$). Several studies [Taylor (1934), Rumscheidt and Mason (1961), Bentley and Leal (1986)] have shown that both in shear and irrotational flow $Ca_{crit.}$ approached a minima at viscosity ratio

levels near unity. Irrotational (extensional) flows has been found, however, to be more conducive to drop deformation and breakup; while a pure shear flow was incapable of dispersing a drop with viscosity ratios above ~3.5, extensional flows are able to breakup droplets with much larger viscosity ratios [Grace (1982)].

The typical dispersion modes in Newtonian fluids have been found to be thread fracture or tip streaming during which the elongated thread is broken through the Rayleigh instabilities. Various modes of dispersion have been, however, reported for the breakup of viscoelastic drops; At high shear rates the viscoelastic drop may form a stretched sheet parallel to flow direction before rupture into the smaller drops [Lindt and Ghosh (1992); Sundararaj and Mocosko (1995); Lin et al. (2003a)]. The first normal stress differences across the drop interface created at high deformation rates can also cause vorticity elongations perpendicular to the flow direction [Hobbie and Migler (1999); Migler (2000) ; Mighri and Huneault (2001)] . Lin et al. (2003b) reported a surface erosion breakup mechanism through which simple shearing can breakup droplets with viscosity ratios much larger than 3.5. Mighri and Carreau [(1997); (1998)] showed how the extent of drop deformation in shear and elongational flow can be influenced by phase elasticities; using constant viscosity Boger fluids they found that increasing the elasticity of the matrix polymer facilitates the drop deformation while increasing the dispersed phase elasticity increases the resistance to deformation and breakup.

In spite of strong shear and elongational flow fields created in the mixing devices the final morphology of concentrated polymer blends can be much coarser than predictions based on droplet breakup mechanism theories. This shows the importance of droplet coalescence in the morphology development of polymer blends.

2.1.2 Coalescence

Coalescence phenomena can be generally categorized into two different types: quiescent (static) coarsening and flow induced (dynamic) phase coalescence. The driving force for coalescence in both processes is the thermodynamic tendency of the system to reduce the interfacial area and minimize the free energy. Both processes are essentially composed of the following sequences: droplet approach, film drainage, film rupture and confluence. There have been a number of studies investigating the static coalescence phenomenon [Fortelny and Kovar (1988); Crist and Nesarikar (1995) ; Fortelny and Zivny (1995); Wallheinke et al. (1999) ; Yuan and Favis (2005)]; these studies showed that the extent of coalescence in a quiescent process is a function of phase concentration, interfacial mobility (mobile, partially mobile or immobile interface) and the instability factors contributing the film drainage phenomenon (Brownian motions, shape relaxation, gravitational forces and van der Waals forces).

In the case of dynamic coalescence the particle approach is favored by the velocity gradient imposed by the external flow. Early studies on flow induced coalescence go back to the work of Smoluchowski (1917) who proposed a coalescence model describing the coagulation rate in the absence of particle-particle interactions. Following Smoluchowski (1917) further studies were conducted to account for hydrodynamic interactions which could deviate the particle trajectories from the streamlines of the bulk flow [Batchelor and Green (1972); Wang et al. (1994)]; the influence of hydrodynamic interactions on the deformation of the interface and consequently on the velocity profile of the thinning film was later investigated by Chester (1991) and Davis et al. (1989) who studied the drainage phenomenon in different ranges of interfacial mobility; it was shown that going from a rigid to a fully mobile interface, the coalescence is

facilitated through the increased tangential circulating flow inside the droplets, which reduces the resisting force and favors the particles' collision.

Coalescence in molten polymer blends has not been completely understood yet. The difficulty encountered in these systems is that the direct visualization of the colliding drops is often limited and the phenomenological coalescence parameters such as the drainage time (t_d) or the critical film thickness (h_c) at the point of rupture can be hardly evaluated. To study the size evolution of the particles under flow, rheological devices are often employed to provide a controlled flow condition and microscopic measurements are subsequently performed to examine the blends morphology. In these studies steady or transient morphological states of the blends as a function of strain rate or strain are investigated. In an attempt to evaluate the effect of the shear history on the final steady state morphology of polymer blends, Minale et al. (1997) performed a series of transient shear measurements at different shear rates; the resulting morphology at the steady state was then evaluated using subsequent dynamic measurements and by applying the Palierne emulsion model (1990). It was shown that there is a critical shear rate above which the final morphology is independent of the initial blend morphology. The dependency to the initial blend morphology resulted in a morphological hysteresis for the two rounds of shearing experiments (increasing or decreasing shear rate) as shown in Fig. 2.1. The morphological hysteresis was then described using theoretical models that can predict the limiting curves for breakup and coalescence. The limiting curve for breakup was determined using the empirical relation proposed by de Bruijn (1989):

$$\log\left(\frac{\eta_m|\dot{\gamma}|R}{\alpha}\right) = -0.506 - 0.0994\log(k) + 0.124\log^2(k) - \frac{0.115}{\log(k) - \log(k_{cr})} \tag{2.4}$$

wherein k is the viscosity ratio and k_{cr} is the viscosity ratio above which drop breakup is impossible (~3.5 for rotational flow).

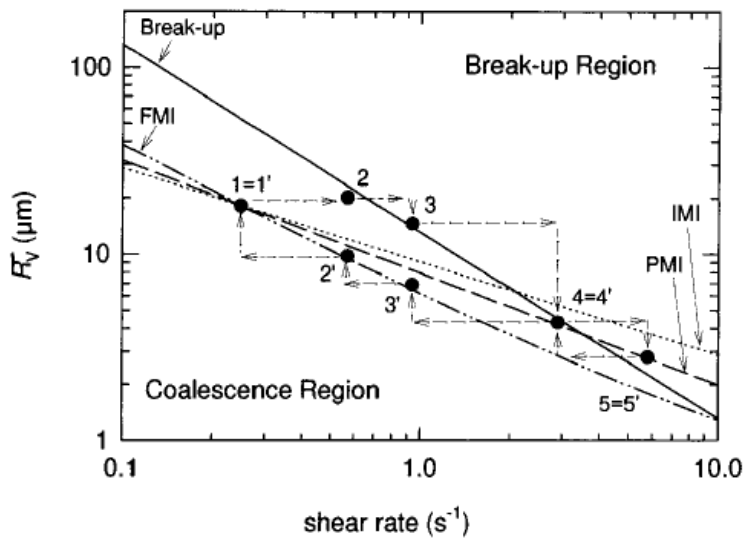

Fig. 2.1. Morphological hysteresis in different sequences of increasing shear and decreasing shear rate [Minale et al. (1997)].

For the coalescence limits the capability of three different coalescence models was evaluated. They differed in the way in which the interface between two approaching droplet is treated. Assuming that the limiting drainage time scales with $1/\dot{\gamma}$ the following three equations were used to determine the limiting curve for coalescence for fully mobile interface (FMI), partially mobile interface (PMI) and the immobile interface (IMI) respectively:

$$R\ln(\frac{R}{h_{cr}}) = \frac{2}{3}\frac{\alpha}{\eta_m \dot{\gamma}} \tag{2.5}$$

$$R = (\frac{4}{\sqrt{3}}\frac{h_{cr}}{k})^{2/5}(\frac{\alpha}{\eta_m \dot{\gamma}})^{3/5} \tag{2.6}$$

$$R = (\frac{32}{9})^{1/4}(\frac{h_{cr}\alpha}{\eta_m \dot{\gamma}})^{1/2} \tag{2.7}$$

wherein R is the drop radius, α is the interfacial tension, η_m is the matrix viscosity and h_{cr} is the critical film thickness. The factor h_{cr} was used as an adjustable fitting parameter so that the coalescence curve passes through point 1=1'. As shown in Fig.2.1 the critical shear rate almost coincides the crossover of the limiting curves for the coalescence and the breakup regions. In fact decreasing the shear rate in the region below the critical value favors the coalescence so that the droplet size increases up to the point beyond which the drainage time becomes too long and coalescence do not occur. Increasing the shear rate in this region causes drop breakup and the droplet size decreases up to the point below which the interfacial forces overcome the hydrodynamic forces and breakup becomes impossible. As shown the critical shear rate can be well described by applying partially mobile interface. Further experiments at different temperatures revealed that the agreement between the experimental values and the prediction of the FMI model becomes better as the viscosity ratio decreases whereas with increasing viscosity ratio the prediction of the IMI model is improved.

To evaluate the transient morphology evolution under shear flow Martin et al. (2000) performed a series of creep experiments using a parallel plate rheometer. The blend morphology was studied in situ by freezing the sample under the rotating plate. To achieve rapid and efficient cooling, samples were quenched by blowing cold dry nitrogen on the fixture. The efficiency of the cooling method was verified by using several different cooling rates; no significant changes in the final morphology was observed meaning that coalescence or shape recovery play no

significant role in the time scale of the cooling process. The evolution of the blend morphology during shearing at the selected shear stresses is shown in Fig. 2.2 (note the difference in magnification of the micrographs).

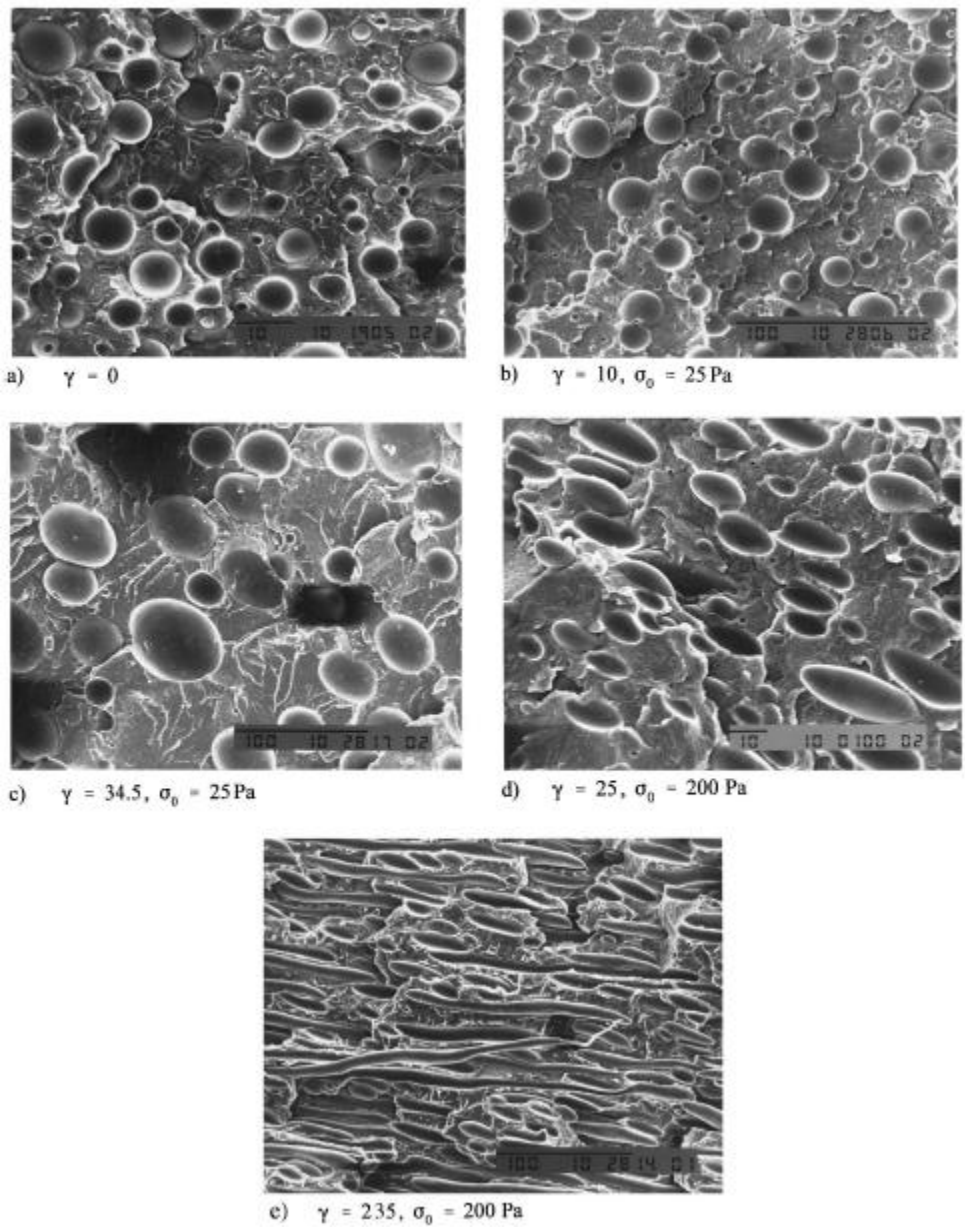

Fig. 2.2. Transient morphology evolution of PS/HDPE 80/20 blend during shearing [Martin et al. (2000)].

The volume average diameter d_v of the particles versus the total strain for the applied stresses is shown in Fig 2.3. For low stresses (25 Pa) the particles of high density polyethylene (HDPE) in the polystyrene matrix remained approximately spherical even after a long time shearing (large shear strain). However, important coalescence was detected and d_v increased by almost 7 times as the strain level reached 34.5 (Fig 2.2.a and Fig 2.2.c). For larger applied stresses (100 Pa and especially 200 Pa), the initial matrix droplet morphology were first transformed into ellipsoids and as shown at 200 Pa the deformation became large enough to result in head to tail collisions. The difference in domain sizes reported for 25 and 200Pa in Fig. 2.3 suggests that coalescence resulting from head to tail collisions at low shear rate is significantly less frequent than coalescence resulted from the collisions of particles on different path lines.

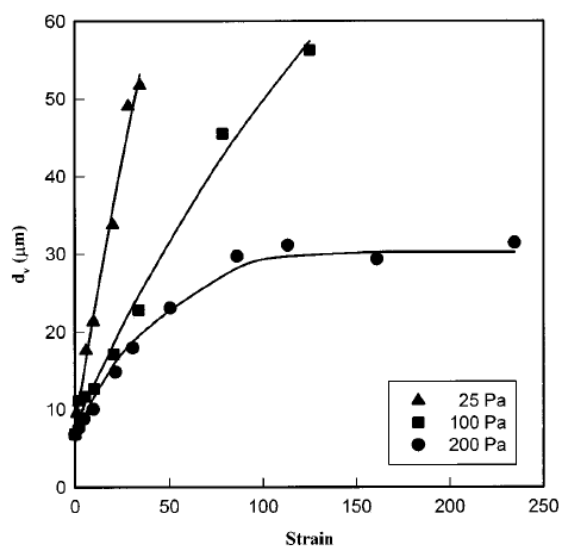

Fig. 2.3. Volume average equivalent diameter of the minor phase versus strain during creep experiments at different applied sheared stresses [Martin et al. (2000)].

Lyu et al. (2000) investigated the transient coalescence behavior of PS/HDPE blends of different viscosity ratios, different volume fractions and different amounts of added copolymer

compatibilizer. Coalescence was monitored by shearing the samples at different shear rates, all below 10 s^{-1} (the shear rate used for the initial preshearing). The capability of Smoluchowski's theory (1917) as well as trajectory [Wang et al. (1994)] and film drainage [Janssen and Meijer (1995)] models in predicting the coalescence behavior were also investigated in their following study [Lyu et. al (2002a)]. It was shown that the coalescence rate decreases with decreasing volume fraction and increasing the amount of block copolymer. Coalescence was also delayed with increasing strain rate. No any monotonic trend was established for the influence of viscosity ratio on the coalescence. The coalescence models were found to be limited to qualitative predictions of the phase morphology evolution.

2.1.3 Role of interfacial modifications

Interfacial modifiers or in other words compatibilizers can influence the morphology development through both drop breakup and coalescence processes. Compatibilizers can contribute to the drop breakup phenomenon by lowering the interfacial tension and consequently reducing the magnitude of the critical capillary number. It has been however found that the main contribution of compatibilization in morphology evolution is through the stabilization of phase morphology against coalescence and not facilitating the drop breakup [Sundararaj and Macosko (1995), Lyu et al. (2002b)]. This can be indirectly understood by considering the experimental observations showing that the presence of compatibilizer can hardly influence the droplet size at low concentrations where the collisions between the particles are rare [Sundararaj and Macosko (1995); Beck Tan et al. (1996); Milner and Xi (1996)].

There are generally two main mechanisms of coalescence inhibitions which have received a particular attention in the literature: streric repulsive interactions [Sundararaj and

Macosko (1995); Macosko et al. (1996)] and Marangoni stresses [Milner and Xi (1996)]. The stress in both proposed mechanisms is on the retarded film drainage process due to the increased hydrodynamic pressure in between of the two approaching droplets. We recall that the film drainage is the squeezing flow of the matrix fluid in the gap between the coalescing particles as illustrated in Fig. 2.4.

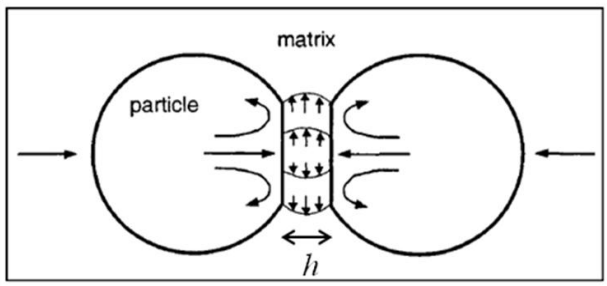

2.4 Illustration of the film drainage process during collision of two deformable drops [Lyu et al. (2002a)].

The time span of coalescence is governed by the average velocity of the thinning film u_{int} and can be scaled by the following relation [Chesters (1991)]:

$$-\frac{dh}{dt} = \frac{2h}{r} u_{\text{int}}$$

where h is the film thickness and r is the drop radius. The velocity profile inside the gap is in turn determined by the pressure gradient between the center of the film and the bulk region out of the interfacial layer. In a non modified interface this pressure can be scaled with capillary pressure at the droplet surface, O(2α/R) where α is the interfacial tension and R is the drop radius [Yiantsios and Davis (1990); Chesters (1991)]. In the presence of compatibilizers this approximation is not however valid as explained by the proposed mechanisms for coalescence inhibition; a schematic of the two stabilization processes is illustrated in Fig 2.5.

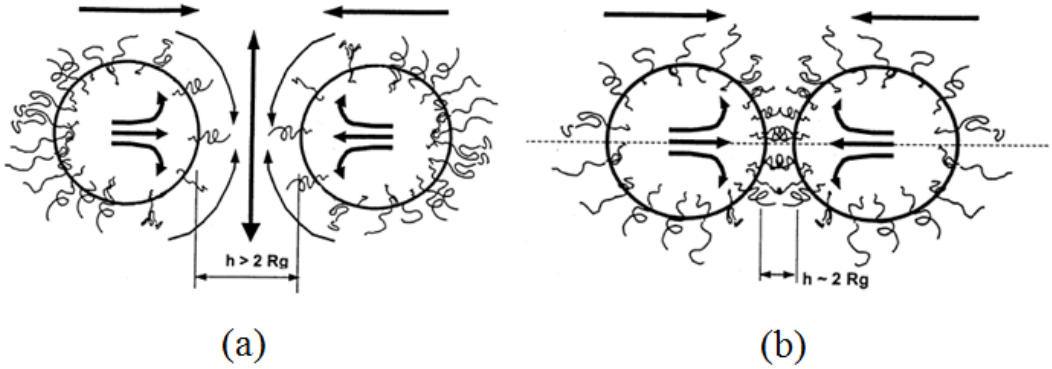

Fig. 2.5. Mechanisms proposed for coalescence inhibition using copolymer compatibilizers: (a) interfacial tension gradient (Marangoni force) and (b) steric repulsion [Lyu et al. (2002b)].

The Maranagoni effect is explained by the interfacial tension gradient created by the movement of the copolymers on the interface; as the particles approaches to each other the drainage flow sweeps the copolymer back to the drop surface and the resulting concentration gradient of the copolymer creates a repulsive force (Fig 2.5.a); the thermodynamic work required to resist such a repulsive interaction was estimated to be in the order of several k_BT [Milner and Xi (1996)]. Lyu et al. (2002b) estimated that for a pair of droplets with diameter d immersed in a matrix with viscosity η and subjected to shear flow with a shear rate of $\dot{\gamma}$, the minimum coverage of the block copolymers required for complete suppression of coalescence due to the Marangoni force would be:

$$\Sigma_{\min} = \frac{5}{32}\frac{d\eta\dot{\gamma}}{kT} \tag{2.8}$$

The steric repulsion stabilization mechanism is based on the assumption that the copolymers are attached to the interface and the repulsive force resisting the droplet approach originates from the

compression of the copolymer layers as shown in Fig 2.4.b. Macosko et al (1996) estimated that the critical concentration required for complete suppression of coalescence due to steric repulsion forces is independent of shear and is a function of the square mean end to end distance of the block copolymer molecules as below:

$$\Sigma_{\min} = \frac{20}{27\pi\langle r_0^2 \rangle} \tag{2.9}$$

To examine the validity of the proposed mechanisms Lyu et al. (2002) performed a series of steady shear experiments on polystyrene/high density polyethyelene (PS/HDPE) systems compatibilized using different types of PS-PE block copolymers. It was shown that non of the proposed models can quantitatively predict the coverage of the block copolymer at the critical saturation concentration; however the minimum coverage of the block copolymer was found to be independent of shear rate and varies with the copolymer architecture; it was shown that the copolymers with a longer corona layer (i.e. larger portion of the outer block) are more efficient in coalescence suppression. Also the copolymers with small molecules (compared to the critical gap at the point of film rupture) were found to be inefficient to inhibit the coalescence. These observations showed that the steric repulsion theory can better explain the role of copolymers in coalescence suppression.

It should be noted that these mechanisms can not describe the behavior of all compatibilized blends. Bhadane et al. (2008) found that the amount of the reactive compatibilizer required to achieve the minimum droplet size in polyamide/poly(isobutylene-co-*p*-methylstyrene) (PA/IMSM) system can be several times larger than the concentration of copolymer needed to saturate the interface and completely suppress the capillary breakup. It was shown that the reaction between the functionalized compatibilizer (brominated poly(isobutylene-

co-*p*-methylstyrene, BIMSM) with PA molecules results in the formation of very high viscosity grafted PA-IMSM molecules which then migrate from the surface of IMIS drops mainly due to the viscosity mismatch as shown in Fig. 2.6. This phenomenon termed as "*interfacial erosion*" exposes the fresh surface to form new copolymers and the successive removal of the newly formed PA-IMSM copolymers results in the development of very fine dispersed phase morphology.

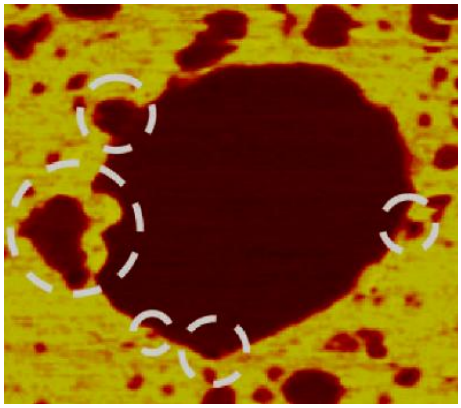

Fig. 2.6. Atomic force micrograph depicting the interfacial erosion in reactively compatibilized BIMSM/PA blend [Bhadane et al. (2008)].

Huitric et al. (2007) investigated the coalescence behavior of reactively compatibilized blends of polyethylene and polyamide systems. Their study showed that the coalescence intensity can not be truly evaluated using conventional criterion (d_n / d_{n_0} or d_v / d_{v_0}) (number and volume average droplet diameters, respectively, normalized by their initial values). This was attributed to the increased collision frequency in the compatibilized blend with finer initial morphology. To obtain a better criterion for coalescence intensity a new parameter was suggested in which the difference in the initial collision frequencies was accounted for.

Sailer and Handge (2008) also reported unexpected rheological and morphological behaviors in reactively compatibilized blends of polyamide 6 (PA6) and a styrene acrylonitrile (SAN) copolymer; It was shown that in the blends with a SAN matrix phase addition of maleic anhydride grafted SAN terpolymer (SANMA) results in the formation of interconnected domains (Fig. 2.7). This was accompanied by low frequency power law behavior of storage and loss modulus in shear oscillation, strain hardening behavior in transient elongation and an enhanced elasticity during recovery. The presence of a local maximum in the variation of loss tangent with frequency showed that the blends feature long range inter particle interactions and behave as materials in the vicinity of the liquid-solid transition. It was concluded that the reactive compatibilization in these blends did not prevent the particle agglomeration but rather delays the coalescence through the formation of cluster like domains.

Deleo and Velankar (2008) also showed that the behavior of reactively compatibilized systems could drastically deviate from the behavior of the blends compatibilized by pre-made copolymers. Their system consisted polydimethylsioxane and polyisoprene (PDMS/PI 70/30) compatibilized either by premade diblocks of PDMS-PI or multifuncational reactive species capable of forming crosslinked compatibilizer at the interface.

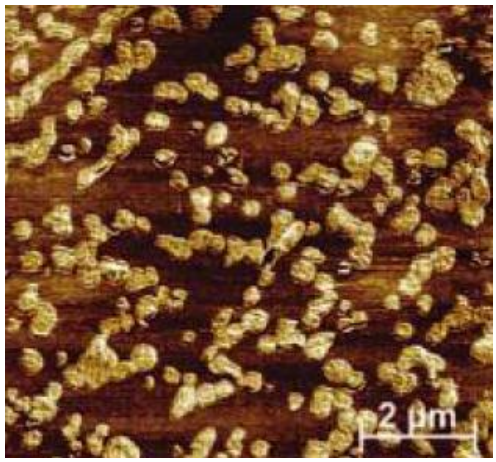

Fig. 2.7. Formation of cluster like morphology in PA6/SAN (30/70) blends compatibilized with 4.8 wt% SANMA compatibilizer [Sailer and Handge (2008)].

While the blend compatibilized by premade copolymer (diblock blend) showed a classical droplet matrix morphology, the formation of crosslinked compatibilizer in the reactive system resulted in an interconnected structure of PDMS inclusions as shown in Fig. 2.8. A similar contrast was also found in the rheological behavior of the two systems; in oscillatory shear measurements the diblock showed a typical liquid like behavior at low frequencies whereas the reactive system featured a gel like behavior with pronounced increase in the elastic moduli; in transient creep experiments the reactive blend showed a high creep recovery at low stresses and large overshoot in the viscosity (not seen in the diblock blend). These behaviors were correlated to the interactions between the clusters of the dispersed PDMS domains. It was concluded that in the reactive system the droplets cluster but do not coalesce due to their crosslinked skin.

It should be noted that compared to premade copolymers, reactive compatibilizers are industrially more important and have been shown to be more efficient in coalescence inhibition. The main advantage of reactive compatibilization is that in this technique the copolymers are formed right at the interface; this issue becomes more important in compatibilization of olefinic systems where the interfacial tensions are generally low and the chance for micelle formation is consequently high.

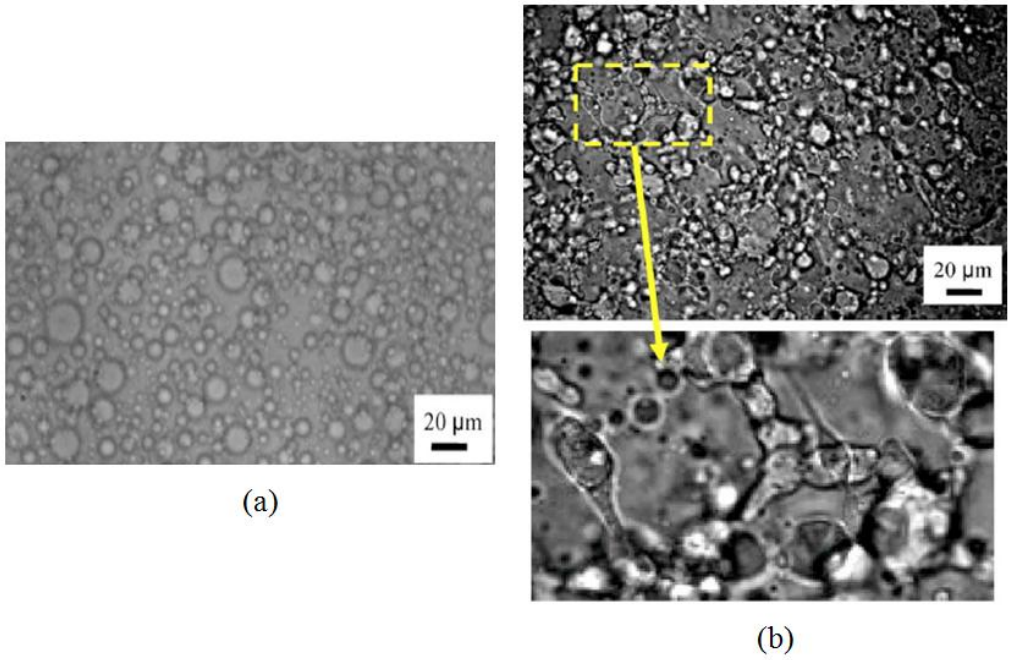

Fig. 2.8. Morphology of compatibilized PDMS/PI (30/70) blends compatibilized by (a) premade copolymers and (b) reactive species [Deleo and Velankar (2008)].

In spite of practical advantages of reactive compatibilization methods over non reactive techniques, the mechanisms of morphology evolution in these systems are often complex and can be hard to understand as discussed in this section. Further studies are still needed to shed light on the rheological and morphological properties of reactively compatibilized polymer blends.

2.2 Rheological models

Studies on the rheology of two phase systems can be tracked back to the work of Einstein (1906) who showed that the viscosity of a dilute suspension of non deformable particles in a Newtonian matrix can be expressed by the matrix viscosity η_m and the volume fraction of the inclusions ϕ:

$$\eta = \eta_m (1 + \frac{5}{2}\phi) \tag{2.11}$$

Later Taylor (1932) extended the Einstein analysis to diluted emulsions of two Newtonian liquids. For small drop deformations (i.e. for relatively spherical drops), Taylor theory predicted the following relationship for the shear viscosity:

$$\eta = \eta_m (1 + \frac{5k+2}{2k+2}\phi) \tag{2.12}$$

in which $k = \frac{\eta_d}{\eta_m}$ the ratio of dispersed to matrix liquid viscosity; in the limit of $k \to \infty$ (very high viscosity drops), Einstein equation is retrieved. It should be noted that in the Taylor analysis the contribution of interfacial tension to the resulting stresses was neglected.

The first rheological model including a parameter for phase relaxation was probably proposed by Frohlich and Sack (1946) who addressed the viscoelastic behavior of diluted emulsions through the following expression:

$$(1 + \tau_1 \frac{d}{dt})\sigma = \eta(1 + \tau_2 \frac{d}{dt})\dot{\gamma} \tag{2.13}$$

wherein:

$$\eta = \eta_m (1 + \frac{5}{2}\phi) \tag{2.14}$$

$$\tau_1 = (\frac{3\eta_m}{2G})(1 + \frac{5}{3}\phi) \tag{2.15}$$

$$\tau_2 = (\frac{3\eta_m}{2G})(1 - \frac{5}{2}\phi) \tag{2.16}$$

σ and $\dot{\gamma}$ are respectively the stress and the rate of deformation tensors and G is the Hookian modulus of the spherical drops. It should be noted however that in this model the predicted elastic behavior of the emulsions was attributed to the elastic recoverable deformation of the spherical drop and not to the interfacial tension.

Following Frohlich and Sack, Oldroyd [(1953); (1955)] proposed his viscoelastic emulsion model in which the contribution of interfacial tension and particle size was accounted for. His constitutive equation for an emulsion of Newtonian monodispersed drops in a Newtonian matrix resulted to the following relation for complex viscosity:

$$\eta^* = \eta_m \left(\frac{1+3\phi H}{1-2\phi H}\right) \tag{2.17}$$

in which :

$$H = \frac{4\alpha / R(2+5k) + i\omega\eta_m (k-1)(16+19k)}{40\alpha / R(1+k) + i\omega\eta_m (3+2k)(16+19k)} \tag{2.18}$$

In the limit of $(\omega \to 0)$ equation (2.17) is reduced to the Taylor relation and for H=1/2 the Einstein equation is retrieved.

The contribution of interfacial tension to the first and second normal stress differences in dilute emulsion was later described by Schowalter et al. (1968) .The constitutive equation of Choi and Schowalter (1975) for semi diluted emulsions of Newtonian fluids resulted in the following expressions for the dynamic moduli:

$$G'(\omega) = \frac{\eta}{\tau_1}\left(1-\frac{\tau_2}{\tau_1}\right)\frac{\omega^2 {\tau_1}^2}{1+\omega^2 {\tau_1}^2} \tag{2.19}$$

$$G''(\omega) = \frac{\eta}{\tau_1}(1-\frac{\tau_2}{\tau_1})\frac{\omega\tau_1}{1+\omega^2\tau_1{}^2} + \omega\eta\frac{\tau_2}{\tau_1} \tag{2.20}$$

in which η, τ_1, τ_2 are the following functions of viscosity ratio *k*, volume fraction ϕ, drop radius *R*, and interfacial tension α:

$$\eta = \eta_m[1+\frac{5k+2}{2k+2}\phi + \frac{5(5k+2)^2}{8(K+1)^2}\phi^2] \tag{2.21}$$

$$\tau_1 = \frac{(19k+16)(2k+3)}{40(k+1)}\frac{\eta_m R}{\alpha}[1+\frac{5(19k+16)}{4(k+1)(2k+3)}\phi] \tag{2.22}$$

$$\tau_2 = \frac{(19k+16)(2k+3)}{40(k+1)}\frac{\eta_m R}{\alpha}[1+\frac{3(19k+16)}{4(k+1)(2k+3)}\phi] \tag{2.23}$$

In order to estimate the dynamic moduli of emulsions of two viscoelastic fluid, the above set of equations can be used in conjunction to the following relation [Gramespacher and Meissner (1992)]:

$$G^* = G^*_{\text{components}} + G^*_{\text{interface}} \tag{2.24}$$

wherein $G^*_{\mathbf{components}}$ is determined based on the complex moduli of the neat components and using a linear mixture rule; $G^*_{\mathbf{interface}}$ is the contribution of the interface to the complex moduli and is calculated by equations (2.19), (2.20) .

Analogous to an electric formalism Palierne (1990) provided a detailed derivation in which the viscoelastic behavior of an emulsion of two viscoelastic incompressible fluids was described by considering interfacial tension, size distribution of the particles and hydrodynamic interactions.

In a general form Palierne model describes the complex modulus as:

$$G_b^*(\omega) = G_m^*(\omega)\frac{1+3\phi\dfrac{E(\omega,R_v)}{D(\omega,R_v)}}{1-2\phi\dfrac{E(\omega,R_v)}{D(\omega,R_v)}} \tag{2.25}$$

where

$$\begin{aligned} E(\omega,R_v) = {} & [G_d^*(\omega)-G_m^*(\omega)][19G_d^*(\omega)+16G_m^*(\omega)]+4\frac{\alpha}{R_v}[5G_d^*(\omega)+2G_m^*(\omega)] \\ & +\frac{\beta'(\omega)}{R_v}[24\frac{\alpha}{R_v}+23G_d^*(\omega)-16G_m^*]+\frac{2\beta''(\omega)}{R_v}[13G_d^*(\omega)+8G_m^*(\omega)] \\ & +24\beta'(\omega)\frac{\alpha}{R_v^2}+16\beta''(\omega)\frac{\alpha+\beta'(\omega)}{R_v} \end{aligned} \tag{2.26}$$

and,

$$\begin{aligned} D(\omega,R_v) = {} & [2G_d^*(\omega)+3G_m^*(\omega)][19G_d^*(\omega)+16G_m^*(\omega)]+40\frac{\alpha}{R_v}[G_d^*(\omega)+G_m^*(\omega)] \\ & +\frac{2\beta'(\omega)}{R_v}[23G_d^*(\omega)+32G_m^*(\omega)]+\frac{4\beta''(\omega)}{R_v}[13G_d^*(\omega)+12G_m^*(\omega)]) \\ & +48\beta'(\omega)\frac{\alpha}{R_v^2}+32\beta''(\omega)\frac{\alpha+\beta'(\omega)}{R_v^2} \end{aligned} \tag{2.27}$$

in which ϕ is the volume fraction of the dispersed phase, R_v is the volume averaged droplet radius and G_d^*, G_m^* are the complex moduli of the dispersed and matrix phases, respectively.

The parameters β' and β'' are the interfacial dilatational and shear modulus and account for the variation of the interfacial tension with interfacial area and the interfacial tension non uniformity. It can be easily shown that in Eq. (2.26) and (2.27) the role of these two parameters can be easily exchanged and hence, to avoid ambiguity in the analysis, one of these parameters is set equal to zero [Jacob et al. (1999)]. It has been shown that for the case of non compatibilized blends or compatibilized systems with fully saturated interface for which the assumption of interfacial tension isotropy is valid both parameters can be set to zero [Riemann *et al.* (1997); Van Hemelrijck (2004); Yee (2007)]. It is worth noting that the Palierne model is adequate in describing the viscoelastic behavior of polymer blends [Vinckier et al. (1996); Lacroix et al. (1998); Xing et al. (2000); Peon et al. (2003)]. It should be noted however that the model is only valid for small deformation ranges and for blends with spherical drop morphology.

To describe the viscoelastic behavior of emulsions in large deformations, Doi and Ohta (1991) proposed a semi-phenomenological model in which the time evolution of the interface was determined by the following relation:

$$\frac{dq_{ij}}{dt} = \frac{dq_{ij}}{dt}\Big|_{flow} + \frac{dq_{ij}}{dt}\Big|_{interfacial\ tension} \tag{2.28}$$

$$\frac{dQ}{dt} = \frac{dQ}{dt}\Big|_{flow} + \frac{dQ}{dt}\Big|_{interfacial\ tension} \tag{2.29}$$

wherein q_{ij} are the components of the anisotropy tensor and Q is the specific interfacial area defined as below:

$$Q = \frac{1}{V}\int dS \tag{2.30}$$

$$q_{ij} = \frac{1}{V}\int dS(e_i e_j - \frac{1}{3}\delta_{ij}) \tag{2.31}$$

in the above equations e_i is the unit vector normal to the interface, δ_{ij} is the Kronecker delta, V is the total system volume and the integrals are over the entire area of the interface S. In equations (2.27) and (2.28) the first term denotes the contribution of the macroscopic flow which enlarges and orients the interface and the second term represents the contribution of interfacial tension which favors the relaxation of the deformed interface. In the Doi and Ohta formalism the contribution of the interface in the morphology evolution was described through a set of first order kinetic equations wherein only the shape relaxation and coalescence processes was explicitly formulated. The stress tensor of their model was expressed using the following formulation proposed for a 50/50 mixture of two Newtonian components with equal viscosities [Batchelor (1970); Doi (1987); Onuki (1987)]:

$$\sigma_{ij} = \eta_m(\kappa_{ij} + \kappa_{ji}) - \alpha q_{ij} - P\delta_{ij} \tag{2.32}$$

in which κ_{ij} are the components of the velocity gradient tensor and P is the isotropic pressure.

Based on the Doi and Ohta theory, Lee and Park (1994) proposed another phenomenological model in which the mismatch in the viscosities of the components was accounted for; the model consisted of three different relaxation mechanisms: shape relaxation, size relaxation (coalescence) and breakup (Fig. 2.9).

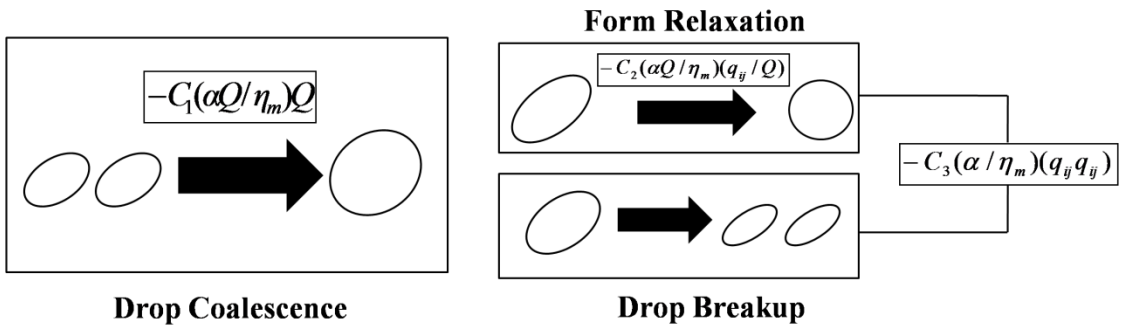

Fig. 2.9. Illustration of different relaxation mechanisms and the corresponding rate equations involved in the Lee and Park model (1994)

Accordingly the time evolution of the interface due to the relaxation mechanisms was expressed by:

$$\frac{d}{dt}\left(\frac{q_{ij}}{Q}\right)\Big|_{\text{relaxation}} = -c_2\frac{\alpha Q}{\eta_m}\left(\frac{q_{ij}}{Q}\right) \tag{2.33}$$

$$\frac{d}{dt}Q\Big|_{\text{relaxation}} = -c_1\frac{\alpha}{\eta_m}Q^2 - c_3\frac{\alpha}{\eta_m}q_{ij}q_{ij} \tag{2.34}$$

in which c_1, c_2 and c_3 are dimensionless rate equation coefficients; Eq. (2.32) , (2.33) combined with the contribution of the macroscopic flow to the deformation of the interface resulted in the following set of equations describing the transient morphological state:

$$\frac{dq_{ij}}{dt} = -q_{ik}\kappa_{kj} - q_{jk}\kappa_{ki} + \frac{2}{3}\delta_{ij}\kappa_{lm}q_{lm} - \frac{Q}{3}(\kappa_{ij}+\kappa_{ji}) + \left(\frac{q_{lm}d_{lm}}{Q}\right)q_{ij} - d_1\frac{\alpha}{\eta_m}Qq_{ij}$$
$$- d_1d_3\frac{\alpha}{\eta_m}\left(\frac{q_{lm}q_{lm}}{Q}\right)q_{ij} \tag{2.35}$$

$$\frac{dQ}{dt} = -\kappa_{ij}q_{ij} - d_1d_2\frac{\alpha}{\eta_m}Q^2 - d_1d_3\frac{\alpha}{\eta_m}q_{ij}q_{ij} \tag{2.36}$$

wherein $d_1 = c_1 + c_2$, $d_2 = c_1/(c_1 + c_2)$ and $d_3 = c_3/(c_1 + c_2)$ represent the degree of total relaxation, degree of size relaxation and the degree of shape relaxation and breakup respectively. Eventually the time evolution of the stress tensor can be determined by simultaneous solution of Eq. (2.34) and (2.35) and the following constitutive equation:

$$\sigma_{ij} = [1 + \frac{6(\eta_i - \eta_m)}{10(\eta_m + \eta_i)}\phi]\eta_d \dot{\gamma} - \alpha q_{ij} - P\delta_{ij} \tag{2.37}$$

It was shown by Lacroix et al. (1997) that the first term of equation (2.36) (i.e. the viscosity ratio term) can be alternatively replaced with another expression to obtain a better description of the experimental data:

$$\sigma_{ij} = [\frac{1 + \frac{3}{2}H}{1 - H}]\eta_m \dot{\gamma}_{ij} - \alpha q_{ij} - P\delta_{ij} \tag{2.38}$$

$$H = \phi \frac{2(\eta_d - \eta_m)}{2\eta_d + 3\eta_m} \tag{2.39}$$

It should be noted however that in the Lee and Park theory interfacial deformations are assumed to be affine. Using a thermodynamic approach proposed by Grmela and Ait Kadi (1994) and considering the same relaxation mechanisms as the Lee and Park model (1994), Lacroix et al. (1999) derived a new phenomenological formalism describing the time evolution of the interface. In their proposed model non affine deformation was accounted for through using an additional slip parameter.

We recall that the capability of different viscoelastic models described in this section has been evaluated in several experimental studies concerning rheological behavior of non compatibilized and compatibilized polymer blends [Vinckier et al. (1996); Guenther et al. (1996); Lacroix et al. (1998); Hemelrijck et al. (2004); Huo et al. (2007)]; however viscoelastic behavior of reactively

compatibilized systems has been the subject of only a small portion of these studies. Investigating a reactively compatibilized blend of polypropylene and polyamide, Asthana and Jayaraman (1999) found that the low frequency plateau of storage moludus can be described by considering an additional relaxation mechanism attributed to the product of the interfacial reaction. Huitric et al. (2007) showed that the morphology evolution of reactively modified blends of polyethylene and polyamide can be described using the modified version of Lee and Park model proposed by Lacroix (1999); however the model only showed qualitative agreement with the stress growth viscosity data. Capability of fractional derivative constitutive equations in predicting the viscoelastic behavior of reactively compatibilized systems was recently evaluated by Sailer and Handge [(2007); (2008)] for an interfacially modified blend of polyamide-6 and styrene-acrylonitrile copolymer; while Palierne model failed at predicting the low frequency behavior, a simplified version of the fractional Zener model showed a good agreement with the experimental data over the whole frequency range. The details of these studies and the models employed will be discussed in Chapter 6 where viscoelastic properties of reactively compatibilized blends of thermoplastic olefins are investigated.

2.3 Foaming behavior of polymer blends

Foaming behavior of polymeric foams in general is determined by the cell nucleation and cell growth phenomena. These phenomena are in turn controlled by various parameters such as viscoelastic properties, surface tensions, gas solubility and diffusivity etc. On the other hand polymer blending is an effective technique to achieve materials featuring controlled and selective properties. As such foaming polymer blends can be considered as a persuasive approach in producing high performance polymeric foams with controlled cellular structures. Not only the cellular structure of polymeric foams can be controlled via a proper choice of the neat

constituents but it can be also tuned by varying the morphological properties of the unfoamed blends. This section provides a summary about different aspects concerning cell nucleation and cell growth phenomena in polymer blends.

2.2.1 Nucleation

2.2.1.1 Classical Mechanism of Heterogeneous Nucleation

For the nucleation rate in a homogeneous system Volmer and Weber (1926) proposed the following expression:

$$J \propto \exp\left(\frac{-\Delta G_n^{*}}{kT}\right) \tag{2.40}$$

wherein ΔG_n^{*} is the change in the Gibbs free energy of the system at the critical bubble radius (or the activation free energy for cell nucleation), k is the Boltzmann constant and T is the temperature. In a heterogeneous system the presence of interface changes the activation energy required to achieve a stable nucleolus, so that the second phase can act as a catalyst for nucleation. The thermodynamic energy required for cell nucleation at the interface of a spherical particle can be expressed as [Fletcher (1958); Blander and Katz (1975)] :

$$\Delta G^{*} = \frac{16\pi\alpha_{\lg}^{3}F}{3(P^{*}-P_{sys})^{2}} \tag{2.41}$$

in which $\alpha_{\lg}$ is the gas-liquid interfacial tension, F is a geometrical factor determined by the contact angle at the solid-gas interface as well as the particle radius and the critical radius for cell nucleation, P^{*} is the internal gas pressure of the nucleated bubble with the critical radius and P_{sys} is the pressure inside the gas-liquid solution. It can be estimated that for a wetting angle of 20°,

ΔG^* can be reduced by a factor of 10^{-3} which can have a significant impact on the nucleation rate [Colton and Suh (1987)]. Fig. 2.8 shows a schematic of the function of the second phase in a heterogeneous nucleation.

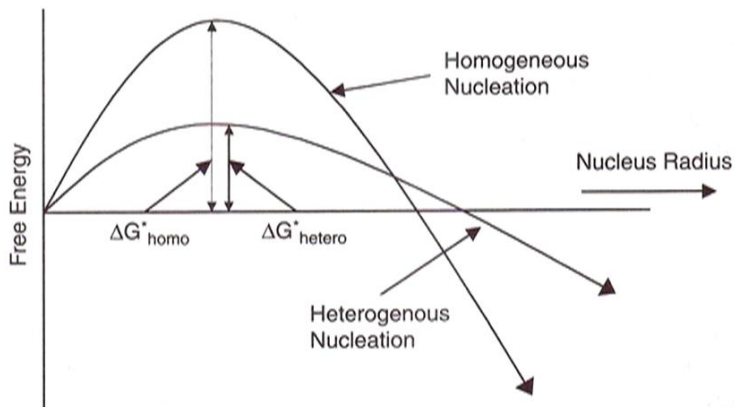

Fig. 2.10. Heterogeneous bubble nucleation $\Delta G^*_{hetero} < \Delta G^*_{homo}$ [Lee et al. (2004)].

Park et al. (2006) showed that a small amount of polystyrene can induce heterogeneous cell-nucleating spots in low density polypropylene (LDPE). While only a small amount of cell nuclei could be obtained for pure LDPE because of high activation energy for nucleation, microcellular foams was produced using LDPE/PS blends. It was shown that by adding 5% PS cell density increased significantly while at higher composition the cell densities were hardly changed. It is believed that the coalescence of initial nuclei is responsible for the trend observed at higher PS content.

Smith et al. (1998) have also reported a significant reduction in foam density in a polystyrene/acrylic polymer system where addition of 10wt% acrylic polymer resulted in foam with densities 18% lower than that of the neat polystyrene foams.

Tejeda et al. (2005) prepared foams of PP/LDPE by extrusion using Azodicarbonamide as the chemical blowing agent. They showed that the foams made of PP/LDPE blend had average cell

sizes between 130 and 300 μm and varied with the blend composition; the minimum cell size was achieved at the 50/50 composition. It was believed that the presence of the second phase acted as a nucleating site and gave foams of smaller cell sizes. Similar observation has been reported by Sahagun et al. (2006) in a PP/HDPE system. Varying composition of the blends, they found that the dispersed phase content increased the nucleation density and the maximum nucleation density was reported for 50/50 system. They concluded that the interaction of the dispersed phase, locally modified the foamability by creating path of least resistance to cell formation and growth and consequently the number of cell increased while the smaller cell sizes were achieved.

More recently Kim et al (2011) investigated the heterogeneous nucleation effect of rubbery particles TPO blends consisting of polypropylene and ethylene octene copolymers. It was found that there is an optimal domain size at which the cell density of the TPO foams became maximum; increasing the domain size beyond this optimal value reduced the particle density hence the number of active sites for cell nucleation. The rubbery particles with a cell size less than the optimal value was found to be inefficient in cell nucleation. This behavior was found to be in agreement with the prediction of heterogeneous nucleation theory.

2.2.1.1 Microvoid Nucleation Mechanism

Microvoid nucleation mechanism was firstly proposed by Ramesh and coworkers [Ramesh et al. (1994a); Ramesh et al. (1994b)]. Their model considered the presence of the micro cavities formed during cooling of the extruded blends. The blend investigated in their study consisted of polystyrene (PS) as the thermoplastic matrix and polybutadiene (PB) as the rubbery dispersed phase. The formation of cavities during cooling was attributed to the marked

difference of the glass transition temperature of the blend components. As the blend cooled down polystyrene

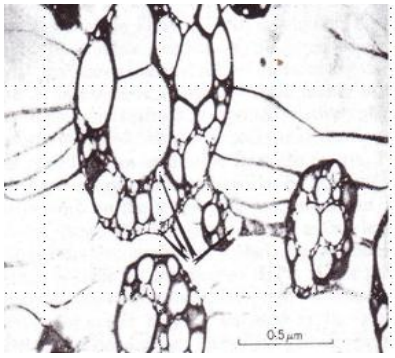

Fig. 2.11. Transmission electron micrograph (TEM) showing the presence of microvoids in PS/PB blend [Keskkula et al. (1986)].

went into the glassy state whereas the rubbery phase was still above the glass transition temperature. This resulted in a threefold difference in the coefficient of thermal expansion; Polystyrene shrank much slower than the rubbery phase and a triaxial tension was created in the rubbery particles. The resulting stresses created the microvoids [Keskkula et al. (1986)], which could later act as nucleating sites (Fig. 2.9).

Compared to the neat polystyrene the nucleated sample yielded foams of much finer cell sizes and with several order of magnitude increases in the cell density (Fig. 2.10). It was also shown that the cell density varied much the same as the rubber particle density and the morphology of the rubbery particles and bubbles showed a similar log-normal size distributions. It was also found that there is a critical size below which the cavities fail at nucleating a bubble embryo. This was attributed to the fact that the very small voids could not survive against the elastic forces resisting the bubble growth hence became inefficient in cell nucleation. It should

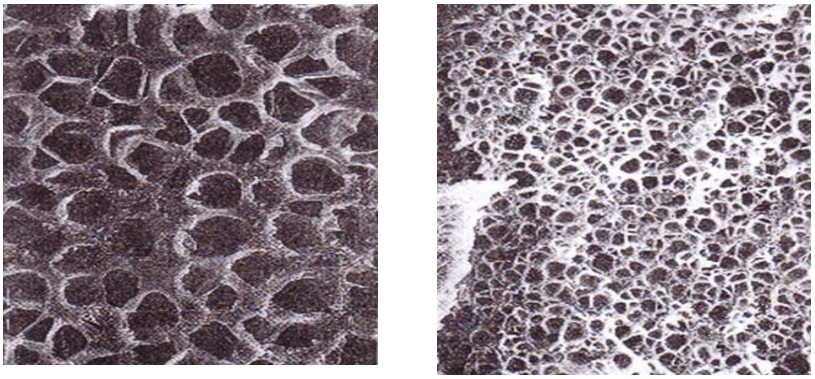

(a) (b)

Fig. 2.12. Scanning electron micrograph of styrenic foams a) polystyrene b) nucleated polystyrene [Ramesh et al. (1994a)]

be noted that this mechanism is mainly proposed for cell nucleation in solid state batch (autoclave) foaming processes where the microvoids are present in the unfoamed sample prior to gas loading and may not be valid for nucleation phenomenon in molten polymer blends.

2.2.2 Growth

The kinematic of cell growth in a polymeric media is determined by the hydrodynamic and interfacial forces on the surface of the growing bubble as well as the diffusion rate of the gas molecules available in the surrounding media; it is therefore expected that the bubble growth in a polymer blend can be strongly controlled by the rheological properties of the surrounding polymers as well as the microstructure and respective positions of different phases involved in the system. Given that the information concerning these issues is quite limited in the literature, bubble growth in polymer blend is still an unclear phenomenon. It has been shown by a number of studies that polymer blending can strongly improve the cellular morphology through the modification of melt rheological properties. A common example of this approach is the addition of branched polypropylene to its linear counterpart [Van Nuffel et al. (1998); Spitael et al.

(2004); Stange et al. (2006)]. Stange et al. (2006) showed that even the addition of low amount (as low as 2%) of a branched polypropylene can significantly improve the foamability of polypropylene blown with Azodicarbonamide as a chemical blowing agent. This improvement can be attributed to the pronounced strain hardening behavior of the blends containing branched polypropylene. During bubble growth cell walls experience extensional stresses; the enhanced elongational viscosity in these blends reduces sag, prevents cell coalescence and consequently promotes the final cellular morphology.

A number of recent studies have been recently devoted at controlling the bubble growth through selective localization of the initial nuclei in the dispersed domains. The main concept of all these studies is based on the significant distinctions in viscoelasticity and solubility of the blend components, which confine the bubble growth in the dispersed inclusions and suppresses bubble coalescence. Otsuka et al. (2008) reported the formation of a nanocellular structure in a blend of polystyrene (PS) and polymethylemthacyrylate (PMMA). The unfoamed blends in their study contained nanosized PMMA domains formed during polymerization of MMA monomers in the polystyrene matrix. The selective localization of the bubbles in the PMMA phase was attributed to the difference in the glass transition temperature of PMMA and PS phases, which resulted in different levels of viscoelasticity. Applying a same approach, Nemoto and Ohshima (2008) showed that in a blend of polypropylene (PP) and polypropylene-ethylene copolymer rubber (PER) the bubble size and location can be highly controlled in the dispersed rubbery domains. Foaming was conducted in batch setup and at 20°C. In this system the crystallinity of the PP phase was found to be responsible for the localization of cell nucleation and growth inside the rubbery domains. To clarify that the bubbles were formed in the dispersed rubbery particles, the initial morphology of the particles was changed by uniaxial extension of the extruded blend

(unfoamed) at the die exit. The elongated sample was cooled down and subsequently foamed at 20°C. The presence of elongated bubbles (Fig. 2.13) in the foamed sample showed that the cellular structure was mainly controlled by the initial morphology of the PER domains.

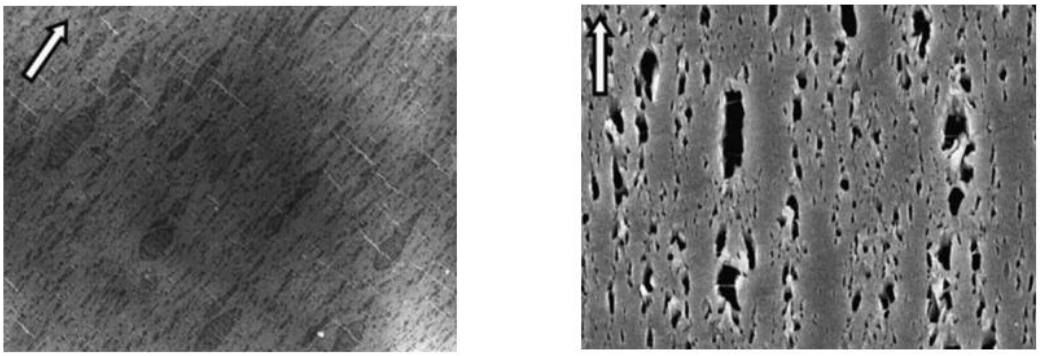

(a) (b)

Fig. 2.13. Micrographs of (a) unfoamed) and (b) foamed PP/PER (50/50) blends. The dark phases represent the PER inclusions and bubbles in the unfoamed and foamed samples respectively.

Similar observations were also reported by [Nemoto et al. (2010); Ruckdäschel (2010)]. It should be noted that in these studies the final positions of different phases could not be determined by direct microscopic observations. All these results, however, suggest that the foaming behavior of polymer blends can be delicately controlled by the blends rheological and morphological properties.

2.4. Summary

Due to the important role of the blend microstructure in controlling the final properties, morphology evolution in immiscible polymer blends has been extensively studied. Several

aspects concerning drop breakup and coalescence have been explored and different techniques have been proposed for coalescence suppression through interfacial modification. It was shown that rheological methods can be considered as unique tools to study the morphology evolution in polymer blends mainly because of the prominent advantage of rheological device in providing controlled flow conditions. While because of limitations in direct visualization techniques flow induced morphological behaviors and more specifically dynamic coalescence have been poorly understood, relating the blend microstructure to the rheological properties can be considered as an encouraging approach. In this view the capability of rheological models in predicting viscoelastic behavior of polymer blends is crucial. This issue becomes more problematic in the case of reactively compatibilized systems for which the binary emulsion models often fail in predicting the viscoelastic behavior. This is mainly due to the presence of newly formed interfacial species as well as formation of complex morphologies in these systems.

Polymer blending can be considered as an efficient technique to achieve foams with controlled cellular structure. Depending on the phase morphology behavior and rheological and thermodynamic properties of the neat constituents, blending can render a variety of materials with different foamabilities. Several studies have proven that the dispersed phase can act as nucleating sites during foaming of polymer blends. It has been also shown that the cell coalescence can be controlled by confining the cell growth inside the dispersed phase. In this regard the microstructure of polymer blends can play a crucial role in determining the cellular morphology. In the literature concerning foaming of polymer blends this point has been addressed rather by varying the blend morphology via changing the viscosity ratio or phase concentration; although these approaches provide different phase morphologies, they are accompanied by changes which are not related to the morphological states of the blends only. In

addition the respective positions of different phases could not be directly determined. These issues will be considered in this study; a reactive compatibilization technique will be employed and its impact on the rheological and morphological properties and consequently on the final cellular structure will be investigated.

CHAPTER 3
OBJECTIVES

In view of the industrial importance of thermoplastic olefin blends and the environmental and economic needs for high performance light weight materials, and due to the lack of literature data on the foaming behavior of polymer blends and its dependency to the blend microstructure and rheological properties, the main objective of this study is:

"***To improve the foaming behavior of thermoplastic olefin blends via controlling the morphological and rheological properties"***

To meet this objective a particular attention is paid to phase coalescence phenomenon which is of crucial importance in controlling the morphology development and rheological properties of polymer blends. The coalescence behavior of the TPOs is investigated using a rheological method through which the coalescence intensity can be evaluated in a controlled homogeneous shear flow field.

In addition the extent of coalescence is controlled by means of a reactive compatibilization practice. The microstructure of the compatibilized TPOs is analyzed in the light of dynamic and transient rheological measurements and morphological data. The ability of different viscoelastic models in describing rheology-morphology interrelationships is also evaluated.

Finally, the role of reactive compatibilization in controlling the foaming behavior of the TPOs is investigated. Also the influence of the initial microstructure of the non compatibilized unfoamed TPOs on the final cellular morphology is examined. The role of the dispersed elastomeric domains as nucleating sites for cell formation is investigated in the light of

microscopic observations. The influence of melt viscolastic properties on the foaming behavior of the TPOs is examined via rheological measurements in shear and elongation.

CHAPTER 4
ORGANIZATION OF THE ARTICLES

The following three chapters contain the articles representing the results of this study:

The first article presented in chapter 4 is entitled "*Coalescence in Thermoplastic Olefin (TPO) Blends under Shear Flow*". This work investigates the coalescence behavior of thermoplastic olefin blends based on polypropylene and three types of ethylene octene copolymers with different viscosities. The capability of transient rheological models in predicting the extent of phase coalescence induced by gentle shearing is evaluated. The viscoelastic behavior and morphological properties of the blends with different concentrations are characterized using dynamic and transient rheological measurements and scanning electron microscopy. This article has been published in *Rheologica Acta* (Volume 50, Issue 11 (2011), Pages 881-895).

The second article presented in chapter 5 is entitled *"Rheological and Morphological Properties of Reactively Compatibilized Thermoplastic Olefin (TPO) Blends".* In this work thermoplastic olefin blends of polypropylene and ethylene octene copolymer compatibilized using a reactive melt blending practice are investigated. The microstructure of the blends is studied in the light of rheological and morphological measurements. Dynamic and transient rheological behavior of the blends is correlated to the morphological data obtained via atomic force microscopy. This article has been published in the *Journal of Rheology* (Volume 56, Issue 3 (2012), Pages 625-647).

.

The third article presented in chapter 6 is entitled *"Foaming Behavior of Microcellular Thermoplastic Olefin Blends (TPO)"*. In this article the influence of reactive compatibilization on the final cellular morphology of TPO foams produced via different batch foaming processes is investigated. The dependency of the cellular morphology to the unfoamed blends microstructure is also studied by altering the initial morphology of the TPOs via static and dynamic coalescence. Dynamic shear measurements and stress growth shear and elongational experiments are performed to characterize the viscoelastic properties of the TPOs. Morphology of different TPOs and the resulting foams are characterized using a microscopic method based on back scattering electron imaging technique. This article has been submitted to the *Journal of Cellular Plastics*.

CHAPTER 5

Coalescence in Thermoplastic Olefin (TPO) Blends under Shear Flow

Amirhossein Maani, Marie-Claude Heuzey, Pierre J. Carreau

Center for Applied Research on Polymers and Composites, CREPEC

Department of Chemical Engineering, École Polytechnique de Montréal

PO Box 6079, Stn Centre-ville, Montreal, QC, Canada H3C3A7

Parts of this work have been presented at the

81st annual meeting of the Society of Rheology (October 2009) and

6th Annual European Rheology Conference (April 2010).

Published in *Rheologica Acta* (Volume 50, Issue 11 (2011), Pages 881-895).

.

Abstract

In this article the capability of the Lee-Park (LP) model (Lee and Park 1994) in predicting the extent of drop coalescence under transient shear has been evaluated. Thermoplastic olefin blends of polypropylene (PP) and three types of metallocene catalyzed ethylene copolymers (EC) with different melt viscosities were investigated. The interfacial tension between the PP and the ECs was determined by means of linear viscoelastic measurements using a simplified version of the Palierne (1990) model as well as the Choi and Schowalter (1975) equation. Flow induced coalescence was investigated by shearing the samples at a very low shear rate of 0.01 s^{-1}. The size evolution and orientation of the dispersed droplets under shear were correlated with the transient rheological data. To account for the non-affine deformation an additional slip parameter (Lacroix et al. 1999) was introduced into the LP model. The modified model (LPL model) was found to predict well the morphological state of all blends in conjunction with the rheological data, whereas in most of the cases, the LP model significantly underestimated the interfacial area (Q). Coalescence was favored by a decrease of the viscosity of the dispersed phase. Smaller viscosity droplets increased the interfacial mobility and, hence, reduced the drainage time promoting the coalescence of two approaching droplets.

Keywords: thermoplastic olefin blends, morphology evolution, shear induced coalescence, transient rheological models

Introduction

With the development of metallocene catalysts technology, a new generation of ethylene α-olefin copolymers with fairly controlled co-monomer compositions and narrow distributions of molecular weight have been commercially produced. These copolymers feature a wide range of elastomeric characteristics and unique rheological properties depending on the type and level content of co-monomer incorporated in their structure (Kim et al. 1996; Bensason et al. 1997; Bin Wadud and Baird 2000; Doerpinghaus and Baird 2003; Patham and Jayaraman 2005). Due to the higher toughening contribution and better processability than other traditional ethylene copolymers, these elastomers are increasingly used as impact modifiers in thermoplastic olefin (TPO) compounding (Nitta et al. 1998; Yu 2001; McNally et al. 2002; Kontopoulou et al. 2003).

As for other types of immiscible polymer blends, the properties of TPOs are crucially dependent on the microstructure of the dispersed phase formed during compounding (Jancar et al. 1993; Yokoyama and Ricco 1998; Van Der Wal et al. 1999; Jiang et al. 2000). The final morphology is determined by the competition between the break-up and coalescence phenomena, which are highly dependent on the type of flow and intensity of the applied stresses during mixing. Since all of the mixing devices generate a complex shear and elongational flow field, the separation of the flow types using rheological devices provides an opportunity for a refined investigation on the flow-induced morphology. Although a large number of studies have been devoted to understand rheology/morphology interrelationships (Guenther and Baird 1996; Minale et al. 1997; Lacroix et al. 1998; Martin et al. 2000; Yu et al. 2005; Schnell et al. 2008), several aspects of breakup and coalescence phenomena still remain to be clarified. As we shall see in the next section, the coalescence process in molten polymer blends is still not well understood, due to its complex nature. The aim of this study is to shed light on the coalescence and break-up behavior

of molten thermoplastic olefin blends under shear flow. The influence of the melt viscosity and concentration of the dispersed phase is investigated, and the results are interpreted using phenomenological models.

Background

The simplest illustration of the flow-induced coalescence of two droplets in a continuous phase can be depicted in three steps. In the first step, droplets widely separated are brought together due to the velocity gradient imposed by the external flow; in the second step, as the separation of the droplets becomes comparable with the droplet radius, the fluid between the approaching particles experiences a squeezing flow (film drainage). In this step, the magnitude of the force due to the external flow as well as the hydrodynamic interactions between the colliding particles controls the film thinning rate. In the third step, when the particle distance becomes comparable with the range of the non-hydrodynamic attractive forces, an instantaneous destabilization in the thinning fluid results in the film rupture and confluence. The first description of flow-induced coalescence was drawn by Smoluchowski (1917). Neglecting all particle-particle interactions and assuming that the colliding particles follow a straight line to the point of contact, he estimated the rate of coagulation in simple shear flow. Further investigations, however, showed that the colliding trajectory may significantly deviate from the straight line due to hydrodynamic interactions between rigid particles (Batchelor and Green 1972) or viscous drops (Wang et al. 1994). Hydrodynamic interactions, moreover, may result in the partial flattening of deformable drops if the hydrodynamic pressure in the thinning film becomes comparable to the capillary pressure at the droplet surface, $O(2\alpha/R)$ where α is the interfacial tension and R is the drop radius (Yiantsios and Davis 1990; Chesters 1991). All these interactions should be considered for the majority of liquid-liquid dispersions when the interface is treated as “partially mobile”. The

important characteristic of partially mobile interfaces is in fact the coupling between the flow in the thinning film and the internal circulating flow inside the droplets. In the case of Newtonian droplets in a Newtonian matrix, scaling concepts were considered by Davis et al. (1989) and Chesters (1991) to analyze the flow in the thinning film. The velocity profile in the film is decomposed into two parts: $u = u_p + u_t$, where u_t is the uniform part of the film velocity corresponding to the velocity at the drop interface and u_p is the pressure driven parabolic portion of the film velocity. The following relation between the velocity components can be deduced under the assumption that the tangential stress is continuous across the partially mobile interface:

$$\frac{u_p}{u_t} \approx k(\frac{h}{a}) \tag{5.1}$$

in which k is the ratio of the dispersed to the continuous phase viscosity, h is the film thickness and a is the lateral extent of the film. This relation implies that a larger viscosity ratio increases the contribution of the pressure driven velocity and, hence, increases the hydrodynamic force resisting the relative motion of the droplets. Indeed, coalescence will never occur between rigid particles ($k \to \infty$), whereas mobile droplets can collide even in the absence of attractive interfacial forces (Davis et al. 1989). By means of a scaling theory, Yang et al. (2001) showed that the drainage time in the collision of two equal size drops is approximately proportional to the viscosity ratio. The experimental study of Yoon et al. (2005), however, suggests that the drainage time scales with $k^{0.8}$. Information on the influence of the viscosity ratio on coalescence in concentrated molten polymer blends is quite scarce. For molten immiscible blends, the phenomenological coalescence parameters such as drainage time (t_d) or critical film thickness

(h_c) at the point of rupture can be hardly evaluated. The difficulty arises in the direct visualization and positioning of colliding molten droplets. It has also been shown that indirect calculations of t_d or h_c using classical coalescence models only result in an order of magnitude estimation. Unsatisfactory predictions were encountered at high concentration of the dispersed phase by Minale et al. (1998) and by Vinckier et al. (1998). This ambiguity was also shown in the studies of Lyu et al. (2000) and Lyu et al. (2002) where the Smoluchowski theory and different types of trajectory models were used to evaluate the coalescence efficiency. The coalescence efficiency in their study was expressed by means of an adjustable coalescence rate parameter for fitting experimental data, and it was demonstrated that the variation of this parameter with the viscosity ratio (k) was not monotonic. It should be noted that in trajectory theories only binary interactions between spherical particles are considered, whereas in concentrated or semi-concentrated systems, where the inter-particle distances are comparable to the drop radii, multiple interactions may occur. Quantifying coalescence efficiency is still a complex matter. Huitric et al. (2007) showed that in some cases the commonly used criterion (d_n / d_{n_0} or d_v / d_{v_0}) (number and volume average droplet diameters, respectively, normalized by their initial values) failed to evaluate the coalescence intensity. For example d_n / d_{n_0} in compatibilized blends was found to be larger than in non-compatibilized system. Indeed the larger collision frequency in the compatibilized blends with finer drops causes d_n / d_{n_0} or d_v / d_{v_0} to increase faster with time, which obviously does not mean that coalescence is facilitated by compatibilization.

In the present study, the capability of the phenomenological model of Lee and Park (1994) and the modified version of Lacroix et al. (1999) to describe the coalescence intensity is evaluated. It

should be noted that due to the very low shear rate used in this study (0.01 s^{-1}), the viscoelastic effects due to the respective properties of the components are expected to be negligible (Park et al. 2003; Guidoa et al. 2003).

Experimental

A. Materials and Sample Preparation

The main characteristics of the polymers used in this study are given in Table 5.1. The TPOs consist of a polypropylene homopolymer (Pro-fax 6523, Basell Polyolefins) as the matrix, while three types of metallocene catalyzed ethylene octene copolymers (Engage Polyolefin Elastomers, Dow Chemical Company) were used as the elastomeric dispersed phase. As shown in Table 5.1, the composition of the ethylene copolymers (ECs) is relatively similar, while their melt flow indices vary significantly (note that the numbers used in the nomenclature are chosen to reflect the melt flow index of the polymers).

Table 5.1 Main characteristics of the neat materials.

Material	M.F.I.(g/10min)	T_m(°C)	η_0 (Pa.s) at 200 (°C)	Octene Content(wt%)
PP	4 (230°C-2.16 kg)	162	6300	-------
EC1	1 (190°C-2.16 kg)	60	7300	38
EC5	5 (230°C-2.16 kg)	60	1400	38
EC30	30 (230°C-2.16 kg)	60	200	40

Blending was performed using a Brabender internal mixer (C.W. Brabender Instruments Inc., Model DDRV501) at a set temperature of 215 °C and with a rotor speed of 50 rpm. TPOs with

compositions of 85/15, 80/20, 75/25, 70/30 w/w PP/EC were investigated. Mixing was carried out for 12 min under a nitrogen atmosphere to prevent degradation. After mixing, samples were extracted from the blades and quenched in liquid nitrogen. For rheological measurements small disks of 25 mm diameter were prepared using a compression molding press at 200 ^{o}C and under a nitrogen atmosphere. Samples were first melted for 8 min and then the pressure load was progressively increased up to 3 tons. The same blending and molding procedures were also applied to the neat materials so that the thermo-mechanical history of the blends and the neat components were the same.

B. Rheological/Morphological Measurements

All the rheological measurements were conducted on a rotational rheometer (Paar Physica MCR-501) with a cone and plate flow geometry of 25 mm diameter and 0.02 rad cone. The maximum ratio of droplet number average diameter to gap size (after shear-induced phase coarsening) was found to be less than 0.15. All measurements were performed under a nitrogen atmosphere at 200 ^{o}C. The neat polypropylene was found to be stable for a period of over one hour. Hence, thermal degradation was assumed to be negligible during the rheological measurements for the blends. Dynamic measurements were carried out in a frequency range of 0.01-100 rad/s and at maximum strain amplitude of 5%, which was found to be in the linear viscoelastic region. Time sweep tests showed that the maximum variation in dynamic data over the time frame of the experiments was less than 5%. The morphological stability of the samples was confirmed by microscopic observations since the variation in droplet size of the blends, before and after the frequency sweep tests, was found to be in the range of the experimental error (±25%). To minimize the morphological non-uniformity due to sample preparation, a shear rate of 0.3 s^{-1} was applied for 1 h to pre-shear the sample before further rheological measurements. Preliminary

experiments showed that at this shear rate all the samples were stable in the cone-plate geometry. To ensure that the spherical shape of the drops was recovered and the initial isotropic condition was fulfilled, the samples were allowed to relax for one more hour after pre-shearing. As discussed further, due to the very low interfacial tension between the TPO components, the recovery time of the deformed droplets in some of the concentrated TPOs (70/30 w/w) may exceed 15 min. Microscopic observations confirmed that 1 h recovery was, however, enough for complete shape relaxation; at the end of the experiments the heating elements were turned off and the relaxed samples were slowly cooled down by natural convection.

The morphology of various samples was examined by scanning electron microscopy (SEM). Samples were firstly fractured in liquid nitrogen and submerged in cyclohexane for 24 h to dissolve the elastomeric phase at the surface. After drying, the inspected surfaces were coated with a gold-palladium alloy and electron micrographs were taken using a Jeol (JSM 840) microscope operated at a voltage of 10 kV. The number and volume average diameters were determined from the surface analysis of at least 300 particles using a semi-automatic method consisting of a digitalizing device and SigmaScan Pro© software. The Schwartz-Saltikov (Saltikov 1967) correction was applied to account for the fact that the observation plane might not cut the particles through their equator.

Results and Discussion

A. Determination of interfacial tension

Several experimental techniques have been so far developed for the measurement of interfacial tension between polymer pairs. A good review of these methods can be found in the work of Xing et al. (2000). Among these techniques, rheological approaches have been found to be a powerful tool for determining the interfacial tension in polymer blends for which the

applicability of other methods becomes limited. In such techniques, the interfacial tension is evaluated from linear viscoelastic measurements and the variation of the complex modulus is correlated to interfacial tension through a constitutive equation.

The dynamic storage modulus data of the neat materials used in this study and of the 70/30 and 85/15 blends are presented in Figure 5.1. As shown, the storage modulus of the blends at low frequencies is larger than the neat components. This behavior is obviously related to the presence of interfacial elasticity and the secondary plateau at low frequencies is a clear indication of the shape relaxation of the deformed droplets subjected to oscillatory shear flow. The dynamic moduli were used to calculate the relaxation spectrum of the blends by a nonlinear regression computation using a commercial software (NLREG©). The relaxation spectra are illustrated in Figure 5.2. As typical behavior of binary systems, two distinct peaks are observed in the time weighted relaxation spectra of the blends. The second peak is directly related to the shape relaxation time of the deformed droplets, while the first broad peak reflects the contribution due to the relaxation of the matrix macromolecules. As shown in Figure 5.2 the second peak for the 70/30 blends appears at longer time as compared to the 85/15 blend. This was expected since in more concentrated systems the droplets are larger and, hence, relax over a longer period of time. In the inserts of Figure 5.2 the interfacial relaxation spectra calculated from the method proposed by Vinckier et al. (1996) are also shown. In this method, the interfacial elasticity is isolated from the contribution of the blend constituents by subtracting the spectra of the components (weighted by the volume fractions) from the blend spectrum. It has been experimentally shown that compared to the time weighted relaxation spectrum, this interfacial spectrum is more sensitive for determining the characteristic relaxation time of the deformed droplets (Vinckier et al. 1996).

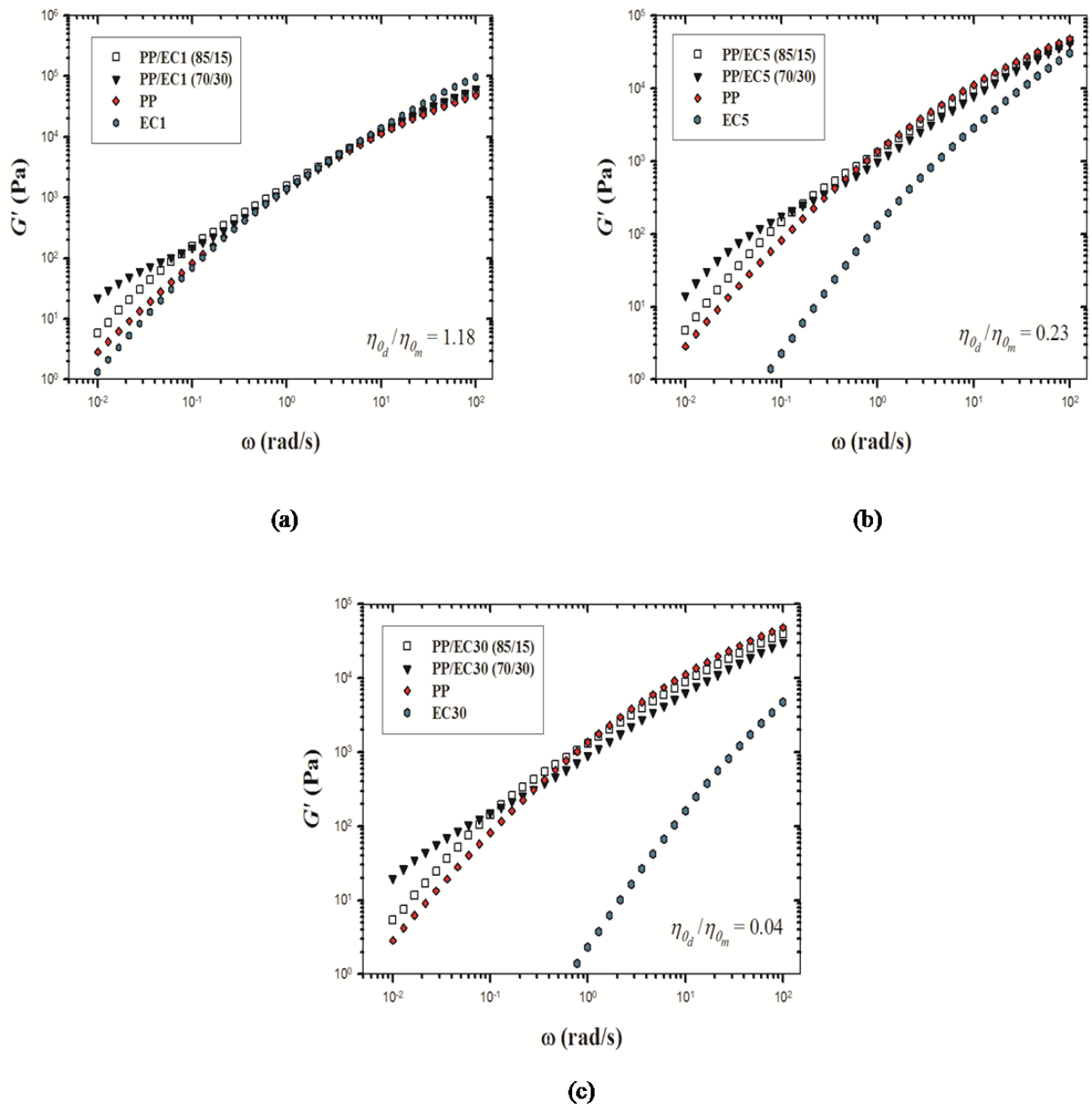

Fig. 5.1 Storage moduli of the neat components and of the 85/15 and 70/30 (w/w) PP/EC blends at 200 ^{o}C; (a) PP/EC1, (b) PP/EC5, (c) PP/EC30.

The interfacial relaxation spectrum of the 85/15 blend shows sharper peaks due to their more uniform morphology as compared to the 70/30 blend. The characteristic interfacial relaxation times can be used along with the microscopic data to estimate the interfacial tension.

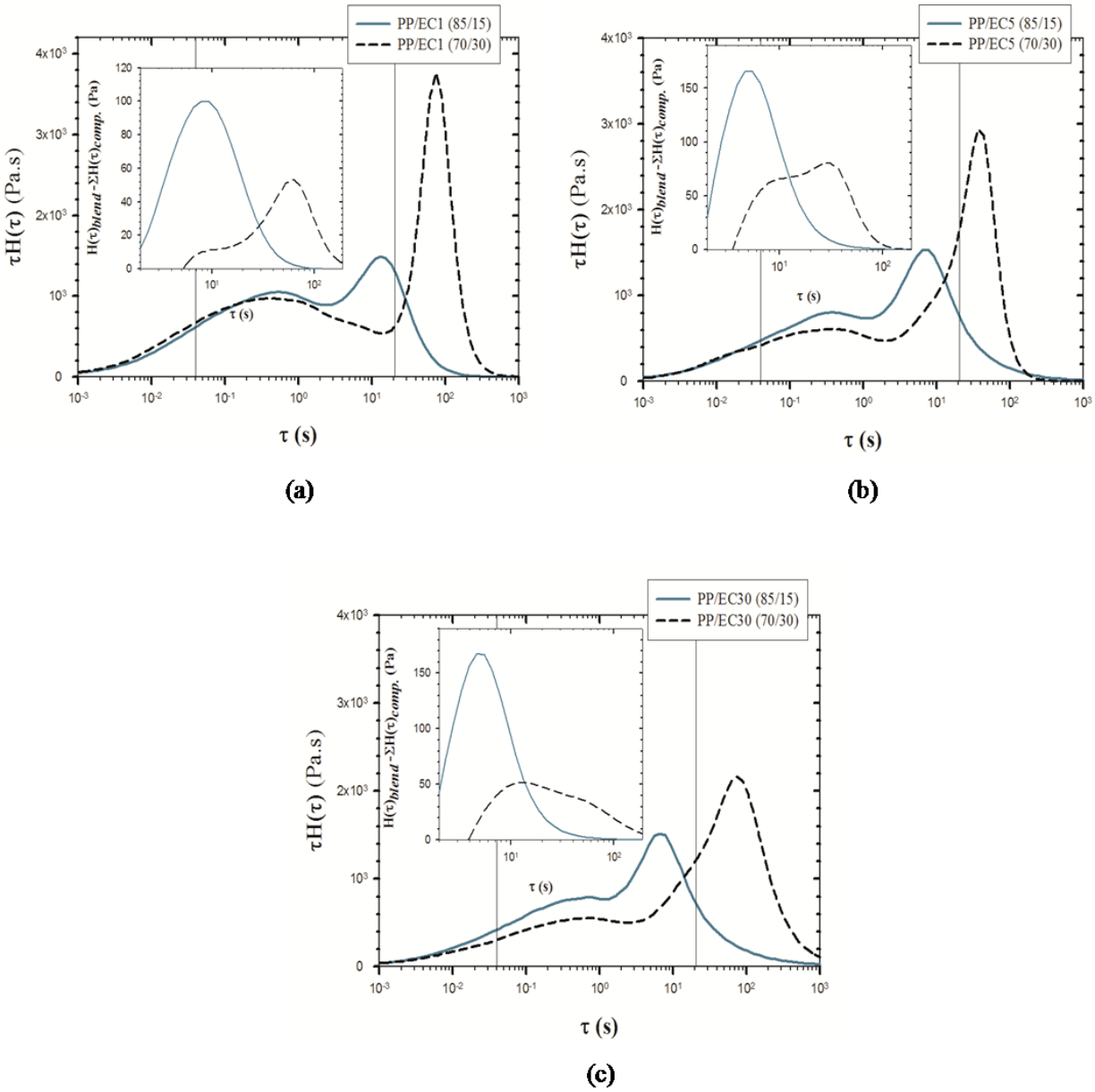

Fig. 5.2. Time weighted relaxation spectrum as well as subtracted relaxation spectrum for the blends containing 15% and 30% dispersed phase. (a) PP/EC1, (b) PP/EC5, (c) PP/EC30. The solid lines indicate the window of validity based on the experimental frequency.

Assuming that at low frequencies the behavior of the components is mostly Newtonian, the Palierne (1990) model gives the following expression for the interfacial tension (Graebling et al. 1993):

$$\alpha = \frac{R_v \eta_m}{4\tau_D} \frac{(19k+16)[2k+3-2\Phi(k-1)]}{10(k+1)-2\Phi(5k+2)} \tag{5.2}$$

in which R_v is the volumetric mean of the droplet radii, α is the interfacial tension, τ_D is the characteristic shape relaxation time, η_m is the matrix viscosity, and Φ is the volume fraction of the dispersed phase. The dynamics of the interface can be also described based on the Choi and Schowalter (1975). Neglecting non-linear terms, the constitutive equation of Choi and Schowalter can be simplified to describe the dynamic storage and loss moduli for an emulsion of two Newtonian liquids as:

$$G'(\omega) = \frac{\eta}{\tau_1}(1-\frac{\tau_2}{\tau_1})\frac{\omega^2 \tau_1^{\ 2}}{1+\omega^2 \tau_1^{\ 2}} \ , \tag{5.3}$$

$$G''(\omega) = \frac{\eta}{\tau_1}(1-\frac{\tau_2}{\tau_1})\frac{\omega \tau_1}{1+\omega^2 \tau_1^{\ 2}} + \omega\eta\frac{\tau_2}{\tau_1} \ , \tag{5.4}$$

with

$$\eta = \eta_m[1+\Phi\frac{5k+2}{2(k+1)}+\Phi^2\frac{5(5k+2)^2}{8(k+1)^2}] \ , \tag{5.5}$$

$$\tau_1 = \tau_0[1+\Phi\frac{5(19k+16)}{4(k+1)(2k+3)}] \ , \tag{5.6}$$

$$\tau_2 = \tau_0[1+\Phi\frac{3(19k+16)}{4(k+1)(2k+3)}] \ , \tag{5.7}$$

where $\tau_0 = \frac{R_v \eta_m}{\alpha} \frac{(19k+16)(2k+3)}{40(k+1)}$ and τ_1 was found by Gramsespacher and Meissner (1992) to be equal to the characteristic relaxation time of the interface. Isolating the contribution of the interfacial stress from that of the neat constituents, Gramespacher and Meissner (1992) suggested the following relation to account for the viscoelasticity of the components:

$$G^*_{\text{blend}} = G^*_{\text{components}} + G^*_{\text{interface}} \quad , \tag{5.8}$$

in which $G^*_{components}$ is the sum of the complex moduli of the components weighted by their volume fractions, and $G^*_{\text{interface}}$ is calculated using Eqs. 5.3 and 4.

The estimated interfacial tension values are given in Table 5.2. Note that the values obtained using the Choi and Showalter equation vary significantly from sample to sample. This is, however, not expected since the co-monomer composition in different ECs is similar (see Table 5.1).

Table 5.2. Interfacial tension and relaxation time obtained by different methods for the (85/15) blends.

			Modified Choi-Schowalter Model		**Palierne Model**	
Blend	**D_v(μm)**	**τ (s)***	**α (mN/m)**	**τ (s)**	**α (mN/m)**	**τ (s)****
PP/EC1	**0.7**	**13.2**	**0.6±0.1**	**10.4**	**0.7±0.1**	**7.8**
PP/EC5	**0.8**	**6.6**	**0.9±0.1**	**8.1**	**0.8±0.1**	**5.5**
PP/EC30	**0.9**	**6.6**	**1.3±0.1**	**5.3**	**0.8±0.1**	**4.7**

***associated with the second peak in the time weighted spectrum**

****calculated based on the subtracted spectrum proposed by Vinckier et al. (1996)**

Also we do not expect a significant variation of the interfacial tension with molecular weight, since for the commercial copolymers used in this study the molecular weight is larger than the critical values above which the interfacial tension is independent of molecular weight (Anastasiadis et al. 1988; Ellingson et al. 1994). In contrast the Palierne model gives very similar values of the interfacial tension for the different systems.

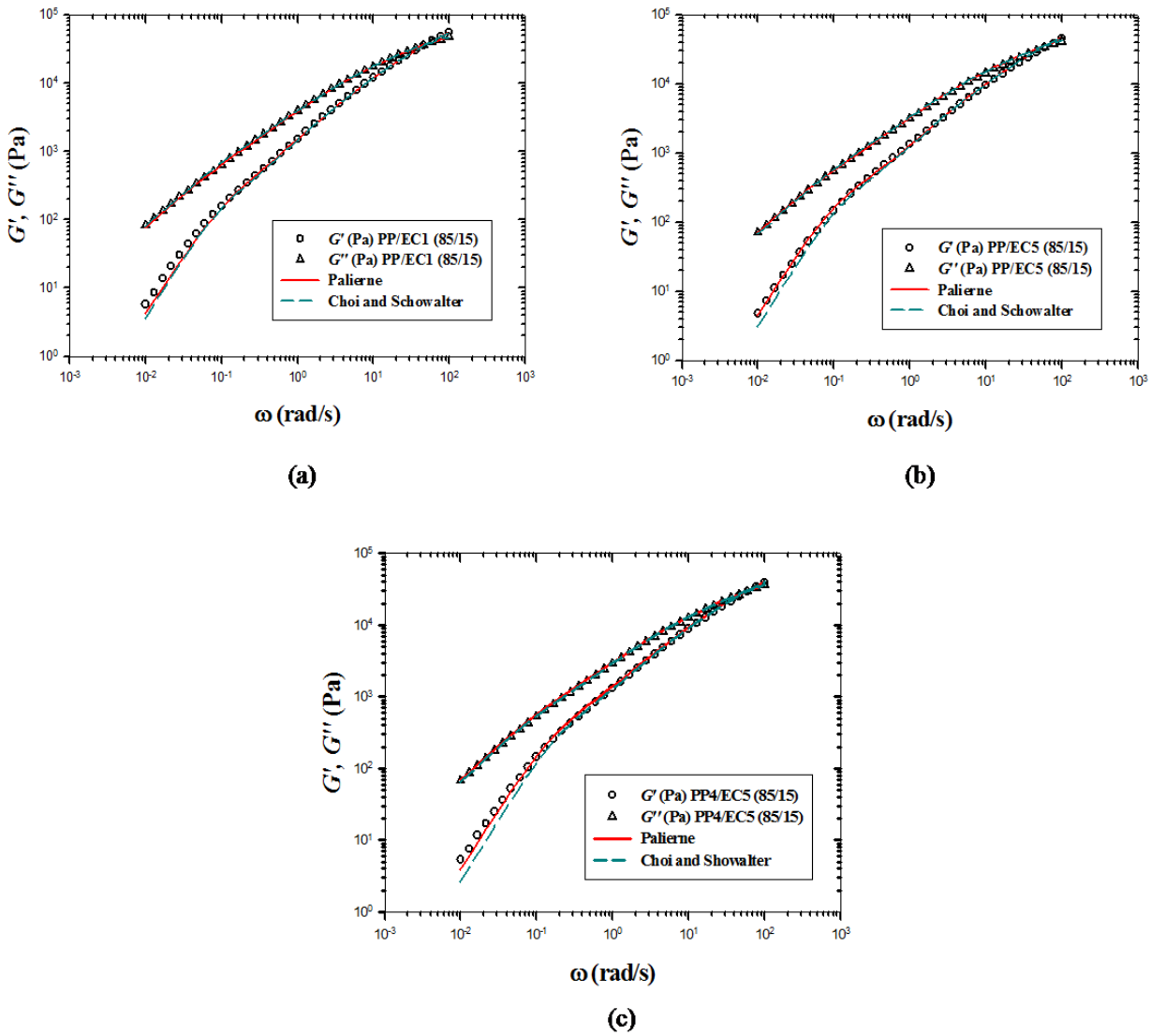

Fig. 5.3 Predictions of the storage and loss moduli of the PP/EC(85/15) blends with the Palierne and Choi-Showalter models. (a) PP/EC1(85/15), (b) PP/EC5(85/15), (c) PP/EC30(85/15).

The predictions for the dynamic moduli are also shown in Figure 5.3. As illustrated, the Palierne model predicts quite well the experimental data, in fact slightly better than the Choi and Showalter theory at low frequency. Considering the better fit obtained by the Palierne model, the interfacial tension values estimated by the latter are used from now on in this work.

B. Morphology evolution under transient shear

In this study, the morphology evolution of the blends was firstly modeled using the phenomenological transient model of Lee and Park (1994). In this approach the micro-structure development of the dispersed phase is described in terms of the specific interfacial area (Q) and the anisotropy tensor (q_{ij}). The model is based on the Doi and Ohta theory (1991), which was originally developed for 50/50 mixtures of Newtonian fluids with equal viscosities. In this model, the time evolution of the interfacial area and the anisotropy due to macroscopic flow are expressed by the following set of coupled equations:

$$\frac{d}{dt}q_{ij} = -q_{ik}\kappa_{kj} - q_{jk}\kappa_{ki} + \frac{2}{3}\delta_{ij}\kappa_{lm}q_{lm} - \frac{Q}{3}(\dot{\gamma}_{ij}) + (\frac{q_{lm}\kappa_{lm}}{Q})q_{ij}$$

$$- d_1\frac{\alpha}{\eta_m}Qq_{ij} - d_1 d_3\frac{\alpha}{\eta_m}(\frac{q_{lm}q_{lm}}{Q})q_{ij} \ , \tag{5.9}$$

$$\frac{d}{dt}Q = -\kappa_{ij}q_{ij} - d_1 d_2\frac{\alpha}{\eta_m}Q^2 - d_1 d_3\frac{\alpha}{\eta_m}q_{ij}q_{ij} \ , \tag{5.10}$$

where κ_{ij} are the components of the velocity gradient tensor, $\dot{\gamma}_{ij} = \kappa_{ij} + \kappa_{ji}$ are components of the rate of deformation tensor, δ_{ij} is the Kronecker delta and the summation over repeated indices is considered. The coefficients d_1, d_2, d_3 represent, respectively, the degree of total relaxation($d_1 = c_1 + c_2$), size relaxation ($d_2 = c_1 / (c_1 + c_2)$) and shape relaxation and breakup ($d_3 = c_3 / (c_1 + c_2)$), where c_1, c_2, c_3 are related to the kinetic equations describing the droplet relaxation mechanisms:

$$\frac{d}{dt}\left(\frac{q_{ij}}{Q}\right)\Bigg|_{\text{relaxation}} = -c_2 \frac{\alpha Q}{\eta_m}\left(\frac{q_{ij}}{Q}\right) \quad , \tag{5.11}$$

$$\frac{d}{dt} Q\Big|_{\text{relaxation}} = -c_1 \frac{\alpha}{\eta_m} Q^2 - c_3 \frac{\alpha}{\eta_m} q_{ij} q_{ij} \, , \tag{5.12}$$

Eq. 5.11 accounts for the decrease in anisotropy due to shape recovery of the deformed droplets. The first term in Eq. 5.12 represents the rate of coalescence and the second term incorporates the contribution of breakup in the evolution of the interfacial area. The constants are dimensionless and positive and may be functions of volume fraction and possibly other material characteristics such as the dispersed phase viscosity. In contrast to the real behavior of stable emulsions, the c_1 term in Eq.5.12 causes the Q value to vanish even in the absence of flow. As proposed by Doi and Ohta (1991), the first term in Eq. 5.12 can be replaced by $-c_1 \frac{\alpha}{\eta_m}(\sum q_{ij}^2)^{1/2} Q$ to account for the morphological stability under no flow condition and, hence:

$$\frac{d}{dt} Q = -\kappa_{ij} q_{ij} - d_1 d_2 \frac{\alpha}{\eta_m}(\sum q_{ij}^2)^{1/2} Q - d_1 d_3 \frac{\alpha}{\eta_m} q_{ij} q_{ij} \quad , \tag{5.13}$$

The stress tensor can be then calculated as the summation of the viscosity ratio term, the interfacial (morphology dependent) term and the isotropic pressure term as follows:

$$\sigma_{ij} = \left[1 + \frac{6(\eta_i - \eta_m)}{10(\eta_m + \eta_i)} \Phi\right] \eta_m \dot{\gamma}_{ij} - \alpha q_{ij} - P\delta_{ij} \quad , \tag{5.14}$$

where η_i is the viscosity of the inclusions. It was shown by Lacroix et al. (1997) that depending on the rheological properties of the pure components, the following equation might be alternatively used to obtain a better description of the experimental data:

$$\sigma_{ij} = \left[\frac{1 + \frac{3}{2} H}{1 - H} \right] \eta_m \dot{\gamma}_{ij} - \alpha q_{ij} - P\delta_{ij} \,, \tag{5.15}$$

where

$$H = \Phi \frac{2(\eta_i - \eta_m)}{2\eta_i + 3\eta_m} \quad , \tag{5.16}$$

Setting $Q_0 = 6\Phi / d_{v_0}$ and $q_{ij_0} = 0$ as the initial conditions, Eqs. 5.9, 13, 14 (or 15) are simultaneously solved to find out the interfacial area as well as the anisotropy and stress tensors.

In order to account for the non-affine deformation of the droplets, Lacroix et al. (1999) introduced a slip parameter ξ in the thermodynamic formulation for the time evolution of the interface derived by Grmela and Ait-Kadi (1994). The governing equations can then be expressed as follows:

$$\frac{d}{dt} q_{ij} = -q_{ki}\kappa_{kj}(1 - \frac{\xi}{2}) + \frac{\xi}{2} q_{ki}\kappa_{jk} - q_{kj}\kappa_{ki}(1 - \frac{\xi}{2}) + \frac{\xi}{2} q_{kj}\kappa_{ik} + \frac{2}{3}(1-\xi)\delta_{ij}\kappa_{lm}q_{lm} - \frac{Q}{3}(1-\xi)\dot{\gamma}_{ij}$$

$$+ (1-\xi)(\frac{\kappa_{lm}q_{lm}}{Q})q_{ij} - d_1 \frac{\alpha}{\eta_m} Q q_{ij} - d_1 d_3 \frac{\alpha}{\eta_m} (\frac{q_{lm}q_{lm}}{Q}) q_{ij} \,, \tag{5.17}$$

$$\frac{d}{dt} Q = -\kappa_{ij} q_{ij}(1-\xi) - d_1 d_2 \frac{\alpha}{\eta_m} Q^2 - d_1 d_3 \frac{\alpha}{\eta_m} q_{ij} q_{ij} \quad , \tag{5.18}$$

and by introducing the slip parameter the expression of the Lee-Park model for the extra stress tensor becomes:

$$\sigma_{ij} = \eta_m \frac{1 + \frac{3}{2} H}{1 - H} \dot{\gamma}_{ij} - \alpha(1-\xi) q_{ij} - P\delta_{ij} \,, \tag{5.19}$$

In the limit of $\xi = 0$, affine deformation is described by the lower convected time derivative while for $\xi = 2$ the evolution tensor is governed by the upper convected time derivative. In the case of $\xi = 1$, macroscopic flow causes only rotational and translational motions and the extra stress due to the interfacial tension vanishes.

Figure 5.4 reports transient shear viscosity of the PP/EC (70/30) blends along with predictions of the Lee-Park (LP) and the modified Lee-Park (LPL) models. Considering that the imposed shear rate in these experiment was small (0.01 s^{-1}), the overshoot observed is clearly due to the evolution of the morphological anisotropy. At large strains, a relatively stable viscosity was established for the PP/EC1 blend whereas a progressive decrease can be observed for the PP/EC5 and especially for the PP/EC30 blend. This behavior reflects the more intense coalescence in the PP/EC5 and PP/EC30 blends as compared to the PP/EC1. As shown in Figure 5.4, both the LP and LPL models predict quite well the transient viscosities. For the PP/EC1 and PP/EC5 blends, the LP and LPL models result in very similar predictions of the viscosity data. This is, however, not surprising since the interfacial slip parameter ξ used in the LPL model was found to be quite small for both blends. Similar values for the degree of total relaxation (d_1) and size relaxation (d_2) were obtained from both models for these blends (see Table 5.3). However, the specific interfacial area at the end of the experiment ($Q_{Model}/Q_{Exp.}$) is best predicted by the LPL model.

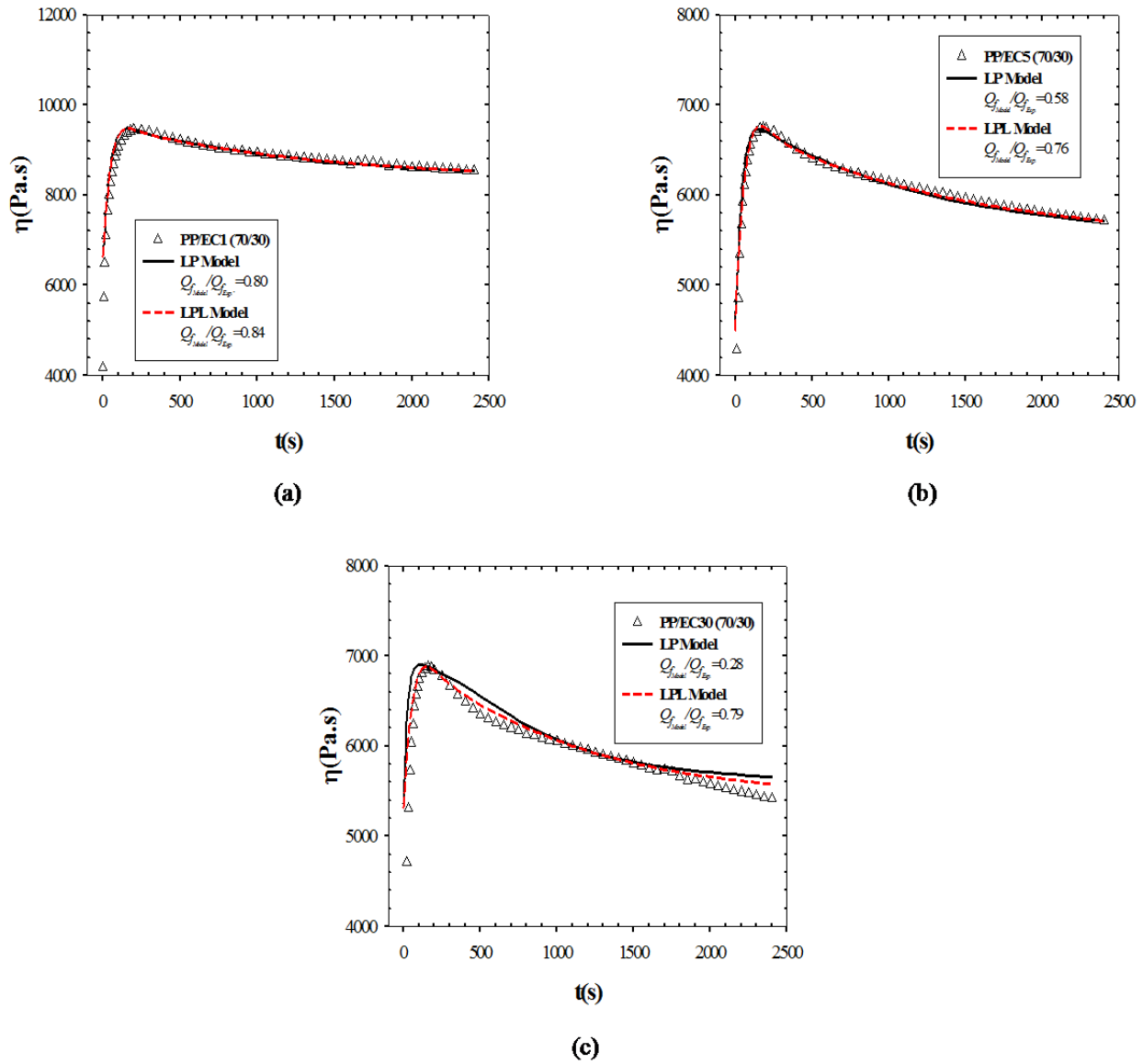

Fig. 5.4 Comparison between the stress growth viscosity data and predictions of the LP and LPL models for the PP/EC (70/30) blends at T=200°C, (s^{-1}). a) PP/EC1(70/30); b)PP/EC5(70/30); c)PP/EC30(70/30).

The LP model significantly underestimates the *Q* values determined from SEM, especially for the PP/EC30 blend. These results show the capability of the LPL model to predict the morphology coarsening in these blends, strictly based on rheological data.

The time evolution of the specific interfacial area predicted by the LPL model is shown in Figure 5.5. The behavior is similar to that for the transient viscosity. In the case of the PP/EC1 blend, *Q* approaches a plateau (steady-state value), implying that equilibrium has been established between the breakup and coalescence phenomena. The rate of decrease of *Q* for the PP/EC5 and PP/EC30 blends is, however, much faster.

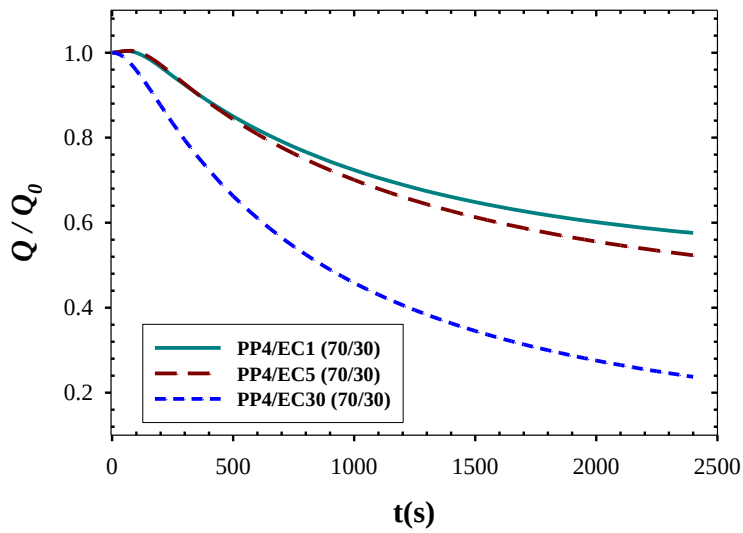

Fig. 5.5 Variation of the normalized specific interfacial area with time for the PP/EC (70/30) blends at T=200°C, $\dot{\gamma} = 0.01$ (s^{-1}).

Examples of the morphology of the blends at the beginning and at the end of the stress growth experiment carried out at $\dot{\gamma} = 0.01\,\mathrm{s}^{-1}$ are illustrated in the micrographs of Figure 5.6.

(a) PP/EC1 (70/30)

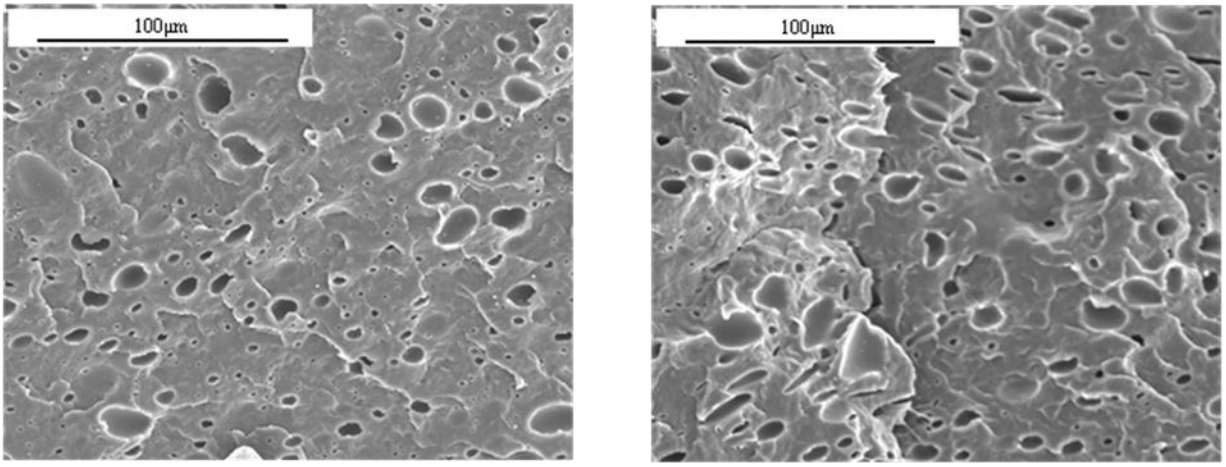

(b) PP/EC30 (70/30)

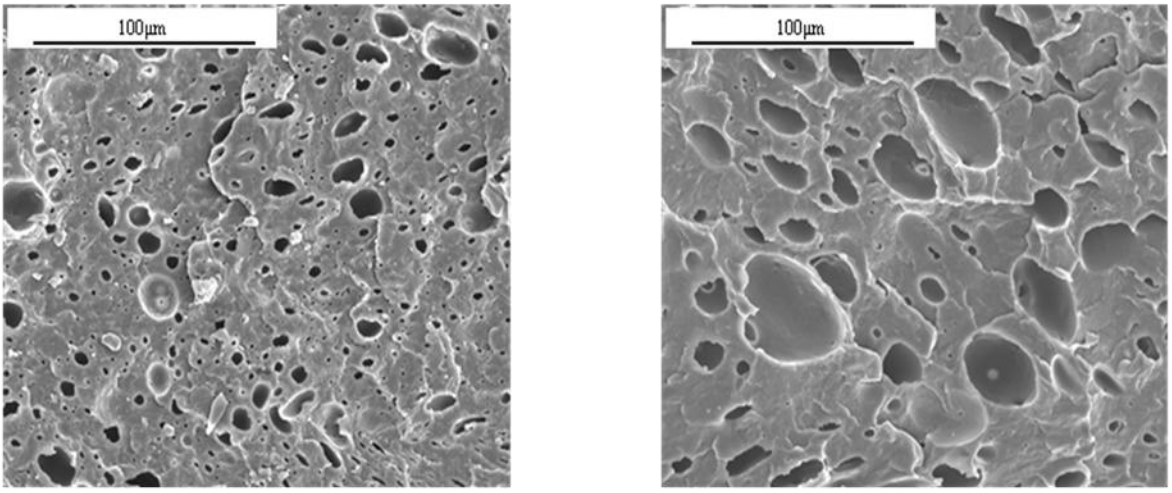

Fig. 5.6. Micrographs showing coalescence after shearing. Left micrographs: initial morphology; right micrographs: after 40 min. shearing at $\dot{\gamma} = 0.01$ s^{-1}. a) PP/EC1(70/30)); b) PP/EC30(70/30). The ratio of final to initial droplet size (d_{v_f} / d_{v_0}) was measured to be 1.3 and 3 for PP/EC1(70/30) andPP/EC30(70/30) blend respectively.

As shown, the coalescence in the PP/EC30 is much more intense than in the PP/EC1, in agreement with the model predictions. While the initial morphology in both blends is similar, the final droplet size in the PP/EC30 blend is almost two times larger.

As mentioned previously, for the same matrix viscosity, reducing the droplet viscosity (hence, viscosity ratio) promotes the interfacial mobility and facilitates the film drainage and coalescence. This is in agreement with the transient morphological observation of this study. The increased interfacial mobility can be also analyzed from the rate of droplet relaxation as a lower viscosity of the dispersed phase can facilitate the motion of the drop surface during recovery. The rate of the shape relaxation in the PP/EC1 and EC30 blends can be compared by considering the time required for the complete recovery of the sheared drops. For this purpose, these blends were sheared at a relatively high shear rate (0.3 s^{-1}) for 1 h and then the flow was stopped for recovery. Figure 5.7 presents the morphology of the sheared sample after 15 min recovery along with the rheological data. While the droplets of the PP/EC1 remain elongated, almost spherical shapes are observed for the PP/EC30 blend. This microscopic observation was also confirmed by a subsequent startup test after the 15 min recovery, carried out at a low shear rate of 0.01 s^{-1}. The absence of an overshoot in the second run of the startup test for the PP/EC1 indicates that the anisotropic morphological state was retained at the end of the rest time, while the transient viscosity data for PP/EC30 shows the typical behavior of an isotropic system. The increased interfacial mobility is also reflected in the slip parameter ξ. As shown in Table 5.3, this parameter increases from 0.03 for the PP/EC1 blend to 0.35 for PP/EC30. This means that the reduced droplet viscosity facilitates the droplet deformation, responsible for non-affine deformation (or more hydrodynamic interaction).

(a) PP/EC1 (70/30)

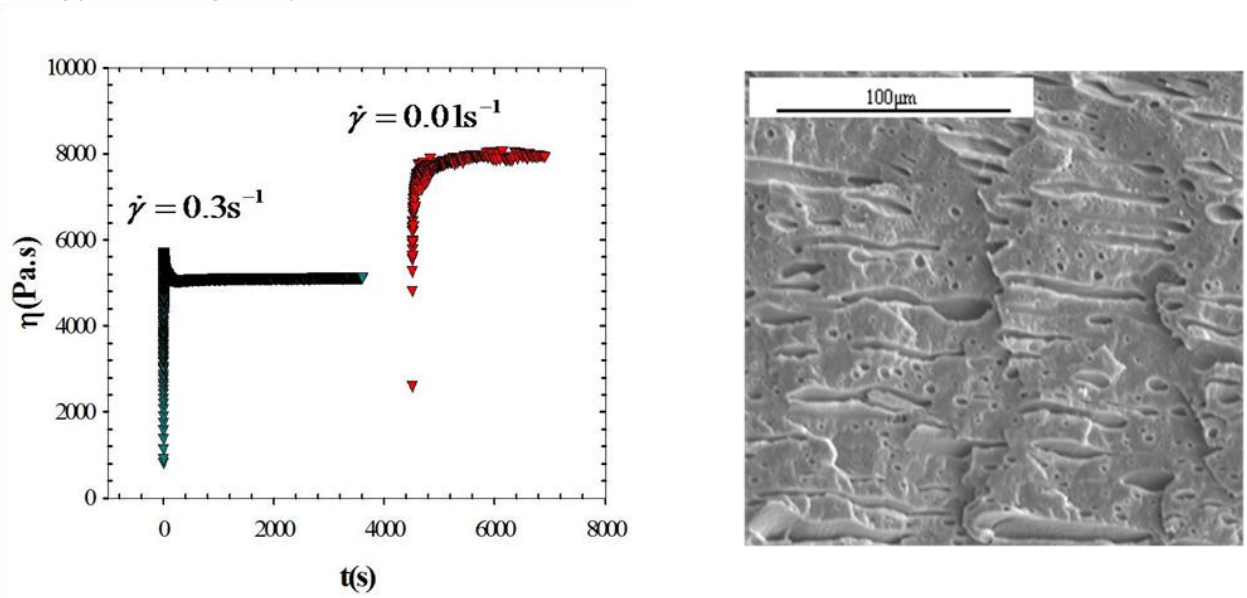

(b) PP/EC30(70/30)

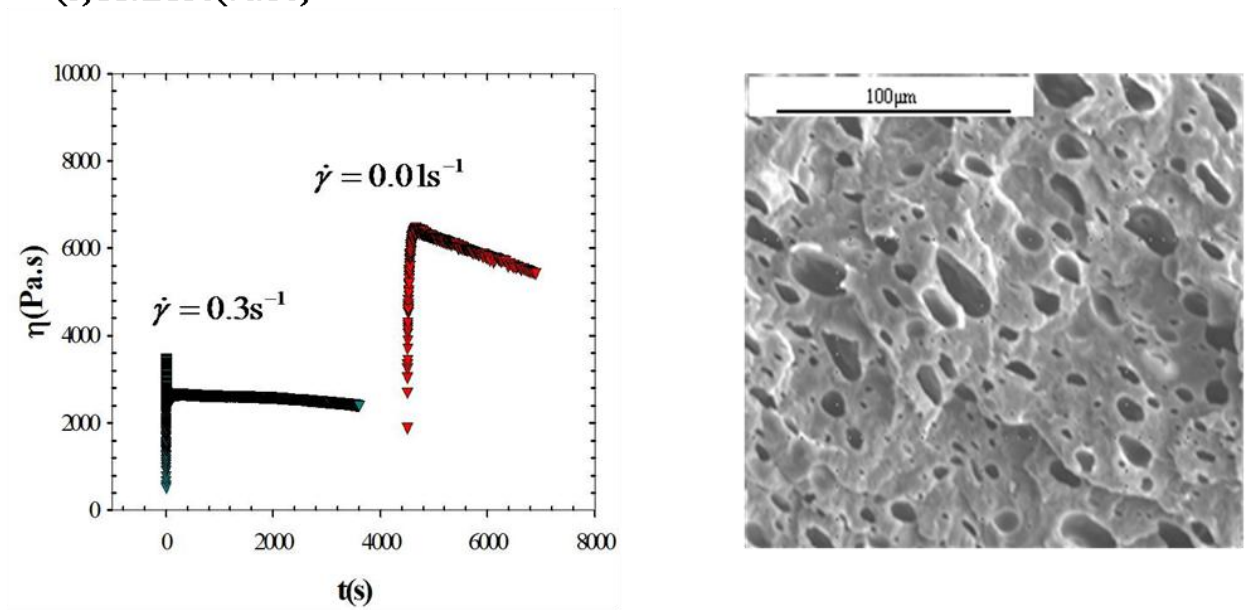

Fig. 5.7. Stress growth viscosity and morphological data for two consecutive stress growth experiments, at $\dot{\gamma} = 0.3\,s^{-1}$ and $\dot{\gamma} = 0.01\,s^{-1}$. The micrographs were taken after 15 min recovery following the first stress growth. a) PP/EC1(70/30); b) PP/EC30(70/30).

Table 5.3 Parameters used for predicting the transient shear viscosity of different blends with LP and LPL models at 0.01(s^{-1}).

			LP Model				LPL Model				
Blend	Q_o(m^{-1})x10^{-5}	Q_f(m^{-1})x10^{-5}	d_1	d_2	d_3	Q_f(m^{-1})x10^{-5}	d_1	d_2	d_3	ξ	Q_f(m^{-1})x10^{-5}
PP/EC1(70/30)	**2.6**	**1.8**	**0.52**	**0.35**	**0.70**	**1.4**	**0.48**	**0.35**	**0.70**	**0.03**	**1.5**
PP/EC5(70/30)	**2.2**	**1.5**	**0.69**	**0.41**	**0.70**	**0.8**	**0.45**	**0.40**	**0.70**	**0.11**	**1.1**
PP/EC30(70/30)	**2.5**	**0.8**	**1.20**	**0.67**	**0.70**	**0.2**	**0.38**	**0.58**	**0.70**	**0.35**	**0.6**
PP/EC30(75/25)	**4.4**	**1.4**	**1.92**	**0.6**	**0.75**	**0.2**	**0.36**	**0.50**	**0.75**	**0.51**	**1.2**
PP/EC30(80/20)	**5.0**	**1.6**	**1.36**	**0.29**	**0.80**	**0.9**	**0.69**	**0.26**	**0.80**	**0.27**	**1.6**
PP/EC30(85/15)	**5.4**	**1.7**	**1.86**	**0.20**	**0.85**	**1.1**	**1.71**	**0.20**	**0.85**	**0.04**	**1.2**

The capability of the LP and LPL models for evaluating the extent of coalescence was also examined in blends of different concentrations. For this purpose, PP/EC30 blends at concentrations of 85/15, 80/20 and 75/25 w/w were also prepared and subjected to a steady shear rate of 0.01 s^{-1}. The transient shear viscosity of the blends is presented in Figure 5.8. As expected, the overshoot is reduced as the dispersed phase concentration is decreased. However, the magnitude of the transient viscosity increases, reflecting the more important contribution of the viscous matrix. The predictions of both LP and LPL models for the *Q* value of the 85/15 blend are in good agreement with the SEM measurements. For this blend the value of the slip parameter ξ is negligible (see Table 5.3) and as expected both models yield similar values for the other parameters. For the other blends, however, the LP model largely underpredicts the *Q* values; the LPL model gives better predictions of the final morphology, but a slip parameter different from zero has to be used.

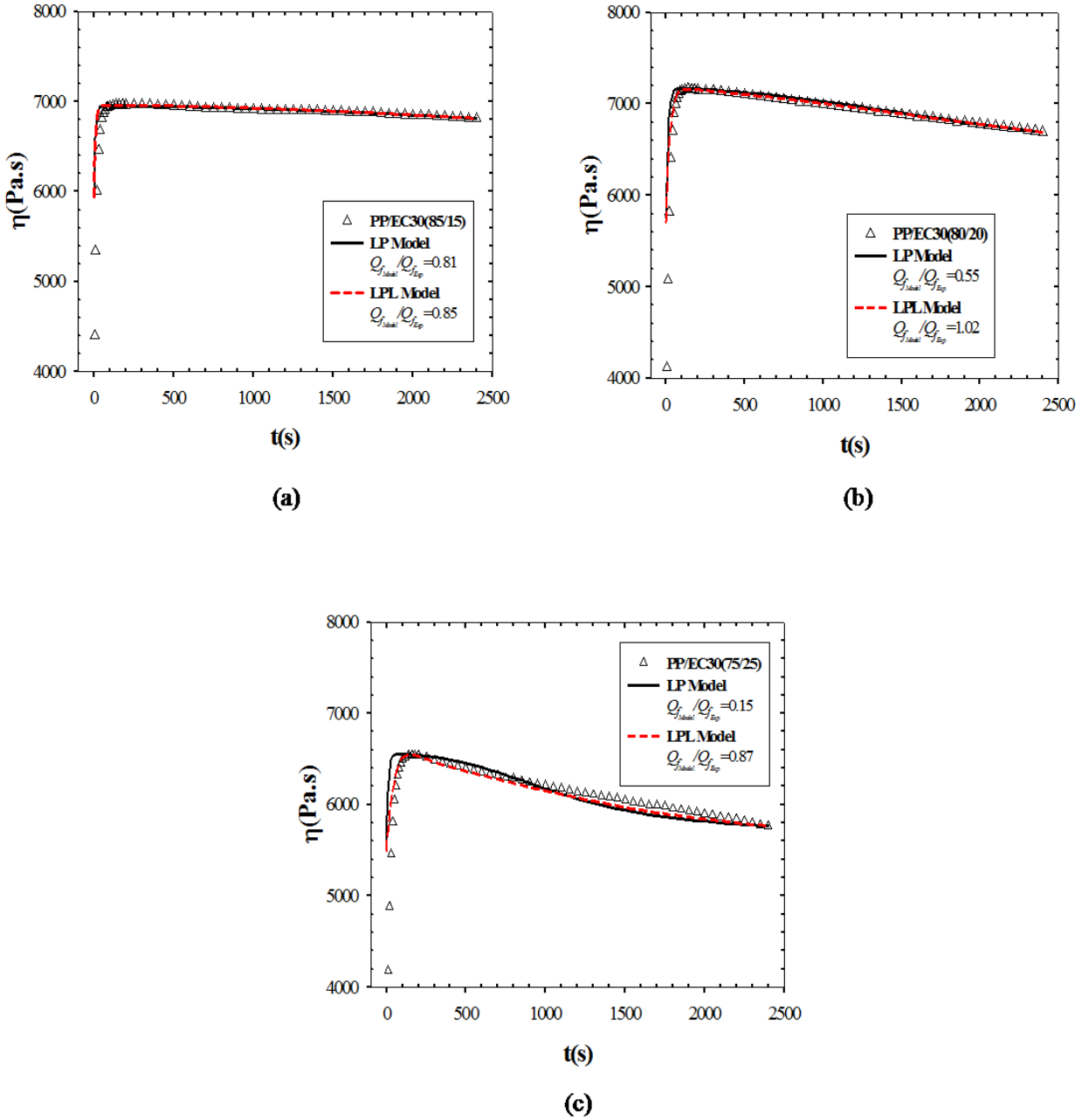

Fig. 5.8. Comparison of stress growth viscosity data and predictions of the LP and LPL models for PP/EC30 blends at 200°C, $\dot{\gamma} = 0.01\,\mathrm{s}^{-1}$. a) PP/EC30(85/15); b) PP/EC30(80/20); c) PP/EC30(75/25).

To examine the coalescence intensity of the blends at different concentrations we firstly examine the ratio of the final to the initial experimental droplet size, d_{v_f} / d_{v_0}. As illustrated in Figure 5.9 (data shown by blank squares) this ratio is nearly the same (~ 3) for all concentrations, although the initial droplet size varied from 1.6 μm for the (85/15) PP/EC30 to 7.2 μm for the (70/30) PP/EC30 blend. As mentioned previously, the d_{v_f} / d_{v_0} ratio does not account for the initial droplet density, which affects considerably the collision frequency and, hence, coalescence. Using the Smoluchowski theory (1917) the collision frequency for the PP/EC30 (85/15) blend is estimated to be almost 11 times larger than for the PP/EC30 (70/30) blend. In fact the d_{v_f} / d_{v_0} ratio can reflect the coalescence intensity only when the initial droplet sizes are in the same range. This is of course a difficult condition to meet experimentally. We simulate the situation using the LPL model assuming that the parameters are independent of the morphological state of the blends. Here we assume that the PP/EC30 blends of different concentrations have the same initial droplet size of 4 μm. The calculated d_{v_f} / d_{v_0} ratio from $Q = 6\Phi / d_v$ is reported in Figure 5.9 (data shown by filled triangles) as a function of the volume fraction of the dispersed phase, Φ. As expected, d_{v_f} / d_{v_0} monotonically increases with Φ. Hence, the effect of the collision frequency on coalescence is well accounted by the LPL model. To verify that the model parameters obtained from one set of rheological/morphological data are applicable for predicting the behavior of the same blend for different initial morphologies, we carried on the following final experiment for the (75/25) PP/EC30 blend, initially pre-sheared at 0.02 s^{-1} for 600 s. This caused the initial droplet size to change from 3.4 to 6.3 μm. After 15 min rest, the sample was subjected to a shear rate of 0.01 s^{-1}. The transient shear viscosity at 0.01 s^{-1} for the sample pre-sheared at 0.02 s^{-1} is presented in Figure 5.10. The predictions of the LPL

model using the same constants as determined from previous experiments (see Table 5.3) are also shown. The model predictions are in good qualitative agreement with the experimental viscosity data and final morphology as well. These observations prove the usefulness of such phenomenological models to predict morphological changes in polymer blends during processing.

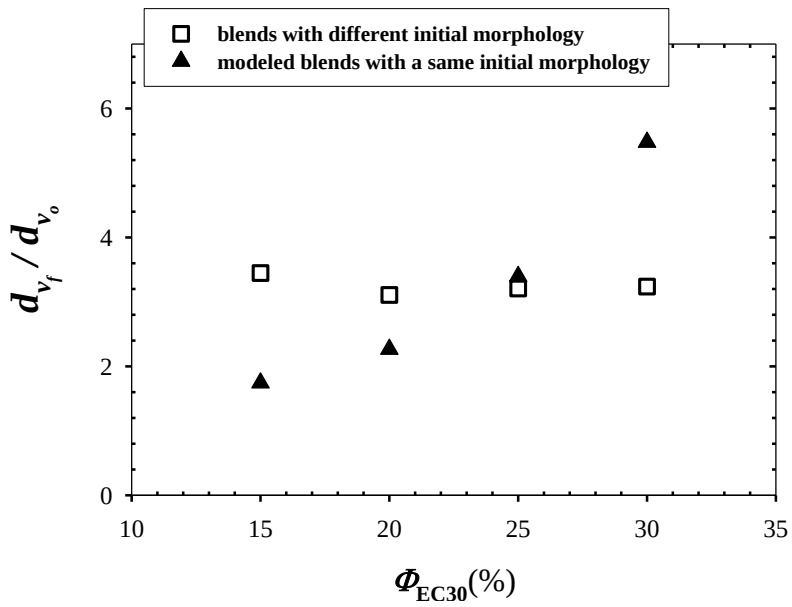

Fig. 5.9. Variation of the final droplet size normalized by the initial value for the blends with different initial morphologies (□) and simulated blends with a same initial droplet size (▲).

Finally, we stress that the phenomenological models used in this work are based on drastic assumptions and it is unrealistic to believe that they could be fully predictive. Nevertheless, the variations of the model parameters with concentration of the dispersed phase can be explained partly as follows. As the volume fraction decreases the shape recovery is more rapid explaining the increase in d_1 reported in Table 5.3. At low volume fractions, the contribution of coalescence becomes weak and as such d_2 (μ in Lee-Park), which is indeed indicating the contribution of

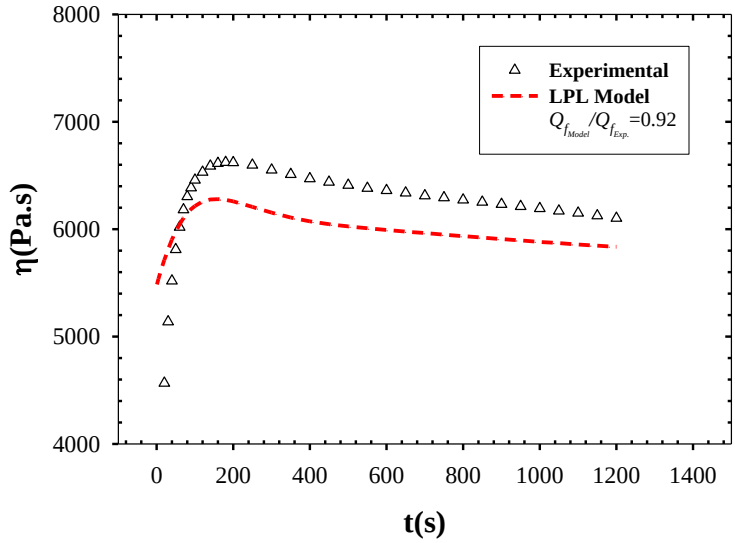

Fig. 5.10. Comparison between the predictions of the PLP model and experimental data for PP/EC30(75/25) blend pre-sheared at 0.02 s^{-1} for 600 s.

coalescence compared to shape recovery, should decrease with volume fraction. The parameter d_3 was taken equal to (1-ϕ) as suggested by Lee and Park (1994). The dependency of the slip parameter on volume fraction is, however, more complicated. An important consequence of the variation of volume fraction is the change in the inter-particle distance; at low volume fractions the particles are far from each other and, hence, hydrodynamic (particle-particle) interactions play a minor role resulting in a small value of the slip parameter. As the concentrations increases the particles become closer to each other and the larger slip values account for the stronger hydrodynamic interactions. However, the interparticle distance is not the only consequence of the increased volume fraction. We recall that the viscosity of the dispersed phase in the case of PP/EC30 blend is significantly smaller than the matrix. Hence, for these blends, an increase in volume fraction results into a reduction of the bulk shear stress, which is at the origin of hydrodynamic interactions. Considering all the influencing parameters, it is difficult at this point

to establish a clear relationship between the model parameters, volume fraction and component properties. Obviously, more work is needed to assess the models for more severe conditions encountered in industry and possibly develop a more adequate model.

Concluding remarks

The effect of the viscosity of the dispersed phase on the flow-induced coalescence in thermoplastic olefin blends (TPOs) under transient shear flow was investigated. To model the morphology evolution under steady shear, the interfacial tension of the blends was determined by applying different emulsion linear viscoelastic models. It was shown that compared to the Choi and Showalter theory, the Palierne model gives a better estimation of the low frequency data. Also the Palierne model predicts almost the same value of the interfacial tension for the different blends, as expected from their similar composition. The Lee and Park (LP) model can predict well the transient viscosity data for all blends, but in most cases it underpredicts the interfacial area, Q. Using a slip parameter (ξ) the modified Lee-Park model (LPL model) predicts fairly well both the transient viscosity data and the Q values. The value of the slip parameter was found to correlate with the viscosity of the dispersed phase, suggesting more affine deformation for larger viscosity droplets. The enhanced coalescence and faster relaxation rate of the morphology imply that the interfacial mobility increases with decreasing droplet viscosity. The final to initial droplet size ratio was found to be a poor indicator of coalescence. The LPL model was used to simulate the transient morphological behavior of the blends to account for increased coalescence intensity and indirectly for increasing frequency collision with volume fraction of the dispersed phase.

Acknowledgments

This project has been funded by a grant of NSERC-Center of Excellence Network "The Automobile of the 21st Century". The authors also want to thank Dr. Costeux from the Dow Chemical Company for the elastomers he provided.

References

Anastasiadis SH, Gancarz I, Koberstein JT (1988) interfacial tension of immiscible polymer blends: temperature and molecualr weight dependence. Macromolecules 21: 2980-2987

Batchelor GK, Green JT (1972) Hydrodynamic interaction of two small freely-moving spheres in a linear flow field. Journal of Fluid Mechanics 56: 375-400

Bensason S, Stepanov EV, Chum S, Hiltner A, Baer E (1997) Deformation of elastomeric ethylene-octene copolymers. Macromolecules 30: 2436-2444

Bin Wadud SE, Baird DG (2000) Shear and extensional rheology of sparsely branched metallocene-catalyzed polyethylenes. Journal of Rheology 44: 1151-1167

Chesters AK (1991) Modelling of coalescence processes in fluid-liquid dispersions. A review of current understanding. Chemical Engineering Research and Design 69: 259-227

Choi SJ, Schowalter WR (1975) Rheological properties of nondilute suspensions of deformable particles. Physics of Fluids 18: 420-427

Davis RH, Schonberg JA, Rallison JM (1989) The lubrication force between two viscous drops. Physics of Fluids A (Fluid Dynamics) 1: 77-81

Doerpinghaus PJ, Baird DG (2003) Separating the effects of sparse long-chain branching on rheology from those due to molecular weight in polyethylenes. Journal of Rheology 47: 717-736

Doi M, Ohta T (1991) Dynamics and rheology of complex interfaces. I. Journal of Chemical Physics 95: 1242-1248

Ellingson PC, Strand DA, Cohen A, Sammler RL, Carriere CJ (1994) Molecular weight dependence of polystyrene/poly(methyle methacrylate) interfacial tension probed by imbedded fiber-retraction. Macromolecules 27: 1643-1647

Graebling D, Muller R, Palierne JF (1993) Linear viscoelastic behavior of some incompatible polymer blends in the melt. Interpretation of data with a model of emulsion of viscoelastic liquids. Macromolecules 26: 320-329

Gramespacher H, Meissner J (1992) Interfacial tension between polymer melts measured by shear oscillations of their blends. Journal of Rheology 36: 1127-1141

Grmela M, Ait-Kadi A (1994) Comments on the Doi-Ohta theory of blends. Journal of Non-Newtonian Fluid Mechanics 55: 191-195

Guenther GK, Baird DG (1996) An evaluation of the Doi-Ohta theory for an immiscible polymer blend. Journal of Rheology 40: 1-20

Guidoa S, Simeonea M, Greco F (2003) Effects of matrix viscoelasticity on drop deformation in dilute polymer blends under slow shear flow. Polymer 44: 467-471

Huitric J, Moan M, Carreau PJ, Dufaure N (2007) Effect of reactive compatibilization on droplet coalescence in shear flow. Journal of Non-Newtonian Fluid Mechanics 145: 139-149

Jancar J, DiAnselmo A, DiBenedetto AT, Kucera J (1993) Failure mechanics in elastomer toughened polypropylene. Polymer 34: 1684-1694

Jiang W, Tjong SC, Li RKY (2000) Brittle-tough transition in PP/EPDM blends: effects of interparticle distance and tensile deformation speed. Polymer 41: 3479-3482

Kim YS, Chung CI, Lai SY, Hyun KS (1996) Melt rheological and thermodynamic properties of polyethylene homopolymers and poly(ethylene-α-olefin) copolymers with respect to molecular composition and structure. Journal of Applied Polymer Science 59: 125-137

Kontopoulou M, Wang W, Gopakumar TG, Cheung C (2003) Effect of composition and comonomer type on the rheology, morphology and properties of ethylene-α-olefin copolymer/polypropylene blends. Polymer 44: 7495-7504

Lacroix C, Aressy M, Carreau PJ (1997) Linear viscoelastic behavior of molten polymer blends: A comparative study of the Palierne and Lee and Park models. Rheologica Acta 36: 416-416

Lacroix C, Grmela M, Carreau PJ (1998) Relationships between rheology and morphology for immiscible molten blends of polypropylene and ethylene copolymers under shear flow. Journal of Rheology 42: 41-62

Lacroix C, Grmela M, Carreau PJ (1999) Morphological evolution of immiscible polymer blends in simple shear and elongational flows. Journal of Non-Newtonian Fluid Mechanics 86: 37-59

Lee HM, Park OO (1994) Rheology and dynamics of immiscible polymer blends. Journal of Rheology 38: 1405-1425

Lyu S-P, Bates FS, Macosko CW (2000) Coalescence in polymer blends during shearing. AIChE Journal 46: 229-238

Lyu S, Bates FS, Macosko CW (2002) Modeling of coalescence in polymer blends. AIChE Journal 48: 7-14

Martin P, Carreau PJ, Favis BD, Jerome R (2000) Investigating the morphology/rheology interrelationships in immiscible polymer blends. Journal of Rheology 44: 569-583

McNally T, McShane P, Nally GM, Murphy WR, Cook M, Miller A (2002) Rheology, phase morphology, mechanical, impact and thermal properties of polypropylene/metallocene catalysed ethylene 1-octene copolymer blends. Polymer 43: 3785-3793

Minale M, Mewis J, Moldenaers P (1998) Study of the morphological hysteresis in immiscible polymer blends. AIChE Journal 44: 943-950

Minale M, Moldenaers P, Mewis J (1997) Effect of shear history on the morphology of immiscible polymer blends. Macromolecules 30: 5470-5475

Nitta KH, Okamoto K, Yamaguchi M (1998) Mechanical properties of binary blends of polypropylene with ethylene-olefin copolymer. Polymer 39: 53-58

Palierne JF (1990) Linear rheology of viscoelastic emulsions with interfacial tension. Rheologica Acta 29: 204-214

Park CC, Baldessari F, Leal LG (2003) Study of molecular weight effects on coalescence: Interface slip layer. Journal of Rheology 47: 911-942

Patham B, Jayaraman K (2005) Creep recovery of random ethylene-octene copolymer melts with varying comonomer content. Journal of Rheology 49: 989-999

Saltikov SA (1967) The determination of the size distribution of particles in an opaque material from a measurement of the size distribution of their section. In: Elias H (ed) Stereology. Springer-Verlag, New York, pp 163-173

Schnell M, Ziegler V, Wolf BA (2008) Evolution of viscosities and morphology for the two-phase system polyethylene oxide/poly(dimethylsiloxane). Rheologica Acta 47: 469-476

Smoluchowski V (1917) Versuch einer mathematischen Theorie der Koagulationskinetik kolloidaler Lösungen. Z Phys Chem 92: 129-168

Van Der Wal A, Verheul AJJ, Gaymans RJ (1999) Polypropylene-rubber blends: 4. The effect of the rubber particle size on the fracture behaviour at low and high test speed. Polymer 40: 6057-6065

Vinckier I, Moldenaers P, Mewis J (1996) Relationship between rheology and morphology of model blends in steady shear flow. Journal of Rheology 40: 613-631

Vinckier I, Moldenaers P, Terracciano AM, Grizzuti N (1998) Droplet size evolution during coalescence in semiconcentrated model blends. AIChE Journal 44: 951-958

Wang H, Zinchenko AZ, Davis RH (1994) Collision rate of small drops in linear flow fields. Journal of Fluid Mechanics 265: 161-188

Xing P, Bousmina M, Rodrigue D, Kamal MR (2000) Critical experimental comparison between five techniques for the determination of interfacial tension in polymer blends: model system of polystyrene/polyamide-6. Macromolecules 33: 8020-8034

Yang H, Park CC, Hu YT, Leal LG (2001) The coalescene of two equal-sized drops in a two-dimensional linear flow. Physics of Fluids 13: 1087-1106

Yiantsios SG, Davis RH (1990) On the buoyancy-driven motion of a drop towards a rigid surface or a deformable interface. Journal of Fluid Mechanics 217: 547-573

Yokoyama Y, Ricco T (1998) Toughening of polypropylene by different elastomeric systems. Polymer 39: 3675-3681

Yoon Y, Borrell M, Park CC, Leal LG (2005) Viscosity ratio effects on the coalescence of two equal-sized drops in a two-dimensional linear flow. Journal of Fluid Mechanics 525: 355-379

Yu TC (2001) Metallocene plastomer modification of polypropylenes. Polymer Engineering and Science 41: 656-671

Yu W, Zhou C, Bousmina M (2005) Theory of morphology evolution in mixtures of viscoelastic immiscible components. Journal of Rheology 49: 215-236

CHAPTER 6

Rheological and Morphological Properties of Reactively Compatibilized Thermoplastic Olefin (TPO) Blends

Amirhossein Maani, Bruno Blais, Marie-Claude Heuzey, Pierre J. Carreau

Center for Applied Research on Polymers and Composites, CREPEC

Department of Chemical Engineering, École Polytechnique de Montréal

PO Box 6079, Stn Centre-ville, Montreal, QC, Canada H3C3A7

Parts of this work have been presented at the

82nd annual meeting of the Society of Rheology (October 2010)

Published in the *Journal of Rheology* (Volume 56, Issue 3 (2012), Pages 625-647).

Abstract

Thermoplastic olefin blends of polypropylene (PP) and ethylene octene copolymers (EC) were reactively compatibilized by means of functional reactive compounds capable of forming copolymers at the interface. For this purpose, amine functional groups were firstly incorporated into a polypropylene in a solution reaction. The aminated polypropylene was then used as the reactive compatibilizer during melt mixing. Linear viscoelastic measurements showed that the compatibilized blends feature the characteristics of materials in the sol-gel transition, with a power-law behavior for the dynamic moduli at low frequencies. The gel-like behavior was more pronounced in the blend with a high level of compatibilizer (10 wt%). At high frequencies, however, the dynamic properties of all the blends investigated (compatibilized and non-compatibilized) were identical, suggesting that the bulk properties of the blends were not changed by the reactive compatibilization. The presence of a network structure was also confirmed by microscopic observations. A large transient viscosity with a significant and broad overshoot was observed for the compatibilized blends at low shear rate. In addition, the stress of the compatibilized blends relaxed over a much longer time as compared to the non-compatibilized system. The ability of different linear viscoelastic models in predicting the linear viscoelastic behavior of the compatibilized blends was also examined.

I. Introduction

The major goal in blending polymers is to achieve a balanced or even a synergistic combination of favorable properties of the individual constituents. Aside from the properties of the blend

components, the performance of multiphase polymer blends highly relies on the extent of interfacial area and interfacial interaction of the polymer pairs. To obtain optimal properties in immiscible polymer blends, it is a common practice to use surface modifier species that can locate themselves at the interface, promoting the interfacial interaction and reducing the extent of coalescence of the dispersed phases [Majumdar *et al.* (1994); Tan *et al.* (1996); Hale *et al* (1999); Lin *et al.* (2005)]. Generally, two main mechanisms have been proposed for coalescence inhibition using compatibilizers: steric repulsive forces [Sundararaj and Macosko (1995); Lyu *et al.* (2002)], which originate from the compressed copolymers at the interface, and Marangoni stresses, which originate from the interfacial concentration gradient of copolymers displaced during film drainage [Hemelrijck *et al.* (2004)]. Most attention has been devoted to pre-made copolymers for which the control of the copolymer concentration and architecture can be achieved for laboratory studies [Noolandi and Hong (1982); Cigana *et al.* (1996); Horak *et al.* (2002)]. On the other hand, *in situ* formation of a copolymer during reactive blending has been found to be a more practical and a more efficient strategy for polymer blend compatibilization [Majumdar and Paul (1978); Brown (2003)]. The higher effectiveness of reactive compatibilization is due to the fact that in this technique the copolymer may be formed at the interface, hence diffusion of the copolymer towards the interface is not an issue. This advantage becomes more crucial in compatibilizing thermoplastic olefin blends where the interfacial tension between the blend components is often low and, hence, micelle formation between pre-made block copolymers cannot be avoided. Despite the relatively low interfacial tension between polyolefins in the molten state, the solid state polymer-polymer adhesion at the interface can be highly improved by the addition of an appropriate compatibilizer [Dias *et al.* (2008)]. There is also no doubt that the mechanical properties of rubber toughened thermoplastics are highly

dependent on the size distribution of the rubbery particles [Wu (1985); Jiang *et al.* (1998); Chakraborty *et al.* (2008)].

Impact modification of polypropylene (PP) and metallocene-catalyzed ethylene alpha olefin copolymers has been the subject of many recent studies [Nitta *et al.* (1998); McNally *et al.* (2002); Kontopoulou *et al.* (2003)]. As for other types of olefinic systems, these blends feature a low interfacial tension and therefore reactive blending can be considered as the best option for interface modification. Maleic anhydride-grafted polyethylene octene elastomers are commercially produced and mainly used in compatibilization of toughened polyamide systems [Huang *et al.* (2006); Hassan *et al.* (2006)]. The reaction is a typical example of comb-type graft copolymer formation wherein the end groups of monofunctional chains (e.g terminal amines of polyamide) react with the pendant groups of the multifunctional polymer (e.g cyclic anhydrides of the functionalized elastomer). Because of the absence of functional groups, the compatibilization of polypropylene and maleic anhydride grafted elastomers is often accompanied by the functionalization of polypropylene through which active amine groups are introduced into the PP chains [Datta and Lohse (1991); Kaufman *et al.* (2001)]. The reaction of multifunctional polypropylene and elastomer chains results in the formation of a crosslinked copolymer at the interface [Brown (2003)].

If the number of active groups in the multifunctional polymer is well above unity, the *in situ* formed comb-like or crosslinked copolymer creates a highly viscous interface that can notably change the mechanism for the morphology development in these systems [Sailer and Handge (2007); Bhadane *et al.* (2008)]. The rheological behavior of such reactively compatibilized blends has been the subject of only a few studies. Sailer and Handge (2008) studied blends of polyamide-6 (PA) and styrene-acrylonitrile (SAN) copolymer at a 70/30 wt% (PA/SAN and

SAN/PA) composition, compatibilized using maleic anhydride grafted SAN. They found that particularly at high concentration of maleated SAN the low frequency viscoelastic properties of the blends differed from the liquid-liquid emulsion type behavior and the dynamic moduli as functions of the frequency showed a power-law behavior. In some cases they observed non-spherical aggregated domains of the dispersed phase. The solid-like behavior of these blends at low frequency was attributed to the formation of a network-like structure of the dispersed phase. DeLeo and Velankar (2008) also noted an unusual rheological behavior in blends of polydimethylsiloxane (PDMS) and polyisoprene (PI) at a 70/30 wt% (PDMS/PI) composition where the interface was compatibilized and crosslinked in the presence of multifunctional reactive chains. Similar to the observations of Sailer and Handge (2008) the compatibilized blends featured a cluster-like morphology, a gel-like low frequency behavior in dynamic measurements, a high overshoot of the viscosity in the startup of creep experiments, and an enhanced amount of strain recovered after cessation of the shear stress. The rheological behavior of the system was also explained by the formation of a physical network between the large drop clusters.

In our previous work [Maani *et al.* (2011)] on the shear-induced coalescence of thermoplastic olefin blends, we showed that a larger viscosity of the dispersed phase reduced the interfacial mobility and, hence, hindered film drainage and droplet coalescence. It is the objective of the present study to control the morphology of this type of molten polymer blends by reactive compatibilization where the formation of a copolymer can further immobilize the interface and stabilize the morphology. We also aim at interpreting the phenomenon in the light of rheological measurements.

II. Materials and experimental method

A. Materials

The blends consisted of a polypropylene matrix and a metallocene catalyzed ethylene octene copolymer dispersed phase. General characteristics of the neat polymers are given in Table 6.1. Blends with concentrations of 30 wt% and 15 wt% of elastomer (respectively called PP70 and PP85) and compatibilizer concentration of 0 wt% (n), 5 wt% (m) and 10 wt% (h) have been investigated. The polypropylene homopolymer used was Pro-fax 6523 (PP) with a MFI of 4.0 (dg/min) provided by Basell Polyolefins. The ethylene copolymer (EC) was Exxelor VA1840, a commercial maleic anhydride modified ethylene octene copolymer provided by ExxonMobil Chemical with an octene content of 28 wt% and maleic anhydride level of 0.3 wt% .

Table 6.1. Properties of the polymers used.

Material	MFI[(a)] (g/10min)	$\overline{M}_n$ (g/mol) [(b)]	$\overline{M}_w / \overline{M}_n$ [(b)]	η^*(Pa.s) [(c)]
Pro-fax 6523 (PP)	4	82700	5.1	1000
Exxelor VA1840 (EC)	2	46000	2	1700
Orevac CA 100 (PP-MA)	150-200[(b)]	15000	---	60

(a) Melt flow index, measured at (230 ^{o}C, 2.16 kg).

(b) Values reported by the supplier.

(c) Complex viscosity measured at 215 ^{o}C and angular frequency of 26 rad/s (assuming that the Cox-Merz rule is valid, these values give an estimate of the shear viscosity of the materials during mixing).

B. Compatibilization

Since there is no commercially available polypropylene with amine functional groups (capable of reacting with the maleic anhydride groups of the elastomer), a maleic anhydride

grafted polypropylene PP-MA (Orevac CA100, from Arkema) was modified with a di-functional amine (1,12 diaminododecane) provided by Sigma-Aldrich. For this purpose, the PP-MA was firstly dissolved and diluted in boiling xylene at about 135 ^{o}C. An excess amount of diamine was then added to the solution and after 30 min the heater was turned off and the mixture was cooled down to room temperature to precipitate the polypropylene phase. The two phases were then separated by vacuum filtration and the precipitated powder was further washed in boiling ethanol two times to ensure that the excess diamine was removed from the aminated polypropylene (PP-NH_2). The functionalized polypropylene was then dried in a vacuum oven at 80 ^{o}C for 48 h after which no weight change was detected. The schematic of the reactions involved in the process is shown in Figure 6.1. In the solution reaction the diamine is incorporated to the PP-MA chains, leaving a free amine group. The presence of excess amount of diamine in the reaction media helps avoiding homo-polymerization of maleic anhydride grafted polypropylene chains. Subsequently, the formation of imide-linkages between the maleic anhydride grafted EC chains and the aminated polypropylene during the reactive blending results in the formation of the copolymer compatibilizer. As quoted by the suppliers the number of functional maleic anhydride groups on the PP and EC chains are approximately 2, which implies the possibility of covalent bond formation between multiple chains.

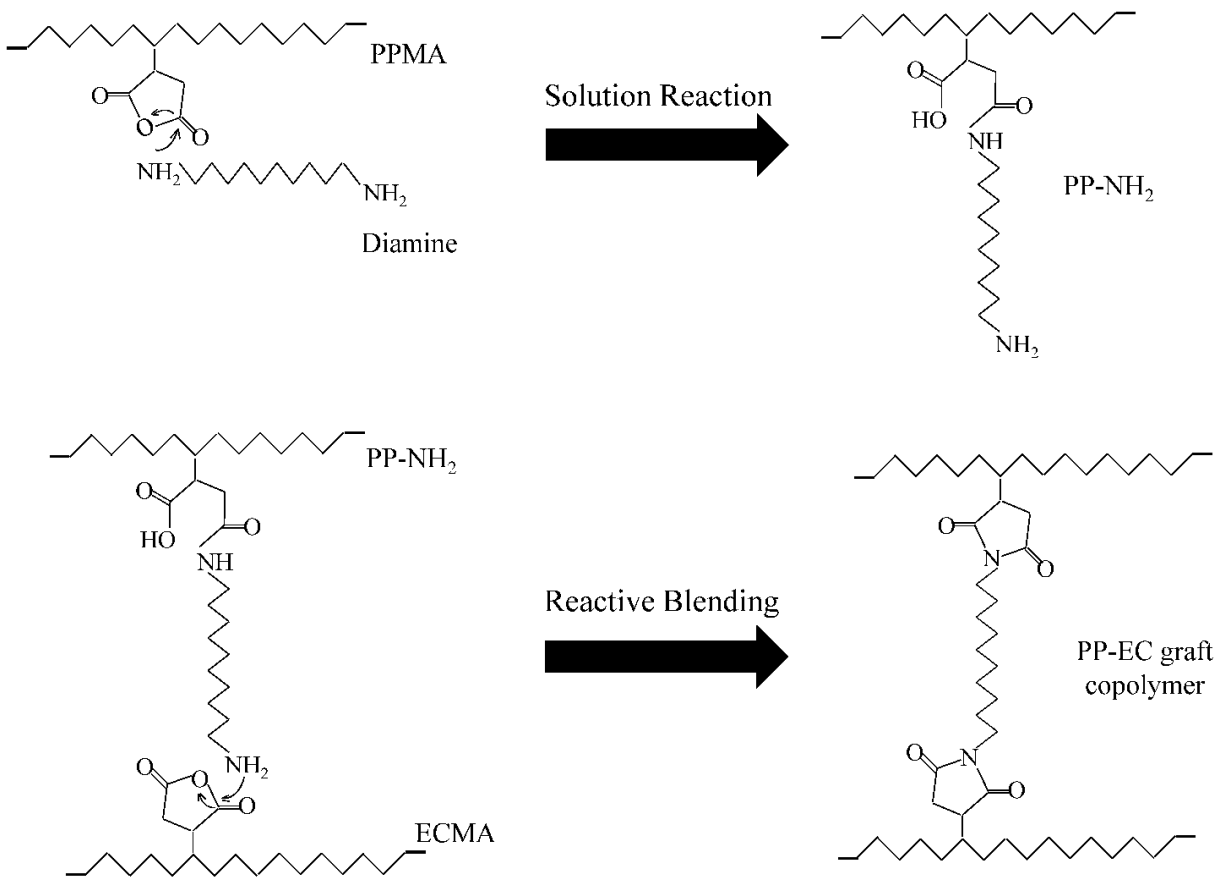

Fig. 6.1. Schematic of the reactions involved in synthesizing the compatibilizer copolymer.

C. Blend preparation

Melt blending of the PP and elastomer was performed in an internal mixer, DDRV501 Brabender (C.W. Brabender Instruments Inc., NJ, USA). The mixing was conducted under a nitrogen atmosphere for 18 min at a set temperature of 215 ^{o}C and using a rotor speed of 50 rpm. For reactive blending, the aminated polypropylene was added to the chamber after 8 min of mixing when a relatively steady-state torque and temperature were established. No indication of a torque increase was detected even 10 min after the addition of PP-NH_2 (end of the mixing), indicating that the formation of the compatibilizer did not influence the processability of the TPO. The presence of traces of C-N-C bonds in the compatibilized samples was confirmed by X-ray photoelectronic spectroscopy (XPS), implying the formation of imide groups during reactive

blending. However, because of the low concentration of the initial NH_2 groups the signal to noise ratio in the spectrum was relatively low; hence results are not shown.

D. Morphology

Two different techniques were used for microscopic observations: scanning electron microscopy (SEM) and atomic force microscopy (AFM). Following imposed shear rate tests, the samples were slowly cooled down and allowed to relax for 1 h. All specimens were firstly planed using a diamond knife-equipped microtome. To cut thin cross sections of the samples after rheological measurements, the specimens were firstly embedded in a mixture of epoxy resin and curing agent and molded at a thickness of 1 mm at room temperature. The AFM imaging was performed using a Nanoscope Dimension™ 3100 microscope (Digital Instrument, CA, USA). Images were captured using intermittent contact imaging (i.e., "tapping mode") and at a scan rate of 1.0 Hz using 125 µm TappingMode™ etched silicon probes (model: ACTA from Applied Nano) with tip radius <10 nm, spring constant of 25-75 N/m and resonant frequency of 200-400 kHz. Imaging was performed using 15-35% tip oscillation damping, which corresponds to a medium force. The images obtained were analyzed using a semi-automatic method via a digitalizing device and SigmaScan Pro© software. To determine the volume-averaged diameter for each sample at least 400 droplets were analyzed, and the Schwartz-Saltykov (1967) correction was applied to account for the fact that the observation plane might not cut the particles through their equator. The specific interfacial area Q (the total area of the interface over the volume of the dispersed phase) was calculated from $Q = 4B/\pi$ [Russ (1986)], in which B is the specific interfacial perimeter (the magnitude of the traced interfaces in the micrograph over

the area of the micrograph). The correlation is valid for any cross section orientation of the images and for any type of non lamellar morphology [Galloway *et al.* (2002)].

E. Rheometry

For rheological measurements, samples were molded into disks of 25 mm diameter using a hydraulic press at 200 ^{o}C and under nitrogen. Samples were first heated for 8 min and then the pressure load was progressively increased up to 3 t and held constant for 2 min. The samples were then cooled to ambient temperature under atmospheric pressure. Rheological measurements were conducted at 200 °C under a nitrogen atmosphere using an MCR-501 rotational rheometer (Anton Paar, Austria) equipped with a cone-and-plate flow geometry of 25 mm diameter and 0.02 rad cone. Stress growth and relaxation experiments were carried out at shear rates ranging from 0.0020 to 0.10 s^{-1}, for which the samples were found to be stable in the geometry and no flow instabilities were detected. Small amplitude oscillatory shear (SAOS) tests were also performed using a strain amplitude of 0.05 within the linear viscoelastic regime. The morphology of the samples was found to be stable during small amplitude oscillatory shear measurements. The neat polymers were also characterized by SAOS tests at 215 ^{o}C.

III. Rheological models

In this work, different rheological models were used to describe the blends behavior. The Palierne model (1990) has proven to be adequate in explaining the dynamic behavior of many kinds of non and compatibilized systems [Graebling *et al.* (1993); Hemelrijck *et al.* (2004); Huo *et al.* (2007)]. The complex modulus of the Palierne model with an isotropic interfacial tension α and a constant interfacial dilatation modulus β' can be expressed as [Jacobs *et al.* (1999)]:

$$G_b^*(\omega) = G_m^*(\omega)\frac{1+3\phi\dfrac{E(\omega,R_v)}{D(\omega,R_v)}}{1-2\phi\dfrac{E(\omega,R_v)}{D(\omega,R_v)}} \tag{6.1}$$

where

$$E(\omega,R_v) = [G_d^*(\omega) - G_m^*(\omega)][19G_d^*(\omega) + 16G_m^*(\omega)] + 4\frac{\alpha}{R_v}[5G_d^*(\omega) + 2G_m^*(\omega)] + \frac{\beta'(\omega)}{R_v}[24\frac{\alpha}{R_v} + 23G_d^*(\omega) - 16G_m^*] \tag{6.2}$$

and

$$D(\omega,R_v) = [2G_d^*(\omega) + 3G_m^*(\omega)][19G_d^*(\omega) + 16G_m^*(\omega)] + 40\frac{\alpha}{R_v}[G_d^*(\omega) + G_m^*(\omega)] + \frac{2\beta'(\omega)}{R_v}[24\frac{\alpha}{R_v} + 23G_d^*(\omega) + 32G_m^*] \tag{6.3}$$

in which ϕ is the volume fraction of the dispersed phase, R_v is the volume averaged droplet radius and G_d^*, G_m^* are the complex moduli of the dispersed and matrix phases, respectively.

To describe the linear viscoelastic behavior of reactively compatibilized systems, Sailer and Handge (2007, 2008) applied a modified version of the Zener model. The mechanical representation of the original Zener model is shown in Figure 6.2a.

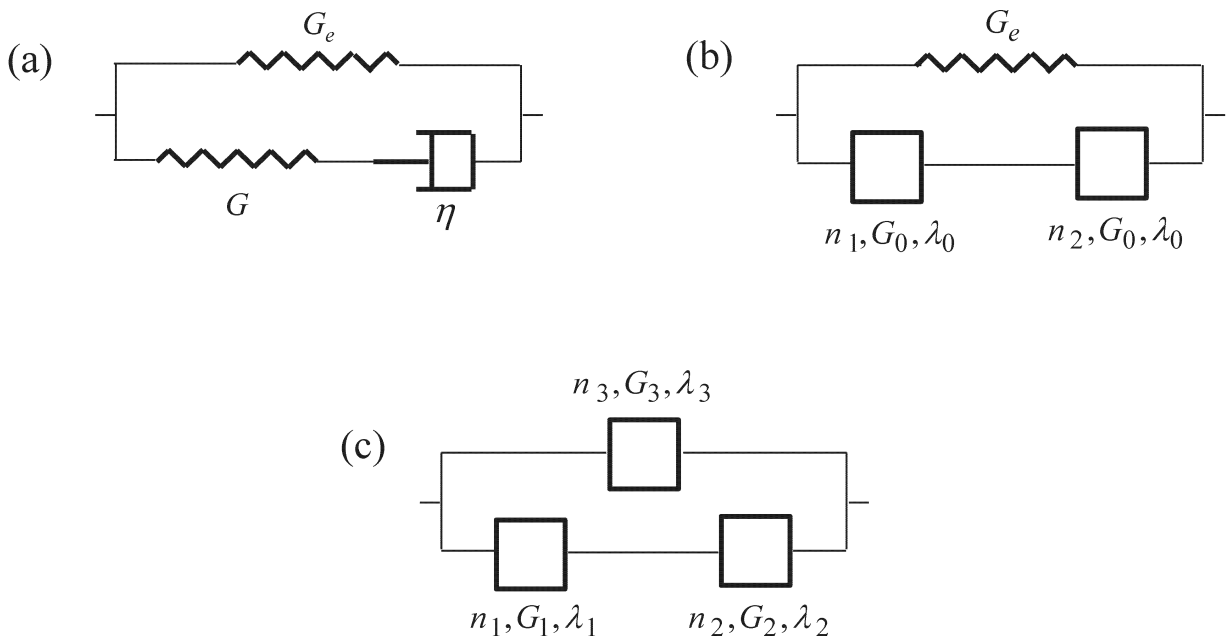

Fig. 6.2. Mechanical representation of a) ordinary Zener model, b) Zener model with two fractional elements [Sailer and Handge (2007)] and c) generalized Zener model (GZM).

This model is a parallel combination of the Maxwell model with a single Hookean spring of elastic modulus G_e. Sailer and Handge (2007) showed that replacing the Maxwell element in this model with so-called fractional elements as shown in Figure 6.2b (identified later as the Zener model with two fractional elements (FE)) could fairly well predict the viscoelastic response of their reactively compatibilized systems. The stress strain relation of the fractional elements includes a fractional order time derivative as below:

$$\sigma = G\lambda^n \frac{d^n}{dt^n}\gamma(t) \tag{6.4}$$

in which σ is the shear stress, γ is the shear strain and G and λ are constants representing the elastic modulus and the relaxation time, respectively. The exponent n can vary between 0 and 1; in the limit of n=0 the equation simplifies to Hooke's law for an elastic solid, while for n=1 the

relation represents Newton's law describing a viscous fluid behavior. It was shown by Schiessel and Blumen (1995) that for fractional values of *n*, the stress-strain relation can be physically achieved by hierarchical arrangements of spring and dashpots with ladders, trees or fractal structures. A good review on the theoretical aspects and applications of constitutive models with fractional derivatives can be found in the work of Friedrich *et al.* (1999).

As we shall see in this article, the Zener model with two fractional elements cannot account for the terminal behavior of the gel-like materials investigated in this study. As such a more general fractional Zener model in which all the three elements are substituted by their fractional counterparts (see Fig.6.2.c) was used. The constitutive equations for the generalized Zener model (GZM) with three fractional elements can be expressed as [Schiessel *et al*. (1995)]:

$$\sigma(t) + \lambda^{(n_1-n_2)} \frac{d^{(n_1-n_2)}\sigma(t)}{dt^{(n_1-n_2)}} = E_0\lambda^{n_1} \frac{d^{n_1}\gamma(t)}{dt^{n_1}} + E_0\lambda^{n_3} \frac{d^{n_3}\gamma(t)}{dt^{n_3}} + E_0\lambda^{(n_3+n_1-n_2)} \frac{d^{(n_3+n_1-n_2)}\gamma(t)}{dt^{(n_3+n_1-n_2)}} \quad (6.5)$$

in which σ and γ are the stress and strain tensors, respectively, and n_1 , n_2 and n_3 are fractional exponents ($n_1 > n_2$) and λ , E_0 and E are defined as:

$$\lambda = (G_1\lambda_1^{n_1} / G_2\lambda_2^{n_2})^{1/(n_1-n_2)} \quad (6.6)$$

$$E_0 = G_1(\lambda_1/\lambda)^{n_1} \quad (6.7)$$

$$E = G_3(\lambda_3/\lambda)^{n_3} \quad (6.8)$$

In the above equations, G_1,G_2, G_3 are relaxation moduli and $\lambda_1, \lambda_2, \lambda_3$ are relaxation times of the fractional elements. The complex modulus is then given by the following expression:

$$G^*(\omega) = E_0 \frac{(i\omega\lambda)^{n_1}}{1+(i\omega\lambda)^{(n_1-n_2)}} + E(i\omega\lambda)^{n_3} \tag{6.9}$$

The mechanical model employed by Sailer and Handge (2007, 2008) (Fig. 6.2b) can be considered as a special case of the above model for two fractional elements. The constitutive equation reduces to:

$$\sigma + \lambda_0{}^{n_1} \frac{d^{n_1}}{dt^{n_1}} \sigma = G_e(\gamma + \lambda_0{}^{(n_1-n_1)} \frac{d^{(n_1-n_1)}}{dt^{(n_1-n_1)}} \gamma) + G_0 \lambda_0{}^{n_2} \frac{d^{n_2}}{dt^{n_2}} \gamma \tag{6.10}$$

The complex moduli can be then written as:

$$G^* = G_e + G_0 \frac{(i\omega\lambda_0)^{n_1}}{1+(i\omega\lambda_0)^{(n_1-n_2)}} \tag{6.11}$$

In our previous work [Maani *et al.* (2011)], we have shown that the transient viscosity of this type of thermoplastic olefin blends could be modeled using a modified version of the Lee-Park model (1994) with in which a slip parameter is incorporated [Lacroix *et al.* (1999)]. For the so-called Lee-Park-Lacroix (LPL) model, the time evolution of the specific surface area of the inclusions Q as well as the components of the anisotropy tensor q_{ij} can be expressed by the following set of coupled differential equations:

$$\frac{d}{dt} q_{ij} = -q_{ki}\kappa_{kj}(1-\frac{\xi}{2}) + \frac{\xi}{2} q_{ki}\kappa_{jk} - q_{kj}\kappa_{ki}(1-\frac{\xi}{2}) + \frac{\xi}{2} q_{kj}\kappa_{ik} + \frac{2}{3}(1-\xi)\delta_{ij}\kappa_{lm}q_{lm} - \frac{Q}{3}(1-\xi)\dot{\gamma}_{ij}$$

$$+(1-\xi)(\frac{\kappa_{lm}q_{lm}}{Q})q_{ij} - d_1 \frac{\alpha}{\eta_m} Q q_{ij} - d_1 d_3 \frac{\alpha}{\eta_m} (\frac{q_{lm}q_{lm}}{Q}) q_{ij} \tag{6.12}$$

$$\frac{d}{dt}Q = -\kappa_{ij}q_{ij}(1-\xi) - d_1 d_2 \frac{\alpha}{\eta_m}Q^2 - d_1 d_3 \frac{\alpha}{\eta_m} q_{ij}q_{ij} \tag{6.13}$$

wherein κ_{ij} are the components of the velocity gradient tensor, and d_1, d_2, d_3 are parameters representing the degree of total relaxation, size relaxation and breakup and shape relaxation, respectively. The slip parameter ξ accounts for non-affine deformation of the particles. In the case of $\xi = 1$, the macroscopic flow causes only rotational and translational motions and the extra stress due to the interfacial tension vanishes. In the limit of $\xi = 0$, affine deformation is described by the lower-convected time derivative, while for $\xi = 2$ the evolution tensor is governed by the upper-convected time derivative.

The stresses are then expressed by:

$$\sigma_{ij} = \eta_m \frac{1 + \frac{3}{2}H}{1-H}\dot{\gamma}_{ij} - \alpha(1-\xi)q_{ij} - P\delta_{ij} \tag{6.14}$$

where,

$$H = \phi \frac{2(\eta_i - \eta_m)}{2\eta_i + 3\eta_m} \tag{6.15}$$

In the above equations, η_i is the viscosity of the inclusions, P is the isotropic pressure and $\dot{\gamma}_{ij}$ are the components of the rate of deformation tensor. The fitting of the model parameters to the experimental data was performed using the nonlinear least square function of the optimization toolbox of Matlab (Matlab software package 7.12.0, The Mathworks Inc.). The Levenberg-Markquardt algorithm was chosen to solve the equations.

IV. Results and Discussion

A. Initial morphology

The microstructures of PP70 blends with different levels of compatibilizer are shown in the AFM micrographs of Figure 6.3. Samples were frozen right after mixing in the internal mixer by submerging them in liquid nitrogen. The presence of non-spherical domains in all the blends shows that the elastomeric phase did not have a sufficient time to relax within the time scale of solidification of the polypropylene phase. The volume-averaged diameter of the dispersed domains were measured to be approximately 1.9, 1.6 and 1.5 μm for the PP70n, PP70m and PP70h blends, respectively. The corresponding specific interfacial areas were calculated to be about 1.3 μm^{-1} for the non compatibilized blend, and 1.7 μm^{-1} for the compatibilized samples. The increase in the compatibilizer concentration from 5 wt% in PP70m to 10 wt% in PP70h does not result in significant morphological changes for these samples. The concentration of the interfacial modifier at which the interface is saturated with copolymer molecules depends on the size of the dispersed phase, tendency of the compatibilizer for micelle formation, molecular structure of the copolymer, etc. A typical value of the critical saturation concentration of the compatibilizer for binary polymer blends with droplet diameter of more than 0.5 μm has been found to be less than 20% of the dispersed phase concentration [Elemans *et al.* (1990); Liang *et al.* (1999); Li and Favis (2002); Huitric *et al.* (2007)]. In the PP70m blend, the concentration of the added PP-NH_2 is around 17% of the dispersed elastomeric phase. Considering that the possibility of micelle formation in reactive compatibilization is low [Brown (2003)], it can be assumed that the interface of the PP70m blend is fairly well covered by the compatibilizer molecules. Hence the PP70h blend that contains a larger amount of compatibilizer should present a similar morphology.

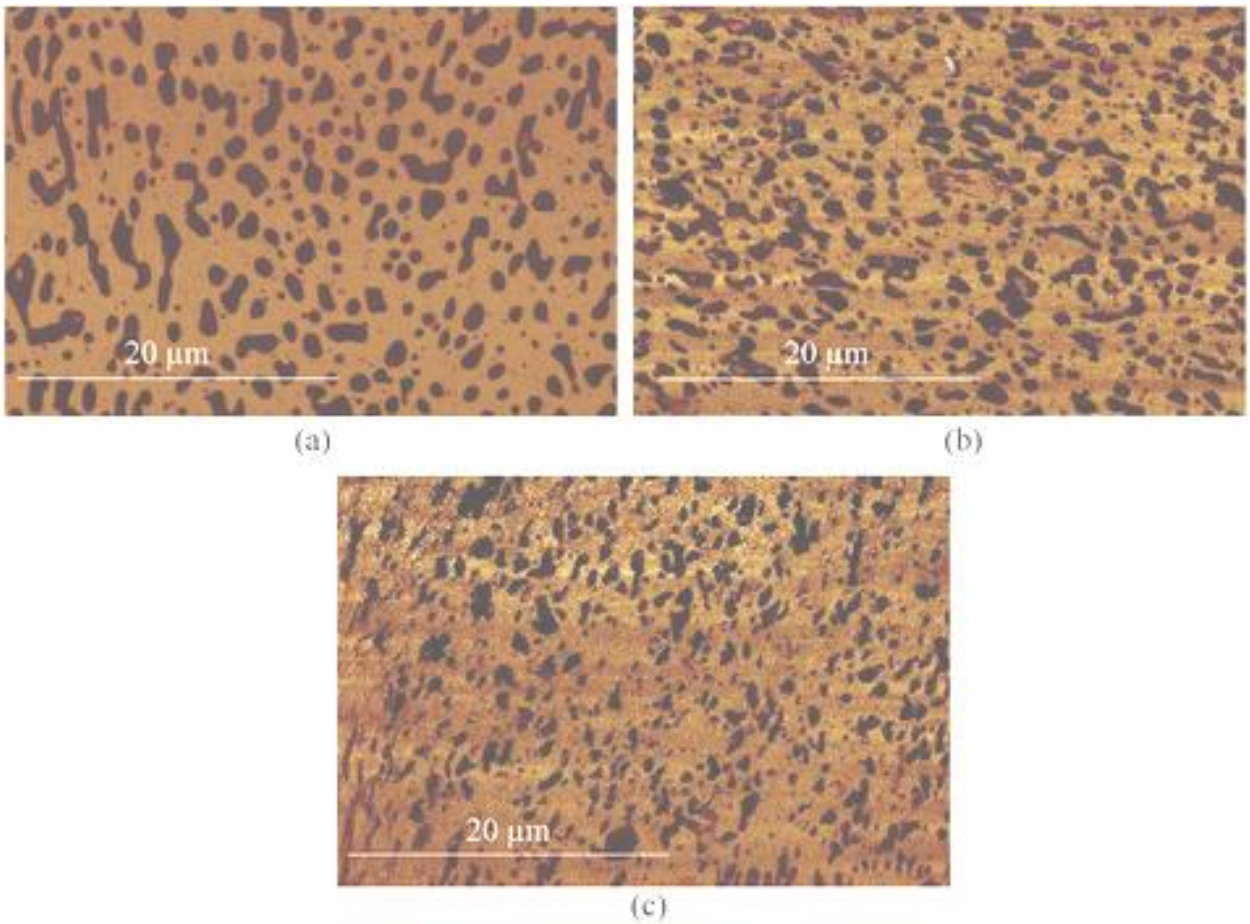

Fig. 6.3. AFM micrographs of PP70 samples quenched right after mixing in the internal mixer: a) PP70n, b) PP70m, and c) PP70h.

Despite the similarity between the frozen morphology of the compatibilized samples collected after mixing in the internal mixer, the microstructures of the blends after molding and conditioning for rheological measurements were found to be quite different. Figure 6.4 shows the morphology of the molded samples which have been squeezed between the gap of the cone and plate flow geometry and heated at 200 ^{o}C for 30 min.

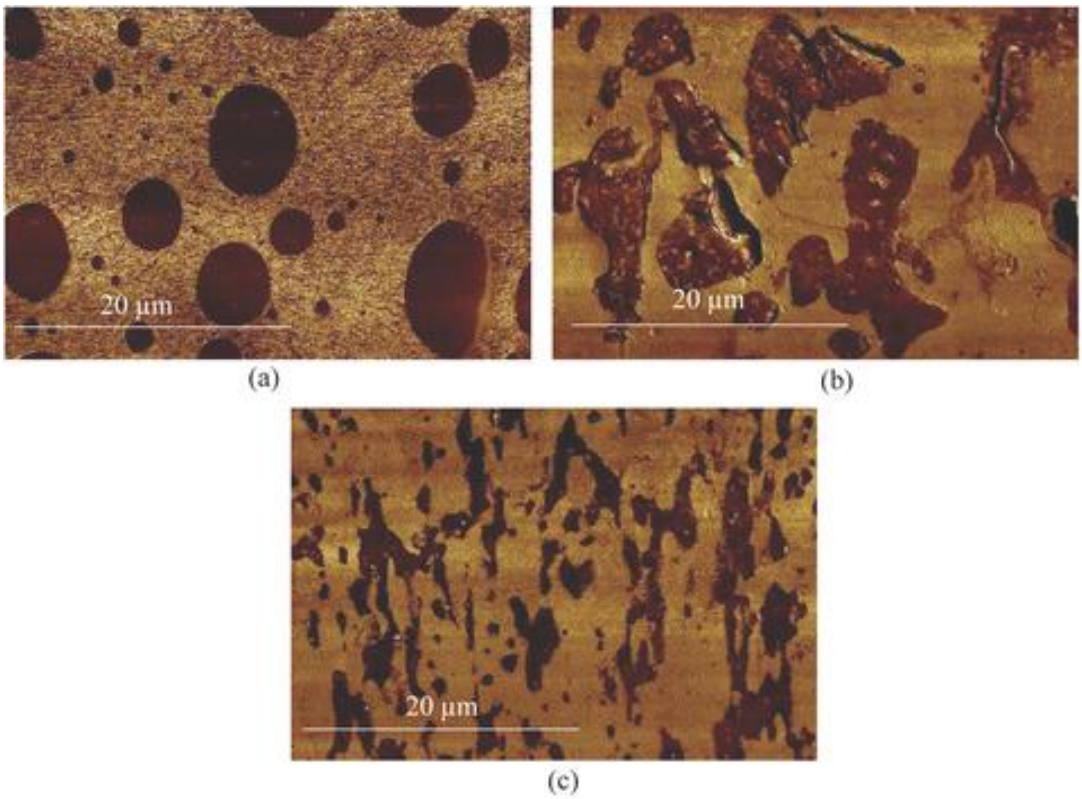

Fig. 6.4. AFM micrographs of PP70 samples after compression molding and squeezing in the gap of the cone and plate geometry at 200 °C for 30 min: a) PP70n, b) PP70m, and c) PP70h.

Even after 30 min of sample annealing, only the droplets of the PP70n blend have recovered their spherical shape (Fig. 6.4a). The morphology of the compatibilized samples features elongated elastomeric domains with irregular shapes which are fairly connected to each other. Compared to the PP70m blend (Fig. 6.4b), the inclusions in PP70h (Fig. 6.4c) are finer and the elongated domains are narrower, providing a larger interfacial area. An estimation of the specific interfacial area *Q* gives values of 0.3 μm^{-1} for the non compatibilized blend (with a droplet size of 6.2 µm), and 0.4 and 0.9 μm^{-1} for the PP70m and PP70h blends, respectively. The retarded interfacial relaxation in the compatibilized blends can be attributed to the improved compatibility at the interface, as well as a reduced mobility of the interface due to the formation of the

compatibilizer. This is in agreement with our previous observations where it was shown that increasing the viscosity of the dispersed phase results in an increased relaxation time of the sheared droplets in similar, but non-compatibilized blends [Maani *et al.* (2011)]. The influence of the formation of the compatibilizer on the rheology of these blends will be discussed in the following section.

B. Dynamic measurements

The storage modulus and complex viscosity of the PP70 blends versus frequency are illustrated in Figure 6.5. With the addition of the compatibilizer, the storage modulus (Fig. 6.5a) at low frequencies shifts to significantly larger values. Compared to the non-compatibilized blend, the storage moduli of the PP70m and PP70h blends at the lowest frequency (0.001 rad/s) are more than 100 and 500 times larger, respectively; however, the storage moduli of all the blends at high frequencies are almost the same. Moreover, none of the compatibilized blends behave as typical binary emulsions at low frequencies where the storage modulus should vary with ω^2. While the slope of the storage modulus of the non-compatiblized blend in the terminal zone (over the first decade) fulfills the criterion of liquid-like behavior (*i.e.* slope of 2), the storage moduli of the PP70m and PP70h blends are found to obey a power-law behavior with very low slopes of 0.4 and 0.2, respectively. The deviation of the viscoelastic properties of the compatibilized blends from the liquid-like behavior is also reflected in the variation of the complex viscosity with frequency (Fig. 6.5b). While at low frequencies the complex viscosity of the PP70n blend tends to level off, the complex viscosities of the compatibilized blends progressively increase as the frequency decreases to low values.

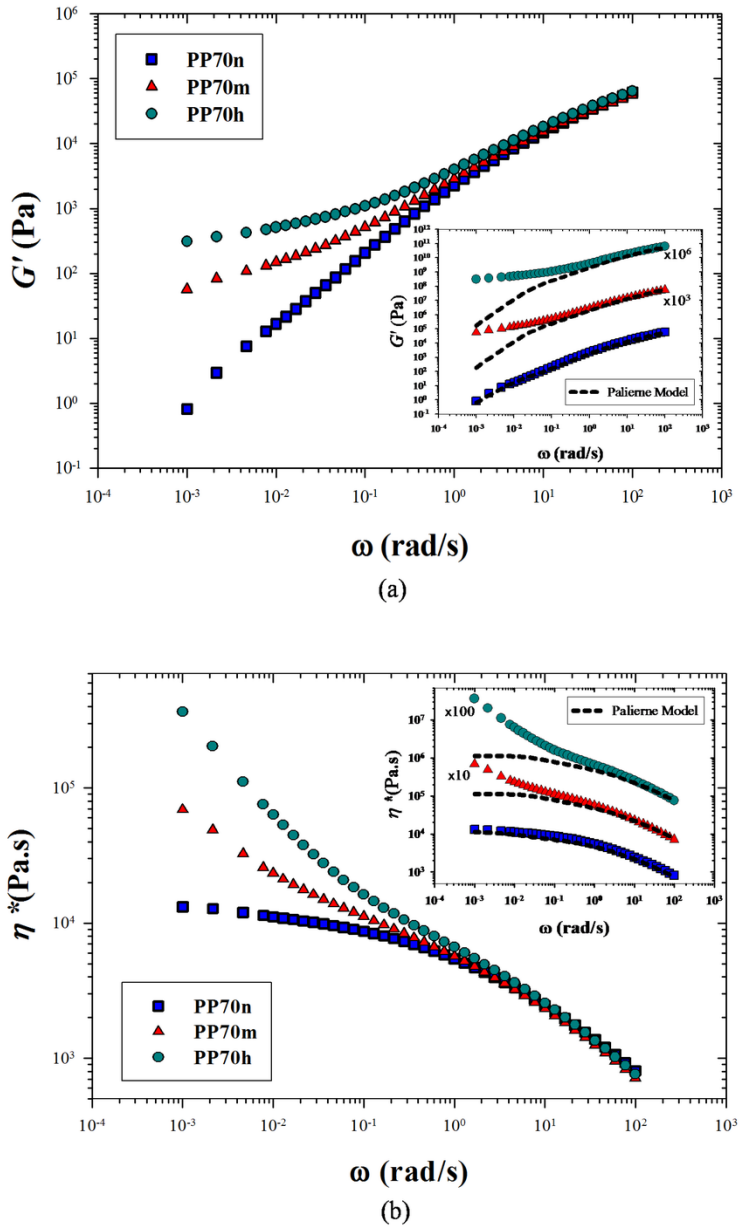

Fig. 6.5. Variations of the storage modulus (a) and the complex viscosity (b) with frequency for the PP70 blends with different levels of compatibilizer. The insertions show the predictions of the Palierne model (data are shifted by factors shown).

Although the increase in the storage modulus at low frequencies in classical compatibilized systems has been reported to be due to increased interfacial area [Graebling *et al.* (1993); Minale

et al. (1997)], the enhanced elasticity observed in the PP70m and PP70h blends cannot be attributed solely to droplet deformation. To better illustrate that the low frequency plateau of *G'* observed in the compatibilized blends is not an extension of the well-known secondary plateau (which is typically observed in binary polymer blends), the Palierne model (1990) was applied. The predictions of the Palierne model for the storage modulus and the complex viscosity of the 70/30 blends are shown in the insertions of Figure 6.5. The behavior of the non-compatibilized sample can be well predicted by the Palierne model using a value of 1.2 mN/m for the interfacial tension (α) and an interfacial dilatational modulus β' of 0.2 mN/m. A low value of β' is expected since for the non-compatibilized case the interfacial tension can be assumed to be isotropic [Riemann *et al.* (1997)]. However, the Palierne model clearly fails in describing the low frequency values of the compatibilized blends (It is worth mentioning that because for the compatibilized blends a true measure of R_v was not obtained, the α / R_v parameter was chosen as the fitting parameter). A similar low frequency behavior of the storage modulus of various immiscible polymer blends has been previously reported. The discrepancy between the predictions of the Palierne model and the experimental data can be explained by considering the morphology of the compatibilized samples shown in Figure 6.4, and taking into account the fact that the Palierne model is restricted to inclusions with equilibrium spherical shape without interparticle interactions. Examining binary blends of polymethylmethacrylate (PMMA) and poly(butylacrylate-co-styrene), Carreau *et al.* (1994) found that above a certain level of the dispersed phase concentration, the storage modulus exhibited an extended plateau at low frequency, which could not be described by the Palierne model. It was shown that by increasing the dispersed phase concentration the particle-particle distance became so small that interparticle forces could attract neighboring particles, bringing them into close contact and finally resulting

in a percolated structure of rubbery domains inside the PMMA matrix. They concluded that the formation of a three-dimensional network of rubbery particles was responsible for the low frequency behavior of the concentrated blends. It is worth noting that the rubbery particles in that system consisted of a crosslinked copolymer of styrene and butylacrylate and were considered as elastic inclusions. Deleo and Velankar (2008), Deleo *et al.* (2011) and Sailer and Handge [(2007); (2008)] also reported the same phenomenon in reactively compatibilized blends with a high concentration (30 wt%) of the dispersed phase. According to them, a percolated structure of the minor phase inside the matrix resulted in a significant upward shift of the storage modulus at low frequencies. These observations are in agreement with the AFM observations discussed in the previous section: the presence of interconnected domains with irregular shapes and extensions of elastomeric phases (more clearly seen in the PP70h blend) confirms the rheological measurements and the gel-type behavior of these systems.

Table 6.2. Fitting parameters of the fractional Zener model with two fractional elements.

Blend	n_1	n_2	λ_0(s)	G_0(Pa)	G_e(Pa)
PP70n	1	0.5	8.9×10^{-1}	9.9×10^{3}	1.0
PP70m	0.7	0.3	4.6×10^{-2}	6.7×10^{4}	65
PP70h	0.7	0.2	3.2×10^{-2}	8.9×10^{4}	4.8×10^{2}

The predictions of the Zener model with two fractional elements for the storage modulus are shown in Figure 6.6. The fitting parameters obtained for the predictions of the two fractional elements Zener model are given in Table 6.2. The experimental data can be fairly well described

by the modified Zener model. Also shown in this figure is the prediction of the Palierne model for the binary blend of a polypropylene matrix with rigid inclusions of infinite elastic modulus. In such a case, the complex modulus is expressed by

$$G_b^*(\omega) = G^*_m\left(\frac{1+3/2\phi}{1-\phi}\right) \tag{6.16}$$

For a dilute suspension in a Newtonian fluid, this is equivalent to the Einstein viscosity equation. As shown, an increase in the storage modulus of the dispersed phase can only shift the high frequency part of the blend storage modulus.

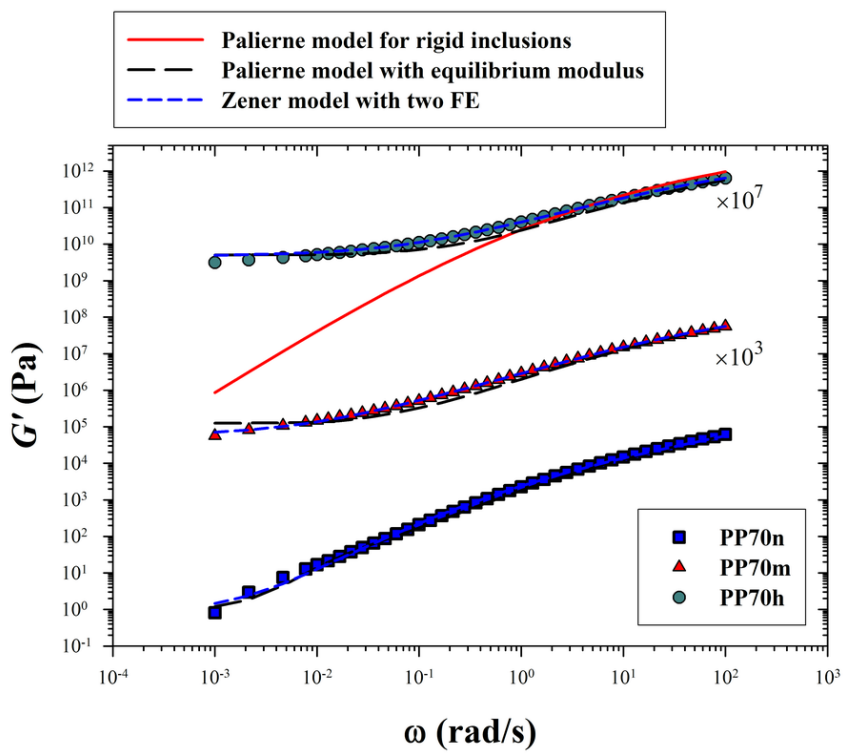

Fig. 6.6. Predictions of the Zener model with two fractional elements (FE) and of the Palierne model with equilibrium modulus for the storage modulus of the PP70h blend (data are shifted by factors shown). The solid line in red represents the behavior of suspensions of rigid particles predicted by the Palierne model for rigid inclusions.

In fact when the blend is subjected to shear, the isolated rigid particles are unable to store mechanical energy; it is only the deformation of a network structure that can introduce a long time relaxation mechanism, giving a broad low frequency plateau.

To account for the low frequency plateau a modified version of the Palierne model was also used wherein an equilibrium modulus was incorporated. The result is also shown in Figure 6.6. Compared to the non-modified Palierne model (Fig. 6.5a) applying the concept of an equilibrium modulus has improved the agreement with the experimental data; however, a qualitative disagreement can still be found in predicting the behavior of the compatibilized blends at very low frequencies both for the modified Palierne and modified Zener models. The discrepancy between the predicted behavior of the storage modulus and the real trend can be better understood by examining the loss tangent values. As shown in Figure 6.7, the loss tangent predicted by the Zener model with two FE and by the modified Palierne model significantly deviate from the experimental data at low frequencies. While these models predict a monotonically decreasing trend for tan δ, the experimental values appear to level off for the compatibilized blends and tend to infinity (liquid-like behavior) for the non-modified system. The deficiency of these models arises from the fact that they always predict a non vanishing equilibrium modulus, hence a solid-like behavior with a zero loss tangent in the terminal zone. The predictions of the generalized Zener model (GZM) for the variation of the loss tangent with frequency are also shown in Figure 6.7. Compared to the other models, the predictions of the GZM model for the low frequency behavior are considerably better, especially for the PP70h blend. The fitting parameters obtained for the different blends are given in Table 6.3. It is worth noting that the sample with a high level of compatibizer shows the smallest values of the n exponent for all the fractional elements, hence a more solid-like behavior.

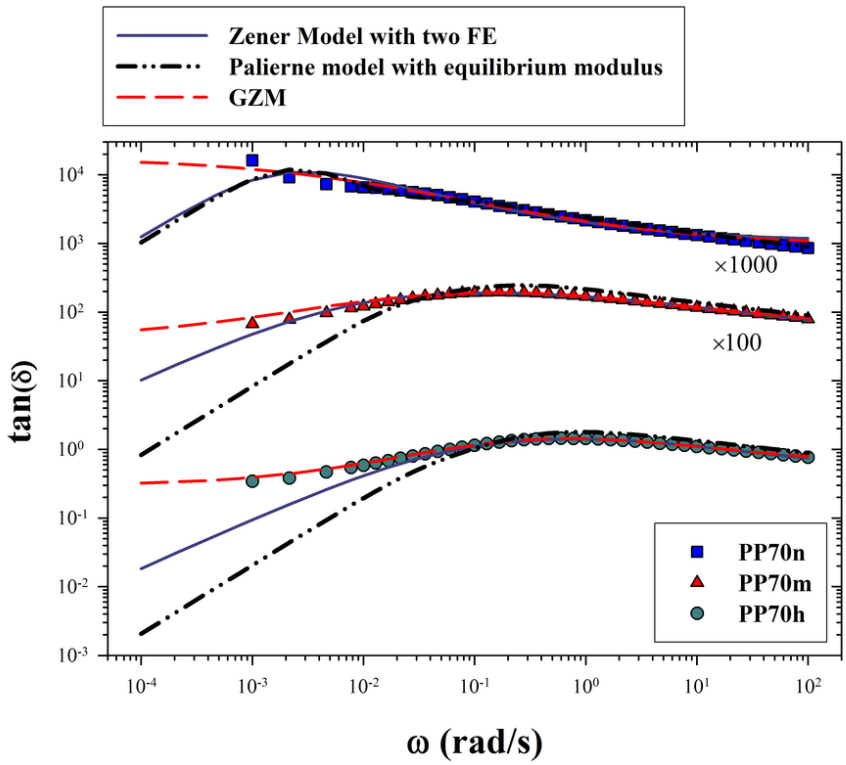

Fig. 6.7. Comparison between the experimental data (shifted by factors shown) and the predictions of the loss tangent versus frequency for the PP70 blends using the modified Palierne model, the Zener model with two FE and its fractional generalization (GZM).

It is also found that in the compatibilized samples, the corresponding relaxation time of the third fractional element (λ_3) is always larger than the relaxation times of the other two elements. Consequently, the response in the terminal zone predicted by the GZM for the compatibilized blends is mainly controlled by the third fractional element, which introduces the longest relaxation mechanism in the system. This can be better realized by a comparison of the n_3 values with the slope of the storage modulus at low frequencies (e.g over the first decade). As mentioned, the storage moduli of the PP70m and PP70h blends at low frequencies obey a power-

law expression with exponents of 0.2 and 0.4, respectively, which are the same as the n_3 values obtained from the GZM.

Table 6.3. Fitting parameters of the generalized Zener model.

Blend	n_1	n_2	n_3	λ_1(s)	λ_2(s)	λ_3(s)	G_1(Pa)	G_2(Pa)	G_3(Pa)
PP70n	0.9	0.4	0.9	2.7	3.6	2.3×10^{-2}	3.2×10^{3}	6.1×10^{3}	1.1
PP70m	0.9	0.4	0.4	95	1.1×10^{3}	4.6×10^{6}	1.6×10^{2}	7.3×10^{2}	2.5
PP70h	0.8	0.3	0.2	9.7	1.5×10^{3}	3.4×10^{7}	1.3×10^{3}	2.2×10^{3}	52
PP85n	1.0	0.5	1.0	2.3	1.7	0.0	3.6×10^{3}	6.3×10^{3}	0.0
PP85h	0.9	0.4	0.2	3.4	6.3	1.8	2.0×10^{3}	7.1×10^{3}	28

The power-law behavior of the storage modulus corresponds to an algebraic decay of the relaxation modulus, which was firstly investigated by Larson (1985) for polymeric liquids. Later Winter and Chambon (1986) and Chambon and Winter (1987) reported a power-law behavior for a cross-linking polydimethylsiloxane system. They showed that for any value of the power-law exponent (n_3 value in the discussion above) less than unity, the material featured the properties of a system in the sol-gel transition, where the zero-shear viscosity goes to infinity, a behavior similar to what was observed in Figure 6.5b. It was also shown by Friedrich and Heymann (1988) that at different stages of a cross-linking reaction, the power-law exponent varies with the reaction time and decreases as the reaction progresses. Later Scanlan and Winter (1991) showed that the exponent *n* increases by diluting the crosslinking media with a non reactive polymer. In fact, smaller *n* stands for a more developed network structure in a cross-linking system. This is

in agreement with the trend observed in this study, where the blend with the highest level of compatibilizer shows the smaller exponents, corresponding to a more interconnected structure as observed in the AFM micrographs.

It has been well established in the literature [Polios *et al.* (1997); Castro *et al.* (2005); Shahbikian *et al.* (2011)] that the formation of interconnected structures or co-continuous phases can cause a gel-like behavior (i.e. significant increase of the storage modulus, with power-law behavior and frequency independency of tan δ). In the case of reactive systems such as the compatibilized blends of this study, the copolymer on the surface of each particle favors the formation of a percolated structure as shown very clearly in Figure 6.4c for the PP70 case. The percolation is not so evident in the case of the lower concentration (PP85) compatibilized blends for which the interparticle interactions are expected to be more limited. The morphologies of the compatibilized and non-compatibilized PP85 blends are shown in Figure 6.8. While all the droplets of the non-compatibilized sample have regained a relaxed spherical shape, some of the elastomeric domains in the compatibilized blend feature irregular shapes, showing again a retarded relaxation behavior. There is no evidence from Figure 6.8b of cocontinuity or percolation for this compatibilized blend. However, the dynamic storage modulus and more so tan δ of the 85/15 blends, illustrated in Figure 6.9, suggest strongly percolation and the formation of irregular elastomeric domains (Fig. 6.8) in PP85h blend and confirm the presence of a copolymer at the interface. The description of the data by the GZM model is excellent as shown in this figure (the fitting parameters are given in Table 6.3). It is obvious that the Palierne model cannot describe the trend for the compatibilized PP85 blend at low frequencies.

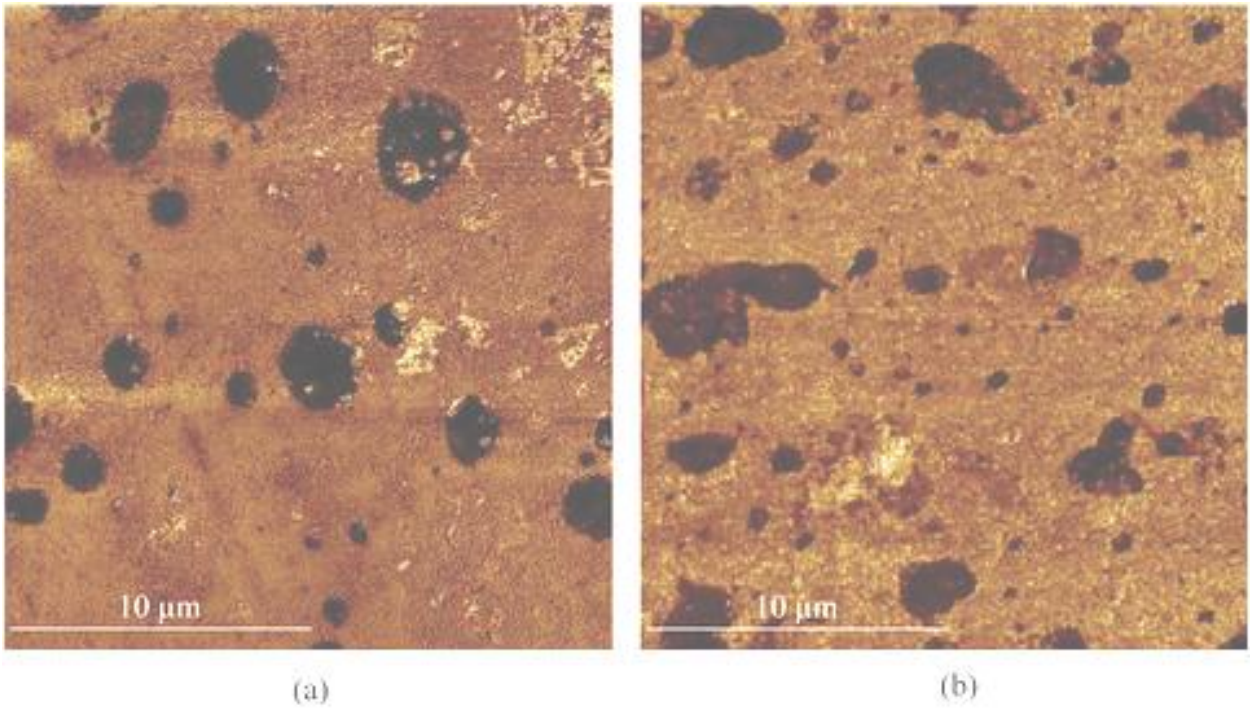

Fig. 6.8. Morphology of the PP/EC (85/15) blends: (a) non-compatibilized (PP85n) and (b) compatibilized with 5wt% PPNH2 (PP85h).

The behavior for the compatibilized PP85 blend is similar to the observations of Asthana and Jayaraman (1999) for low concentrated nylon-6/polypropylene (90/10, w/w) blends compatibilized using maleic anhydride grafted polypropylenes (PPMA) with different levels of maleic anhydride functionalities. An additional relaxation mechanism and significant enhancement in the storage modulus were observed in the blends compatibilized by high functionality PPMA (more than 5 active sites per chain). It was shown by Asthana and Jayaraman (1999) that the incorporation of a non-zero interfacial shear modulus into the Palierne model could better describe the dynamic behavior of their reactively compatibilized systems. To account for the interfacial shear modulus, we have tried the approach of Asthana and Jayaraman (1999) for the compatibilized PP85 blend. However, the use of this generalized Palierne model did not improve significantly the predictions of G' and tan δ for the compatibilized PP85 blend.

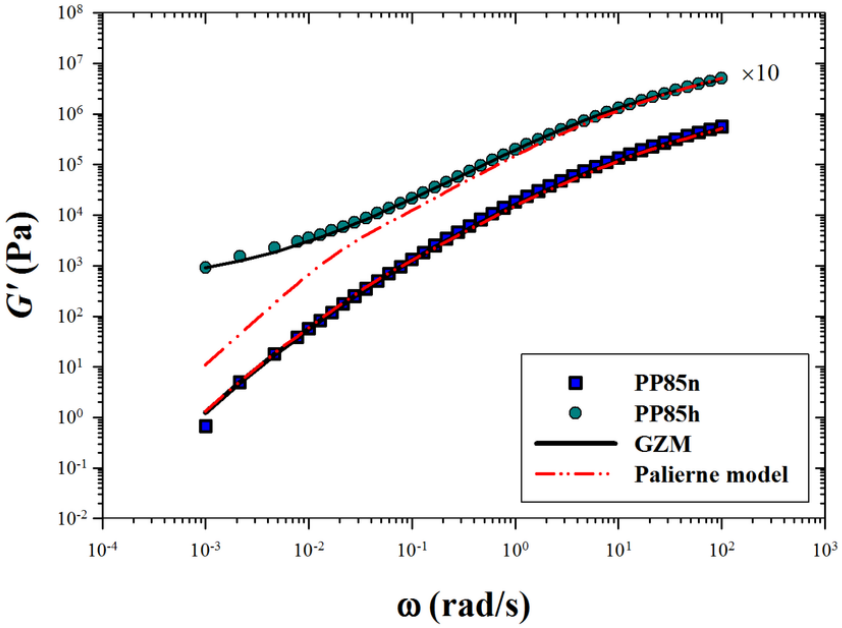

(a)

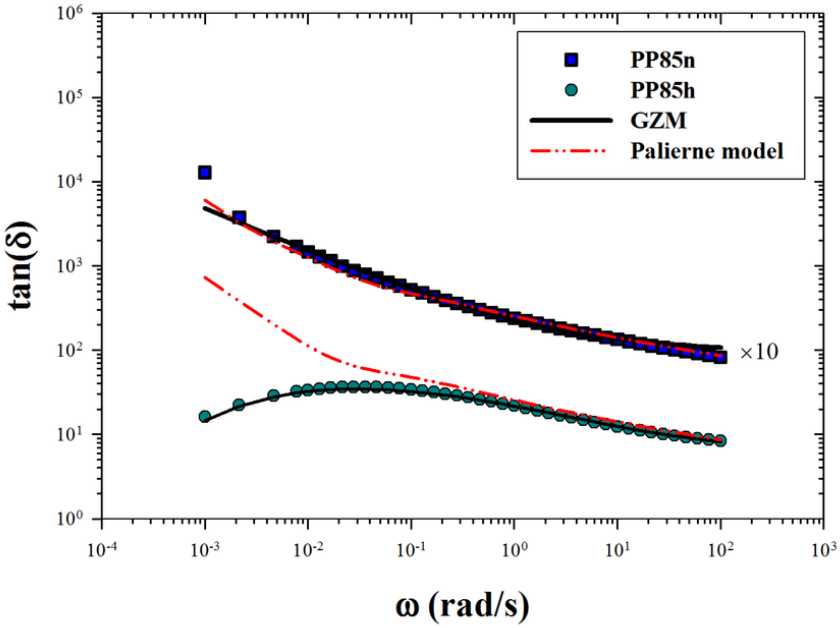

(b)

Fig. 6.9. Storage modulus (a) and loss tangent (b) as functions of frequency for PP85n and PP85h blends, along with the predictions of GZM and the Palierne model.

Similarly to the prediction of the classical version of the Palierne model, the Palierne model with an interfacial shear modulus failed to predict the significant increase of the storage modulus observed in the compatibilized blend.

C. Transient rheological /morphological behavior

The transient (stress growth) shear viscosity of the PP70n and PP70m blends for applied shear rates of 0.01 and 0.1 (s^{-1}) is shown in Figure 6.10. For the PP70h blend, the measurement at 0.1 (s^{-1}) was not possible due to its larger elasticity, which caused secondary flows pushing the sample out of the gap.

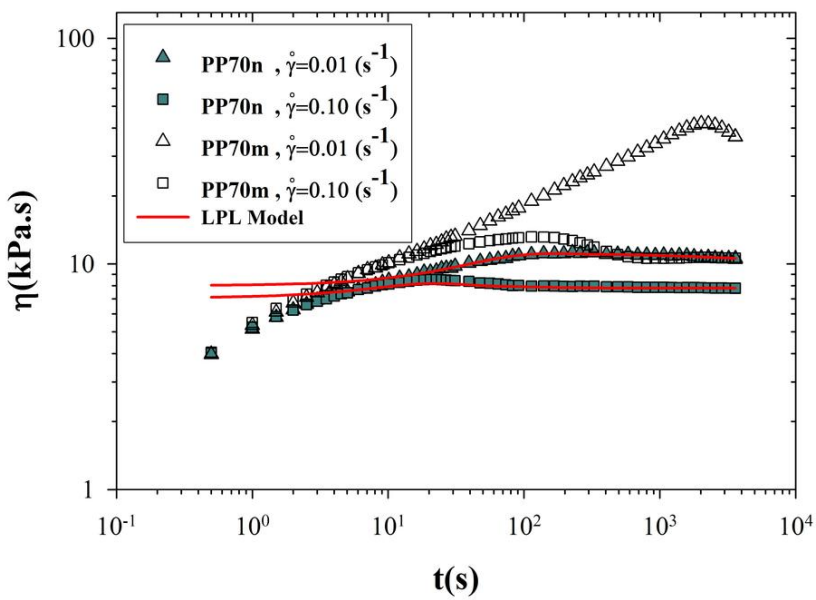

Fig. 6.10. Stress growth data for the PP70n and PP70m blends at $\dot{\gamma} = 0.01$ and $\dot{\gamma} = 0.1\,s^{-1}$. Solid lines represent the predictions of the LPL model for the PP70n blend.

For this system lower shear rates had to be used and the results are reported in Figure 6.11. As shown in Figure 6.10, the transient shear viscosity of the PP70m blend at both shear rates is larger than that of the non-compatibilized sample, in accordance with the complex viscosity at

low frequencies. The predictions of the modified Lee-Park model (LPL) as shown in the figure for the non-compatibilized system are in good agreement with the experimental values, except at short times for which the model is not capable of describing the linear viscoelastic response.

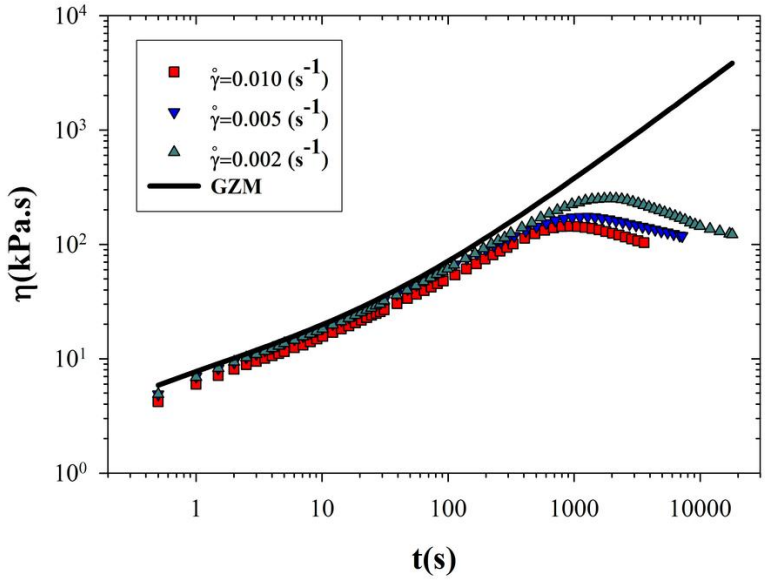

Fig. 6.11. Stress growth data for the PP70h blend at $\dot{\gamma} = 0.01$, $\dot{\gamma} = 0.005$ and $\dot{\gamma} = 0.002\,s^{-1}$, along with the predictions of the generalized Zener model (GZM).

The parameters used to fit the data are provided in Table 6.4. In addition, the model predictions are within 10% the final droplet sizes, d_{v_f} (7.9 μm for shearing at 0.01 s^{-1} and 7.3 μm for shearing at 0.1 s^{-1}). The LPL model, however, fails in predicting the transient viscosity of the PP70m blend both at low and high shear rates (not shown). This was expected since the extra stresses arising from the cross-linked compatibilizer are not accounted for in the LPL model.

Table 6.4. Parameters used for predicting the transient shear viscosity of the PP70n blend.

Shear rate (s^{-1})	d_1	d_2	d_3	ξ
0.01	0.2	0.2	0.7	0.3
0.10	0.4	0.6	0.7	0.0

The influence of a network formation on the magnitude of the transient viscosity is much more significant in the PP70h blend, as seen in Figure 6.11. At 0.01 s^{-1}, the maximum stress value at the overshoot in this sample is almost 13 times larger than that of its non-compatibilized counterpart (144 kPa.s for PP70h compared to11 kPa for PP70n). Figure 6.11 also shows the evolution of the transient viscosities of the PP70h blend at the lowest shear rates (0.002 and 0.005 s^{-1}). Note that fairly large overshoots are still observed, but they appear at very long times as compared to the non-compatibilized blend (Fig. 6.10). Using the fitting parameters presented in Table 6.3 (obtained from the oscillatory data), the transient viscosity in the linear viscoelastic regime can be also described by the GZM using the following equation:

$$\eta^{+}(t) = \int_0^t [E_0 (t/\lambda)^{-\beta} M_{n_1-n_2,1-n_2}(-(t/\lambda)^{(n_1-n_2)}) + \frac{G_3}{\Gamma(1-n_3)}(t/\lambda_3)^{-n_3}]dt \qquad (6.17)$$

in which $M_{x,y}(z) = \sum_{k=0}^{\infty} \frac{z^k}{\Gamma(xk+y)}$ denotes the generalized Mittage-Leffler function and $\Gamma(\ )$ is the Gamma function. As shown in Figure 6.11, the GZM describes the data, but only at the beginning of the stress growth experiment (the first 200 s). At all the deformation rates shearing

brings a non linearity in the stress response, which the GZM cannot describe (we recall that the GZM is a linear viscoelastic model).

The relaxation of the shear stress for the PP70 blends, after cessation of shearing at 0.01 s^{-1}, is shown in Figure 6.12. The initial stress is significantly larger in the compatibilized samples, and the blends relax over a considerably longer time as compared to the non-compatibilized system.

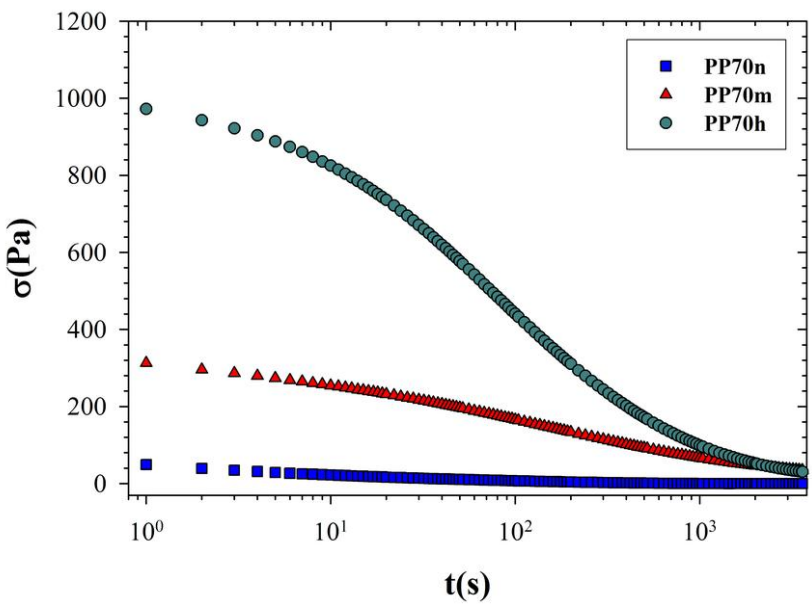

Fig. 6.12. Stress relaxation behavior of the PP70 blends after cessation of shearing at $\dot{\gamma} = 0.01\,s^{-1}$.

This behavior is once more a consequence of the network structure, which incorporates long time relaxation mechanisms into the system. It should be mentioned that the GZM significantly overpredicts the stress relaxation data (results not shown), primarily because of the large deformations imposed during the previous steady shear experiment. Such a deformation during shearing is also accompanied by morphological changes. The morphology of the PP70 blends after 1h of shearing at 0.01 s^{-1} and after 1 h relaxation is shown in Figure 6.13.

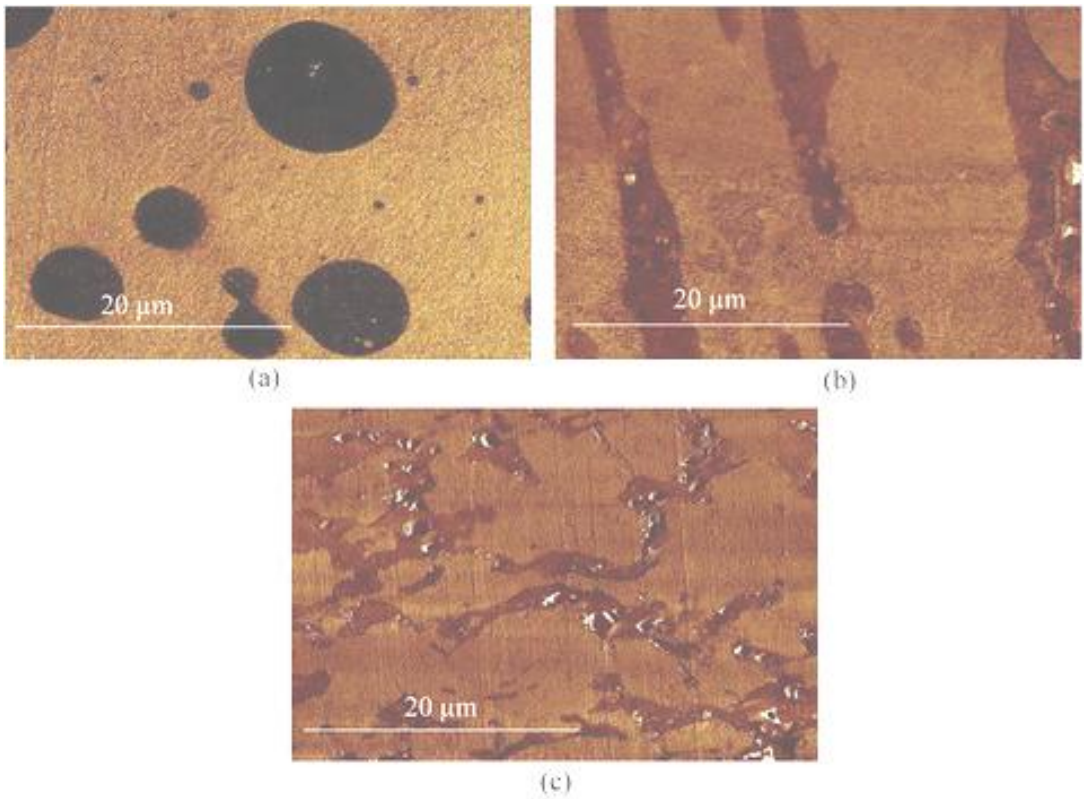

Fig. 6.13. Morphology of blends with different compatibilizer concentrations after shearing at $\dot{\gamma} = 0.01\,\mathrm{s}^{-1}$ for 1h: (a) PP70n, (b) PP70m and (c) PP70h.

Again the non-compatibilized sample (Fig. 6.13a) exhibits a droplet-like morphology, in contrast with the compatibilized blends that show interconnected structures (Figs. 6.13b and c). The specific interfacial area *Q* was found to be 0.2, 0.3 and 0.6 μm^{-1} for PP70n, PP70m and PP70h, respectively. Compared to the non-sheared samples (Fig. 6.4), all the blends have undergone some shear-induced coalescence (the corresponding values for the non-sheared samples are 0.3, 0.4 and 0.9 μm^{-1} for PP70n, PP70m and PP70h, respectively). Even in the PP70h blend, the interfacial area has decreased by almost 30%, similarly to the decrease in the non-compatibilized system. It should be noted, however, that the large decrease of the interfacial area in PP70h results from an increased probability for phase contact and coalescence. This is in accordance

with previous findings in reactively compatibilized polyethylene/polyamide systems [Huitric *et al.* (2007)].

V. Concluding remarks

In this study, the effect of a reactive compatibilizer on the morphology and rheological properties of thermoplastic olefin blends was investigated. All compatibilized blends showed a gel-like behavior at low frequencies. The Palierne emulsion model failed in predicting the low frequency behavior of the compatiblized blends, where significant increases in the storage modulus were observed. It was shown that applying a modified version of the Palierne model and also a viscoelastic Zener model with two fractional elements resulted in better predictions of the storage modulus; however, the latter models could not predict the real trend of the loss tangent at low frequencies. A generalized Zener model with three fractional elements was shown to be capable of describing the linear viscoelastic data over the whole frequency range. The compatibilized blends at low frequencies behave as materials near the gel point, i.e infinite zero shear viscosity and power-law behavior of the storage moduli at low frequencies with exponents less than unity. The LPL model predicted very well the transient rheological and morphological behavior of the non-compatibilized blend, but failed in predicting the transient response of the compatibilized blends. The rheological properties of the reactively compatibilized blends, including gel-like behavior, enhanced viscosity at low shear rate, transient viscosity developed on very long times and retarded stress relaxation, suggest that these blends feature an interconnected structure linked by the compatibilizer copolymer, as confirmed by atomic force microscopy. The results of this work show the interest of rheological methods in characterizing the microstructure of reactive polymer blends.

Acknowledgements

The authors are grateful to Dr. Chopinez and Mr. Quinebeche from Arkema Inc. and Mr. Lemieux from ExxonMobil Chemical for the information and materials provided. We also thank Mrs. W. Leelapornpisit and Mrs. M. Hamdine for their advice and technical assistance in morphological and rheological measurements. This work was supported by a grant of NSERC.

References

Asthana, H. and Jayaraman, K. "Rheology of Reactively Compatibilized Polymer Blends with Varying Extent of Interfacial Reaction." Macromolecules **32**, 3412-3419 (1999).

Bhadane, P. A., Tsou, A. H., Cheng, J. and Favis, B. D. "Morphology development and interfacial erosion in reactive polymer blending." Macromolecules **41**, 7549-7559 (2008).

Brown, B. S. "Reactive compatibilization of polymer blends." Polymer Blends Handbook. Utracki, L. A., Editor. Netherlands, Kluwer Academic Publishers**:** 339-415 (2003).

Carreau, P. J., Bousmina, M. and Ajji, A. (1994). "Rheological properties of blends: Facts and challenges." Progress in Pacific Polymer Science. New York, Springer-Verlag. **3:** 25-40.

Castro, M., Prochazka, F. and Carrot, C. "Cocontinuity in immiscible polymer blends: A gel approach." J. Rheol. **49**, 149-160 (2005).

Chakraborty, P., Ganguly, A., Mitra, S. and Bhowmick, A. K. "Influence of phase modifiers on morphology and properties of thermoplastic elastomers prepared from ethylene propylene diene rubber and isotactic polypropylene." Polym. Eng. Sci. **48**, 477-489 (2008).

Chambon, F. and Winter, H. H. "Linear viscoelasticity at the gel Point of a crosslinking PDMS with Imbalanced stoichiometry." J. Rheol. **31**, 683-697 (1987).

Cigana, P., Favis, B. D. and Jerome, R. "Diblock copolymers as emulsifying agents in polymer blends: Influence of molecular weight, architecture, and chemical composition." J. Polym. Sci., Part B: Polym. Phys. **34**, 1691-1700 (1996).

Datta, S. and Lohse, D. J. "Graft polymers of functionalized ethylene-alpha-olefin copolymer with polypropylene, methods of preparation, and use in polypropylene compositions." United States Patent Exxon Chemical Patents Inc. **4,999,403**

DeLeo, C., Walsh, K. and Velankar, S. "Effect of compatibilizer concentration and weight fraction on model immiscible blends with interfacial crosslinking." J. Rheol. **55**, 713-731 (2011).

DeLeo, C. L. and Velankar, S. S. "Morphology and rheology of compatibilized polymer blends: Diblock compatibilizers vs crosslinked reactive compatibilizers." J. Rheol. **52**, 1385-1404 (2008).

Dias, P., Lin, Y. J., Poon, B., Chen, H. Y., Hiltner, A. and Baer, E. "Adhesion of statistical and blocky ethylene-octene copolymers to polypropylene." Polymer **49**, 2937-2946 (2008).

Elemans, P. H. M., Janssen, J. M. H. and Meijer, H. E. H. "The measurement of interfacial tension in polymer/polymer systems: The breaking thread method." J. Rheol. **34**, 1311-1325 (1990).

Friedrich, C. and Heymann, L. "Extension of a model for crosslinking polymer at the gel point." J. Rheol. **32**, 235-241 (1988).

Friedrich, C., Schiessel, H. and Blumen, A. "Constitutive behavior modeling and fractional derivatives." Rheology Series. Siginer, D. A., De Kee, D. and Chhabra, R. P., Editors. Netherlands, Elsevier **8:** 429-466 (1999).

Galloway, J. A., Montminy, M. D. and Macosko, C. W. "Image analysis for interfacial area and cocontinuity detection in polymer blends." Polymer **43**, 4715-4722 (2002).

Graebling, D., Muller, R. and Palierne, J. F. "Linear viscoelastic behavior of some incompatible polymer blends in the melt. Interpretation of data with a model of emulsion of viscoelastic liquids." Macromolecules **26**, 320-329 (1993).

Hale, W., Keskkula, H. and Paul, D. R. "Compatibilization of PBT/ABS blends by methyl methacrylate glycidyl methacrylate ethyl acrylate terpolymers." Polymer **40**, 365-377 (1999).

Hassan, A., Othman, N., Wahit, M. U., Wei, L. J., Rahmat, A. R. and Mohd Ishak, Z. A. "Maleic anhydride polyethylene octene elastomer toughened polyamide 6/polypropylene nanocomposites: mechanical and morphological properties." Macromol. Symp. **239**, 182-191 (2006).

Hemelrijck, E. V., Puyvelde, P. V., Velankar, S., Macosko, C. W. and Moldenaers, P. "Interfacial elasticity and coalescence suppression in compatibilized polymer blends." J. Rheol. **48**, 143-158 (2004).

Horak, Z., Hlavata, D., Fortelny, I. and Lednicky, F. "Effect of styrene-butadiene triblock copolymer structure on its compatibilization efficiency in PS/PB and PS/PP blends." Polym. Eng. Sci. **42**, 2042-2047 (2002).

Huang, J. J., Keskkula, H. and Paul, D. R. "Elastomer particle morphology in ternary blends of maleated and non-maleated ethylene-based elastomers with polyamides: Role of elastomer phase miscibility." Polymer **47**, 624-638 (2006).

Huitric, J., Moan, M., Carreau, P. J. and Dufaure, N. "Effect of reactive compatibilization on droplet coalescence in shear flow." J. Non-Newt. Fluid Mech. **145**, 139-149 (2007).

Huo, Y., Groeninckx, G. and Moldenaers, P. "Rheology and morphology of polystyrene/polypropylene blends with in situ compatibilization." Rheol. Acta **46**, 507-520 (2007).

Jacobs, U., Fahrlander, M., Winterhalter, J. and Friedrich, C. "Analysis of Palierne's emulsion model in the case of viscoelastic interfacial properties." J. Rheol. **43**, 1495-1509 (1999).

Jiang, W., Liu, C. H., Wang, Z. G., An, L. J., Liang, H. J., Jiang, B. Z., Wang, X. H. and Zhang, H. X. "Brittle-tough transition in PP/EPDM blends: Effects of interparticle distance and temperature." Polymer **39**, 3285-3288 (1998).

Kaufman, L., Cozewith, C., Gadkari, A. C., Dharmarajan, N. R. and Ellul, M. D. "Thermoplastic olefin compositions." United States Patent Exxon Chemical Patents Inc. **6,245,856**

Kontopoulou, M., Wang, W., Gopakumar, T. G. and Cheung, C. "Effect of composition and comonomer type on the rheology, morphology and properties of ethylene--olefin copolymer/polypropylene blends." Polymer **44**, 7495-7504 (2003).

Lacroix, C., Grmela, M. and Carreau, P. J. "Morphological evolution of immiscible polymer blends in simple shear and elongational flows." J. Non-Newt. Fluid Mech. **86**, 37-59 (1999).

Larson, R. G. "Constitutive relationships for polymeric materials with power-law distributions of relaxation times." Rheol. Acta **24**, 327-334 (1985).

Lee, H. M. and Park, O. O. "Rheology and dynamics of immiscible polymer blends." J. Rheol. **38**, 1405-1425 (1994).

Li, J. and Favis, B. D. "Strategies to measure and optimize the migration of the interfacial modifier to the interface in immiscible polymer blends." Polymer **43**, 4935-4945 (2002).

Liang, H., Favis, B. D., Yu, Y. S. and Eisenberg, A. "Correlation between the Interfacial Tension and Dispersed Phase Morphology in Interfacially Modified Blends of LLDPE and PVC." Macromolecules **32**, 1637-1642 (1999).

Lin, B., Mighri, F., Huneault, M. A. and Sundararaj, U. "Effect of premade compatibilizer and reactive polymers on polystyrene drop deformation and breakup in simple shear." Macromolecules **38**, 5609-5616 (2005).

Lyu, S., Jones, T. D., Bates, F. S. and Macosko, C. W. "Role of block copolymers on suppression of droplet coalescence." Macromolecules **35**, 7845-7855 (2002).

Maani, A., Heuzey, M.-C. and Carreau, P. J. "Coalescence in thermoplastic olefin (TPO) blends under shear flow." Rheol. Acta **50,** 881-895 (2011).

Majumdar, B., Keskkula, H. and Paul, D. R. "Mechanical behaviour and morphology of toughened aliphatic polyamides." Polymer **35**, 1399-1408 (1994).

Majumdar, B. and Paul, D. R. "Reactive compatibilization". Polymer Blends. Paul, D. R. and Bucknall, C. B., Editors. New York, Academic Press. **1:** 539-579 (1978).

McNally, T., McShane, P., Nally, G. M., Murphy, W. R., Cook, M. and Miller, A. "Rheology, phase morphology, mechanical, impact and thermal properties of polypropylene/metallocene catalysed ethylene 1-octene copolymer blends." Polymer **43**, 3785-3793 (2002).

Minale, M., Moldenaers, P. and Mewis, J. "Effect of shear history on the morphology of immiscible polymer blends." Macromolecules **30**, 5470-5475 (1997).

Nitta, K. H., Okamoto, K. and Yamaguchi, M. "Mechanical properties of binary blends of polypropylene with ethylene--olefin copolymer." Polymer **39**, 53-58 (1998).

Noolandi, J. and Hong, K. M. "Interfacial properties of immiscible homopolymer blends in the presence of block copolymers." Macromolecules **15**, 482-492 (1982).

Palierne, J. F. "Linear rheology of viscoelastic emulsions with interfacial tension." Rheol. Acta **29**, 204-214 (1990).

Polios, I. S., Soliman, M., Lee, C., Gido, S. P., Schmidt-Rohr, K. and Winter, H. H. "Late Stages of Phase Separation in a Binary Polymer Blend Studied by Rheology, Optical and Electron Microscopy, and Solid State NMR." Macromolecules **30**, 4470-4480 (1997).

Riemann, R. E., Cantow, H. J. and Friedrich, C. "Interpretation of a New Interface-Governed Relaxation Process in Compatibilized Polymer Blends." Macromolecules **30**, 5476-5484 (1997).

Russ, J. C. Practical Sterelogy. New York, NY, Plenum Press (1986).

Sailer, C. and Handge, U. A. "Melt viscosity, elasticity, and morphology of reactively compatibilized polyamide 6/styrene−acrylonitrile blends in shear and elongation." Macromolecules **40**, 2019-2028 (2007).

Sailer, C. and Handge, U. A. "Reactive blending of polyamide 6 and styrene−acrylonitrile copolymer: Influence of blend composition and compatibilizer concentration on morphology and rheology." Macromolecules **41**, 4258-4267 (2008).

Saltykov, S. A. "The determination of the size distribution of particles in an opaque material from a measurement of the size distribution of their section". Stereology. Elias, H. New York, Springer-Verlag**:** 163-173 (1967).

Scanlan, J. C. and Winter, H. H. "Composition dependence of the viscoelasticity of end-linked poly(dimethylsiloxane) at the gel point." Macromolecules **24**, 47-54 (1991).

Schiessel, H. and Blumen, A. "Mesoscopic Pictures of the Sol-Gel Transition: Ladder Models and Fractal Networks." Macromolecules **28**, 4013-4019 (1995).

Schiessel, H., Metzler, R., Blumen, A. and Nonnemacher, T. F. "Generalized viscoelastic models: their fractional equations with solutions." J. Phys. A: Math. Gen. **28**, 6567-6584 (1995).

Shahbikian, S., Carreau, P. J., Heuzey, M.-C., Ellul, M. D., Nadella, H. P., Cheng, J. and Shirodkar, P. "Rheology/morphology relationship of plasticized and nonplasticized thermoplastic elastomers based on ethylene–propylene–diene–terpolymer and polypropylene." Polym. Eng. Sci. **51**, 2314-2327 (2011).

Sundararaj, U. and Macosko, C. W. "Drop breakup and coalescence in polymer blends: The effects of concentration and compatibilization." Macromolecules **28**, 2647-2657 (1995).

Tan, N. C. B., Tai, S. K. and Briber, R. M. "Morphology control and interfacial reinforcement in reactive polystyrene/amorphous polyamide blends." Polymer **37**, 3509-3519 (1996).

Winter, H. H. and Chambon, F. "Analysis of linear viscoelasticity of a crosslinking polymer at the gel point." J. Rheol. **30**, 367-382 (1986).

Wu, S. "Phase structure and adhesion in polymer blends: A criterion for rubber toughening." Polymer **26**, 1855-1863 (1985).

CHAPTER 7

Foaming Behavior of Microcellular Thermoplastic Olefin Blends

Amirhossein Maani[1], Hani E. Naguib[2], Marie-Claude Heuzey[1], Pierre J. Carreau[1]

1- *Department of Chemical Engineering, École Polytechnique de Montréal, PO Box 6079, Stn Centre-ville, Montreal, QC, Canada H3C3A7*

2- *Department of Mechanical and Industrial Engineering, University of Toronto, Toronto, Ontario, Canada M5S 3G8*

Submitted to the *Journal of Cellular Plastics*.

Abstract

The influence of reactive compatibilization on the foaming behavior of thermoplastic olefin (TPO) blends of polypropylene and a metallocene-catalyzed ethylene octene copolymer was investigated. A batch setup was used to foam the samples using carbon dioxide as blowing agent. Solubility measurements were performed to determine the relative amount of gas concentration in the pressurized polymers before foaming. A microscopic method based on the back scattering electron imaging (BEI) technique was used to determine the respective locations of the bubbles and the dispersed elastomeric domains in the polypropylene matrix. It was shown that the bubbles are preferentially formed in the dispersed elastomeric domains. A clear relationship was established between the microstructure of the blends prepared with different levels of compatibilizer and the final cellular morphology of the microcellular TPO foams. The initial morphology of the blends was also altered by quiescent coarsening as well as shear-induced phase coalescence, and the impact of the morphological transitions on the cellular structure of the resulting foams was investigated. Dynamic shear and transient elongational measurements were performed to characterize the viscoelastic behavior of the TPOs. It was shown that the addition of a compatibilizer resulted in enhanced viscoelastic properties at low frequencies as well as increased levels of strain hardening, especially at low strain rates. The reactive compatibilization could significantly improve the melt foamability through control of the blend microstructure as well as enhancement of the melt rheological properties.

I. Introduction

Since the development of the microcellular foaming process at MIT (Massachusetts Institute of Technology) [1], several research projects have intended to control the cellular structure of thermoplastic foams by exploring the role of different processing parameters [2-5] and material factors [6-8]. The foaming behavior of polymer blends has been, however, the subject of only a small portion of these studies. Earlier investigations on the nucleation mechanisms in microcellular foaming of polymer blends go back to the work of Ramesh et al. [9] who investigated the foaming behavior of blends of polystyrene and polybutadiene. They proposed a heterogeneous nucleation mechanism, which was based on the presence of pre-existing microvoids created during the cooling stage after melt blending. It was argued that due to the higher thermal expansion coefficient of the polybutadiene phase, cooling produced thermal stresses that propagate into the rubbery particles and resulted in the formation of cavities, which could serve as initial nuclei. It was shown that the cell size distribution followed the same pattern as the size distribution of the rubber particles. The proposed nucleation model based on this cavitation mechanism also gave a good prediction for the variation of cell density with the saturation pressure and foaming temperature [10]. Another mechanism, which has been proposed in the literature, is based on the classical nucleation theory for heterogeneous systems [11, 12]; the main concept is that the minimum energy needed for the formation of critical nuclei at the polymer-polymer interface is diminished, and hence the nuclei formed at the interface are thermodynamically more stable [13-18].

Beside the interfacial mechanisms (i.e. nucleation in the pre-existing cavities as well as the reduction of the required energy for cell formation at the interface), the bulk properties of the

phases can also contribute to the preferential localization of the initial nuclei. Ruckdäschel et al. [19] reported that addition of a small amount (2 wt%) of a poly(dimethyl-phenylene ether), PPE, to a poly(styrene-acrylonitrile) increased the nucleation density by 100 times; this was attributed both to the diminished energy of cell nucleation at the interface as well as the higher level of gas solubility in PPE compared to the polystyrene copolymer matrix. Yokoyama and Sugiyama [20] investigated the foaming behavior of a blend of polystyrene and dispersed nanodomains of CO_2-philic fluorinated block copolymers. It was shown that depressurization at a temperature well below the glass transition temperature (T_g) of the polystyrene matrix could localize the cell nucleation solely in the dispersed phase and result in the formation of a uniform nanocellular structure. It was shown that as the foaming temperature approached the T_g of polystyrene, micron-sized cells started to appear, implying that the cell nuclei were formed in both continuous and dispersed phases. Similar observations were also reported by Otsuka et al. [21] in a blend composed of a polystyrene matrix and polymethylmethacrylate (PMMA) nano-sized dispersed domains. The results suggested that at low temperature nucleation and growth were confined in the PMMA domains, although the respective locations of the PMMA domains and the bubbles were not directly determined by microscopic observations.

Apart from nucleation, polymer blending can also influence the cellular structure during the cell growth stage. Depending on the phase in which the nuclei are born, the cell walls may experience different surface tensions and hydrodynamic forces; moreover the rate of gas diffusion into the growing cells is affected by the media in which the cells are located. The role of melt blending in controlling the cell growth of polymeric foams has not been thoroughly addressed in the literature; examples of studies on this subject can be found in the work of Park et al. [22], Van Nuffel et al. [23], Spitael et al. [24] and Stange et al. [25]. The emphasis in all

these studies is on the enhanced elongational viscosity due to the addition of a high melt strength polymer, which reduces sag, prevents cell coalescence and consequently results in larger cell densities.

Due to the unique properties of thermoplastic olefins (TPOs), this class of polymer blends has gained a great interest in the polymer processing industry. However, only a handful of studies can be found on the foaming behavior of these systems. Santoni et al. [26] and Guo et al. [27] investigated the effects of rheological properties and of key injection parameters on the cell formation and surface quality of TPO injected foamed parts. Nemoto and Ohshima [28] showed that the cell size and cell orientation can be controlled by the microstructure of the dispersed rubber phase in blends of polypropylene and styrenic elastomers foamed during a batch physical foaming process. More recently Kim et al. [14] showed that the elastomeric phase enhanced the cell density through the heterogeneous nucleation mechanism; however, in their study, the size change of the dispersed rubber particles was accompanied by a change in the viscosity of the polymers used and hence beside the morphological factors, the foaming behavior was also influenced by the rheological properties and possibly by gas solubility and diffusivity parameters. Moreover, the relative locations of the dispersed phase and the bubbles were not microscopically determined.

In this study we aim at controlling the cellular structure of thermoplastic olefin blends of polypropylene and metallocene-catalyzed ethylene octene copolymer. A reactive compatibilization method [29] is employed to achieve finer morphology, enhanced viscoelasticity and consequently improved foamability. Samples are also subjected to quiescent coarsening and shear-induced phase coalescence to further investigate the effect of the dispersed phase morphology on the final cellular structure. In this approach the material properties of the

constituents remain intact and hence this technique can be employed in future modeling studies concerning nucleation and growth in polymer blends. The results are analyzed in the light of microscopic observations enabling us to determine the respective location of bubbles and blend constituents.

II. Experimental

A. Materials and preparation methods

The TPOs were prepared using a polypropylene (PP) homopolymer (Profax 6523 from Basell Inc.) and a metallocene-catalyzed ethylene octene copolymer (EC) (Exxelore VA1840 provided by ExxonMobil Chemical). The polypropylene used is a linear polymer with a melt flow index of 4 dg/min (230 ^{o}C, 2.16 kg). The elastomer is a short chain branched copolymer with a melt flow index of 2 dg/min (230 ^{o}C, 2.16 kg) and is consisting of 28 wt% randomly distributed octene comonomer and 0.3 wt% maleic anhydride grafted molecules. It should be noted that due to the metallocene-catalyzed polymerization, sparse long chain branches are also incorporated in the copolymer structure [30-32]. For reactive compatibilization, a maleic anhydride-grafted polypropylene (Orevac CA 100, provided by Arkema with a maleic anhydride level of 3 wt%) was firstly aminated with an aliphatic diamine (1,12 diaminododecane provided by Sigma-Aldrich) in a solution reaction and further used as a reactive compatibilizer during melt blending. Details of the amination process can be found elsewhere [29]. Blends of composition 60/40 PP/EC w/w and compatibilizer concentrations of 0, 5, 10 wt% (respectively called PP60n, PP60m and PP60h) were prepared using a Brabender batch mixer (DDRV501, C.W. Brabender Instruments Inc., USA) at a set temperature of 215 ^{o}C under nitrogen. The mixing time and rotor speed were set at 18 min and 50 rpm, respectively. Samples were then molded into disks of 25 mm diameter and thicknesses of 2.5, 1.5 and 1 mm for further rheological and foaming

experiments. Molding was performed using a compression hydraulic press at 200 ^{o}C and a maximum pressure of 3 tons.

B. Rheological experiments

Dynamic and transient shear experiments were conducted using a MCR-501 rotational rheometer (Anton Paar, Austria) equipped with a parallel-plate flow geometry of 25 mm diameter. The linear viscoelastic properties were characterized in a frequency range of 0.01 and 100 rad/s, at a maximum strain amplitude of 0.05. Before measurements, samples were firstly heated at 200 ^{o}C in order to melt the crystalline polypropylene phase and then cooled down to 155 ^{o}C since foaming of the molten samples was also conducted at this temperature. To investigate the influence of phase coalescence on the final cellular morphology, a non-compatibilized blend was subjected to annealing (at 200 ^{o}C for 30 min), which results in quiescent coalescence. The influence of shear-induced phase coalescence was investigated by shearing the annealed sample at a strain rate of 0.01 s^{-1} at 200 ^{o}C for 20 min; at the end of the shearing 15 min annealing was applied for drop relaxation.

Extensional measurements were performed using the SER-HV-A01 dual windup extensional geometry (Xpansion Instruments, LLC, USA) hosted on an ARES rheometer (TA Instruments/Rheometric Scientific, USA). Rectangular samples with dimensions of approximately 18 mm x10 mm x1 mm were cut from the molded disks and placed onto the drums by means of securing clamps. Measurements were performed at Hencky strain rates of 0.025, 0.1 and 1 s^{-1} and a temperature of 155 ^{o}C. Prior to sample loading the oven was heated at a set temperature of 185 for 5 min. Loaded samples were first heated at 185 ^{o}C for 90 s and then cooled down to 155 ^{o}C; a sufficient time (2 min) was then elapsed prior to starting the test to

ensure equilibrium temperature within the specimen. All rheological measurements were performed under a nitrogen atmosphere to avoid thermal degradation.

C. Sorption measurements

The diffusivity and solubility of CO_2 in different samples were determined gravimetrically using a Rubotherm magnetic suspension balance (Rubotherm GmbH, Germany). In this technique the mass change of the sample due to gas absorption is recorded contactlessly via transmitting the suspension force from the pressure chamber to the magnetic microbalance positioned out of the chamber at ambient atmosphere. Technical details of this measuring method can be found in the work of Dreisbach and Losch [33]. Prior to the sorption process, the chamber was evacuated and the sample weight under vacuum ($P \approx 0$) at a set temperature T was recorded as $W(0,T)$. The chamber was then pressurized with the compressed CO_2 and the weight change of the sample was monitored until equilibrium was reached. To account for the buoyancy effect, the volume of the polymer (V_p) at the desired temperature and pressure was obtained using a *PVT* apparatus. The amount of gas dissolved into the sample was then determined as:

$$W_g = W(P,T) - W(0,T) + \rho_{CO_2}(V_B + V_p) \quad (1)$$

in which $W(P,T)$ is the balance reading at pressure P and temperature T , variables ρ_{CO_2} and V_P are the density of CO_2 and the non-swelled volume of the sample at this condition, respectively, and V_B is the volume of the specimen holder. It should be mentioned that in these measurements the contribution of the swollen volume of the sample to the buoyancy force was neglected. The gas solubility was then calculated by dividing the weight gain during sorption (W_g) over the initial mass of the polymer.

D. Foaming

Foams were produced using a batch foaming setup shown in Fig. 1; the pressure chamber is hosted on an MCR-501 rheometer (Anton Paar, Austria) equipped with a C-ETD 300 heating device.

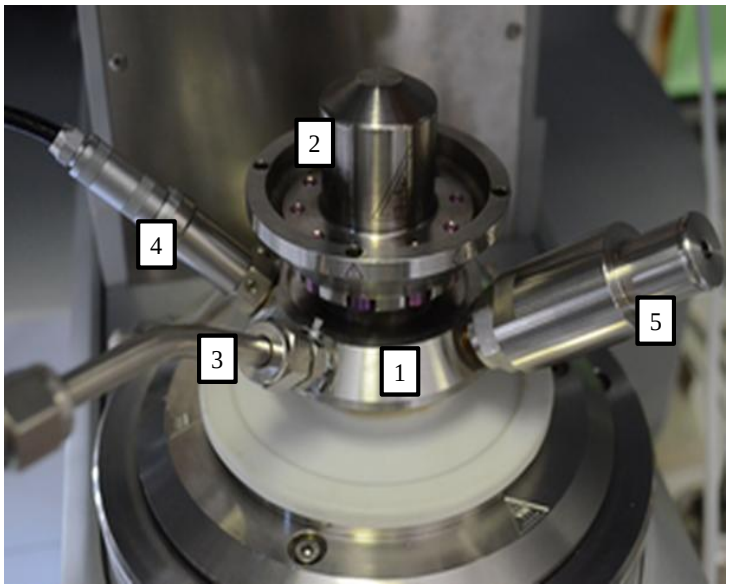

Fig. 7.1. Pressurizing setup used for foaming experiments: 1) high pressure chamber, 2) covering flange, 3) gas inlet (outlet), 4) temperature sensor connection, 5) safety relief outlet.

The connections include a temperature sensor, a safety relief outlet and a gas conduit used for pressurizing/depressurizing the chamber. To examine a wider range of processing conditions met in industry two different foaming methods were used: temperature-induced foaming and pressure-induced foaming. In the temperature-induced foaming method, samples were firstly saturated with CO_2 at room temperature and 4.5 MPa; saturation was conducted in the cylindrical pressure cell of 25 mm diameter. After 12 h the pressure was released and following a 1 min delay the gas-laden sample was submerged in a bath of glycerin at a temperature of 155 ^{o}C. After 15 s the specimen was removed from the glycerin bath and quenched in iced water. In the

pressure-induced foaming method, samples were firstly heated at a temperature of 200 ^{o}C for about 20 min to melt the crystalline phase of the polypropylene. After that the temperature was set at 155 ^{o}C and 1 h was elapsed to ensure temperature equilibrium within the specimen. Molten samples were then pressurized with CO_2 for 6 h and were foamed by instantaneous pressure release.

E. Microscopy

For microscopic observations the unfoamed and foamed specimens were firstly cut using a cryogenic Leica Jung (RM 2165) microtome to create a plane surface. Considering that the foamed TPOs consisted of three different phases (polypropylene matrix, elastomeric phase and bubbles) a new microscopic method was employed to distinguish the different matters. A field-emission gun scanning electron microscope (JEOL 7600F FEG) capable of backscattered electron imaging (BEI) was used for this purpose. Compared to conventional secondary electron imaging (SEI), in BEI the electrons of the incident beam penetrate much deeper and are ejected back to the detector after an elastic interaction with the sample's atoms. The brightness in the scanned images changes with the number of backscattered electrons that reach the detector and is a function of the atomic number of the sample, surface topography as well as the interaction volume of the incident beam throughout the sample. BEI can be used to provide contrast as a function of both elemental composition and surface topography of the sample. Although SEI is capable of high resolution imaging of the fine surface topography, and hence can be used to obtain a contrast between the voids and the surrounding polymer domains, it cannot distinguish the TPO components, which are at a same height on the sample's surface. Therefore, in order to obtain an acceptable level of contrast between the three different phases, samples were scanned using the BEI technique. It was found that after few minute exposure of the sample's surface

with high energy electrons (emitted at 5 kV and 11 mA), the dispersed elastomeric phases appear as milky white domains in a grey background of the polypropylene matrix. Although the atomic structure of the PP and EC phases are the same, the exposure of the samples to high energy electrons can cause superficial phase transitions that create contrast. The origin of these transitions is unclear at this point. This could be either due to the low melting point of the EC phase (61 ^{o}C compared to 161 ^{o}C for PP) or degradation of the EC elastomer under the high current. The accuracy of the technique was however verified by comparing BEI micrographs of the unfoamed binary systems with those obtained using SEI or AFM. The resulting SEM images were further analyzed using a semi-automatic method via a digitalizing device operated with SigmaScan Pro© software. The volume-averaged cell diameters were obtained by analyzing a minimum of 300 bubbles, and the Schwartz-Saltykov [34] correction was applied to account for the fact that the observation plane might not cut the particles through their equator. The number of cells per unit volume of the foamed specimen (*N*, or cell density) was then estimated from the equation $N = \left(nM / A\right)^{3/2}$ where *n* is the number of cells in the analyzed micrograph, *A* is the area of the micrograph and *M* is the microscope magnification. The specific interfacial area *Q* (the total area of the interface over the volume of the dispersed phase) was calculated from $Q = 4B / \pi$ [35], in which *B* is the specific interfacial perimeter (the magnitude of the traced interfaces in the micrograph over the area of the micrograph). The analysis is applicable to any cross-section orientation of the images and for any type of non-lamellar morphology *et al.* [36].

III. Results and discussion

As mentioned in Section II.C, in this work the foaming behavior of the materials was investigated through two different foaming processes. In the first part of the results and

discussion (Section III.A) the foaming behavior of the TPOs as well as of the neat components are examined by using the temperature-induced foaming method. The initial blends morphologies were changed through reactive compatibilization and also phase coalescence induced either by quiescent annealing or shear flow. Section III.B is devoted to the foaming behavior of the TPOs via pressure-induced foaming. Considering that in this process, foaming is performed in the molten state, beside the morphological properties, the rheological behavior of the materials in shear and extensional flow are also investigated in this section.

A. Temperature-induced foaming

Fig. 7.2 presents the morphology of the unfoamed TPOs with different levels of compatibilizer. In all systems, most of the inclusions (the milky white domains in the micrographs) feature a non-spherical shape; indeed the inclusions with larger size did not have a sufficient time to relax over the time scale of solidification of the polypropylene phase. Also the TPO with the highest level of compatibilizer shows a finer morphology; the specific interfacial areas were measured to be 0.3, 0.4 and 0.7 (μm^{-1}) for the PP60n, PP60m and PP60h blends, respectively. The morphology of the resulting TPO foams produced via the temperature-induced foaming process is illustrated in Fig. 7.3. Again the milky white inclusions represent the rubber domains dispersed in the polypropylene matrix (the grey background in the micrograph); the bubbles are the darkest phase (the discontinuous black holes) in the micrographs. This can be understood by taking into account that the holes on the specimen surface reflect considerably less electrons back to the detector. The compatibilized TPO foams (Fig. 7.3b and 7.3c) feature smaller cells compared to the foam produced from the non-compatibilized blend (Fig. 7.3a). The corresponding cell densities and cell sizes were measured to be respectively $2.5 \times 10^9/cm^3$ and 6 µm for PP60n, 7.6 $\times 10^9/cm^3$ and 3µm for PP60m and 8.7 $\times 10^9$ $/cm^3$ and 3µm for the PP60h blend. The increased

cell densities in the compatibilized samples can be correlated to the finer morphology of the dispersed elastomeric phase which can act as nucleating sites in these systems.

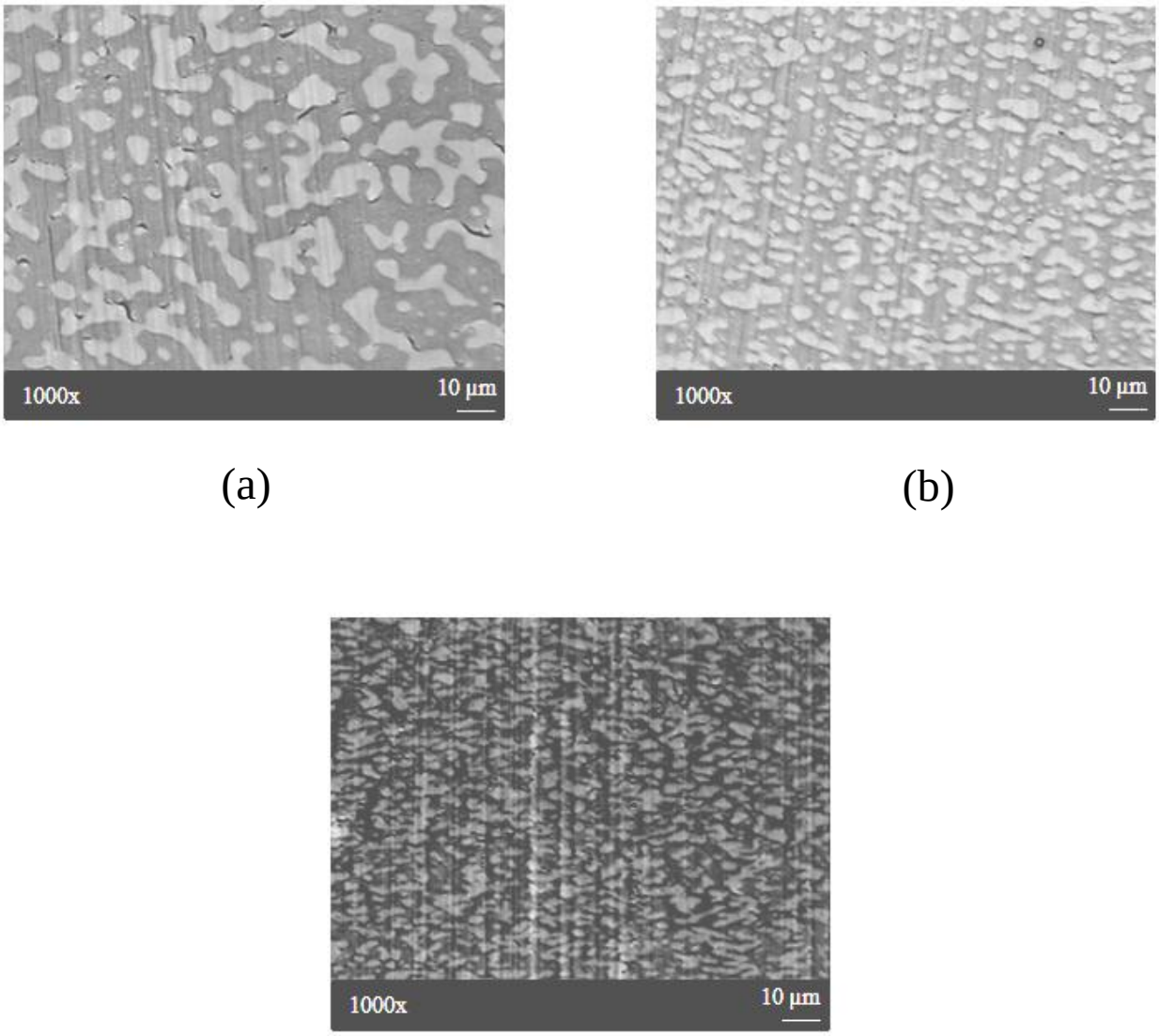

Fig. 7.2. BEI micrographs of the unfoamed TPOs with different levels of compatibilizer: a) PP60n; b) PP60m; c) PP60h.

This can be more clearly understood by examining the bottom row micrographs of Fig. 7.3 taken at a larger magnification. The bubbles are preferentially located in the rubber phase and are in an

elongated form where the rubber domains are highly extended (more clearly seen in the compatibilized samples).

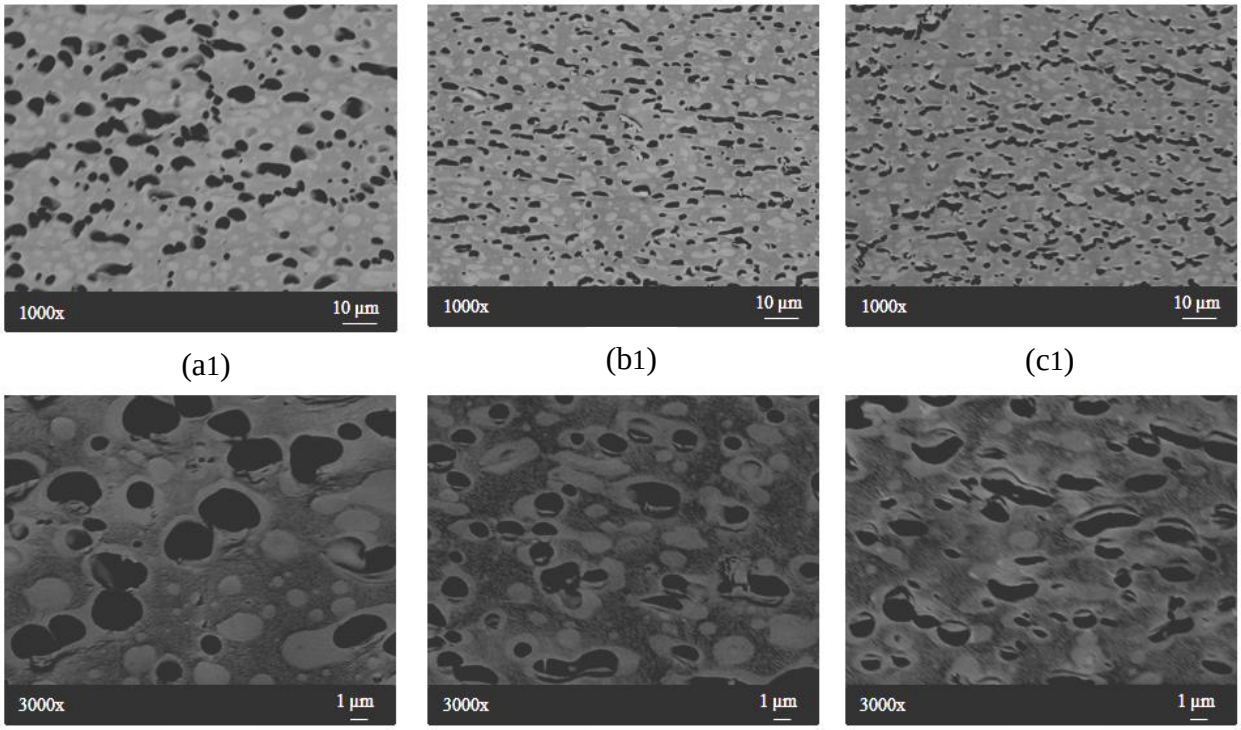

(a1) (b1) (c1)

(a2) (b2) (c2)

Fig. 7.3. BEI micrographs at two different scales of TPO foams with different levels of compatibilizer foamed by temperature-induced foaming: (a1, a2) PP60n; (b1,b2) PP60m; (c1,c2) PP60h.

To our knowledge, there has been no attempt in the literature to report the direct location of the different phases in polymer blend foams using microscopic observations. The microscopic observations of this study allow us to confirm that in these TPO systems the nucleation is directly controlled by the microstructure of the dispersed phase. The fact that the bubbles are located in the elastomer phase can be attributed to: 1) the diminished thermodynamic energy required for cell nucleation at the interface, 2) the different levels of gas solubility and 3) the phase stiffness contrast between the semi-crystalline PP phase and the soft rubber domains [19,

28]. The latter point can be explained by recalling the foaming conditions: in this process, samples are pressurized at room temperature and subsequently foamed in a bath of hot glycerin at 155 ^{o}C, which is below the melting point of PP (161 ^{o}C) and hence the polymer can still retain its semi-crystalline structure. On the other hand this foaming temperature is well above the melting point of the elastomer (60 ^{o}C) and hence the EC domains become quite deformable. This contrast in rigidity between the two different components of the TPO could result in significantly different foaming behaviors. Preliminary foaming experiments were carried on the neat components at 155 ^{o}C: the neat semi-crystalline PP phase was found to be unfoamable (the sample featured only some sparse tiny bubbles, which could be seen at very high magnifications); on the other hand the neat EC foam contained very coarse bubbles (results not shown), attributed to the softness of the elastomer phase that facilitated bubble growth and resulted in a significant coalescence of the nucleated bubbles.

To further explain the differences in foamability of PP and EC, the sorption behavior of CO_2 in the two phases has been examined at 25 and 155 ^{o}C. The diffusivity coefficients and solubility of CO_2 in the PP and EC components and their 60/40 blends are given in Table 1. As expected, due to the crystalline structure of PP the diffusivity coefficient of CO_2 in PP at 25 ^{o}C is significantly less than in EC (almost 10 times). Moreover, CO_2 is shown to be more soluble in the EC phase (31 compared to 22 $mg_{(CO_2)}/g_{(polymer)}$ for PP at 155 ^{o}C). The higher solubility of CO_2 in the EC phase provides a larger amount of gas for cell nucleation and growth, and this can further explain the sharp difference observed in the foamability of these two components.

Table 7.1 Diffusivity and solubility of CO2 in neat PP and EC and their 60/40 (PP/EC) blend

Material	Measurements at 25 ^{o}C		Measurements at 155°C[(a)]	
	Diffusivity (cm^2/s)	Solubility $mg_{(CO_2)}/g_{(polymer)}$	Diffusivity (cm^2/s)	Solubility $mg_{(CO_2)}/g_{(polymer)}$
(EC)	1.1×10^{-6}	35	3.0×10^{-6}	31
(PP)	2.4×10^{-7}	29	2.5×10^{-6}	22
PP/EC(60/40) (PP60n)	5.0×10^{-7}	34	6.2×10^{-6}	31

(a) Prior to measurements samples were firstly heated to 200 ^{o}C and then cooled down to 155 ^{o}C in order to mimic the sorption conditions of the pressure-induced foaming process.

We recall that in contrast to the neat materials, TPO foams featured a very fine cellular morphology, compared to the poor foaming behavior of the neat components. The fine cellular morphology of the TPO foams implies a significant impact of blending on foamability. Indeed foams prepared using TPO blends are characterized by cell densities larger than 10^9 (cm^{-3}) and cell sizes less than 10 µm [1, 37]. The fine cellular structure of these materials provides high strength to weight ratios [38, 39] which is of crucial importance, especially for TPO foams in automotive applications.

Apart from the compatibilization technique, the microstructure of the blends in the molten state can be also altered by either imposing a controlled flow field or quiescent annealing. In our previous work with similar systems [40], we showed how shearing at low shear rates could favor the coalescence of the rubber domains and result in a coarser morphology. Following

the same approach, the PP60n blend was subjected to a steady shear flow at a strain rate of 0.01 s^{-1} for 20 min. This very low shear rate was chosen to avoid overshoots for the neat polymers and favor coalescence in the blend. As we expected that no significant coalescence would occur for the compatilized blends, this test was only performed for the non compatiblized blend. The variations of the transient viscosity of the PP60n blend and of the neat components are illustrated in Fig. 7.4.

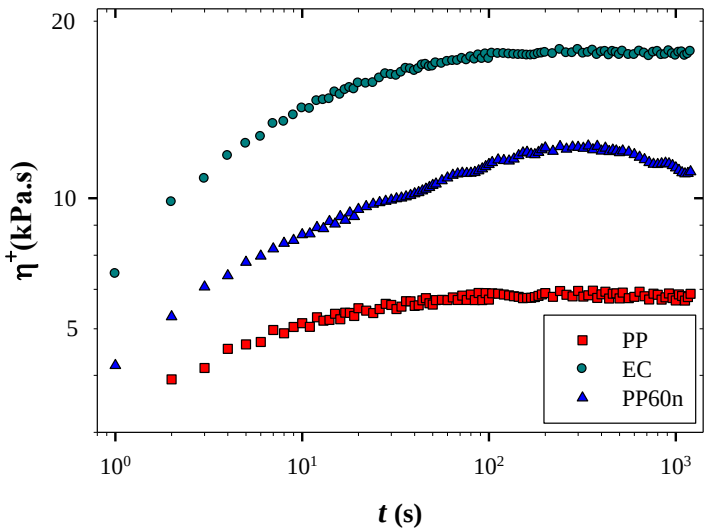

Fig. 7.4. Stress growth viscosity data of the neat PP and neat EC and PP60n blend at 200 ^{o}C at a shear rate of 0.01 s^{-1}.

As expected no overshoots are observed for the two neat components and the steady-state viscosity of the PP is considerably larger than that of the EC component. The presence of an overshoot in the PP60n blend is a clear indication of the deformation and orientation of the rubber domains along the flow direction. Subsequently, coalescence of these particles occurs, which in turn diminishes the interfacial area and reduces the flow resistance. Fig. 7.5 shows the morphological variations in the sample before annealing (Fig. 7.5a), after annealing in the

rheometer at 200 ^{o}C for 30 min (Fig. 7.5b), and at the end of 20 min shearing at 0.01 s^{-1} (Fig. 7.5c).

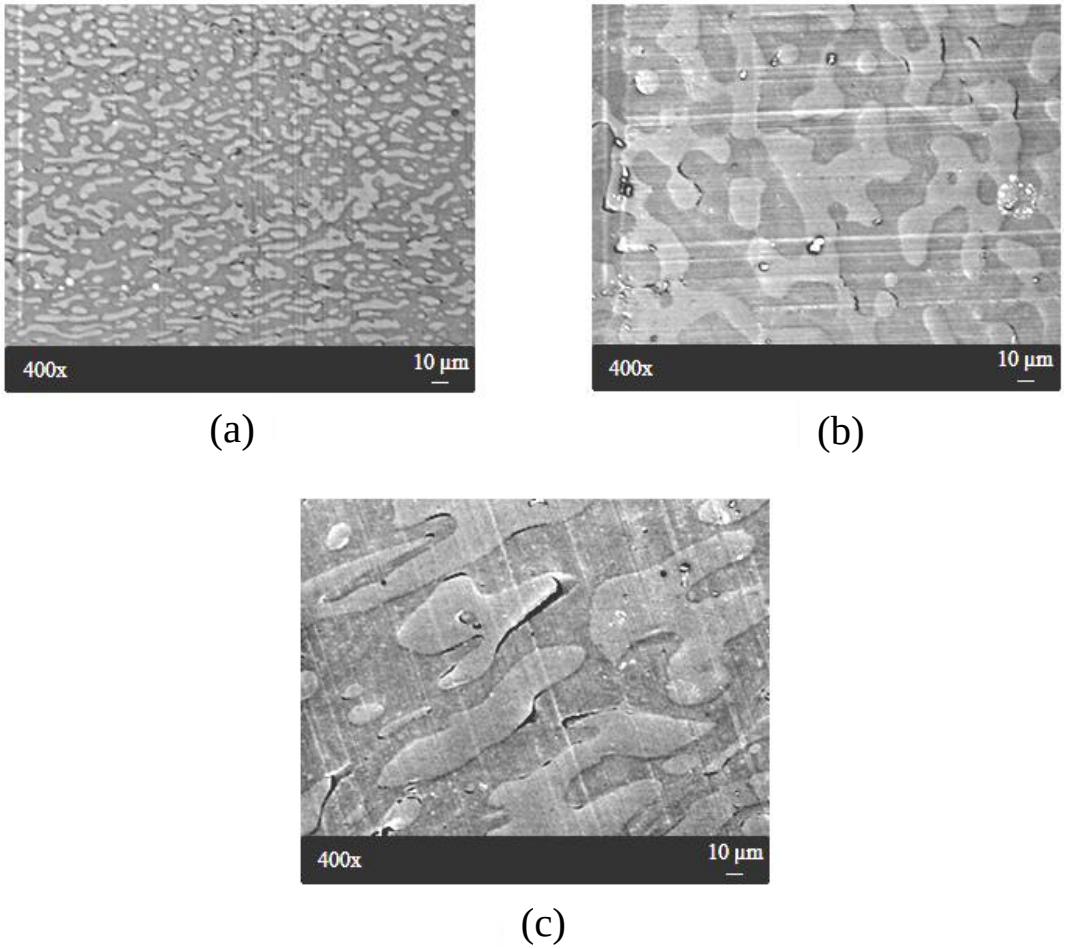

Fig. 7.5. BEI micrographs unfoamed PP60n blends: a) before annealing; b) annealed at 200 ^{o}C; and c) annealed and subsequently sheared at 0.01 s^{-1} and 200 ^{o}C for 20 min.

The corresponding interfacial areas vary from 0.3 μm^{-1} in the initial sample to 0.08 μm^{-1} in the annealed sample and to 0.06 μm^{-1} in the sheared blend. The impact of such a morphological transition on the final cellular morphology is shown in Fig. 7.6. The averaged cell diameter changes from 3 µm in the case of foam made from the non-annealed sample (Fig. 7.6a) to 25 and

42 µm in the foams made from the annealed (Fig. 7.6b) and sheared blends (Fig. 7.6c), respectively.

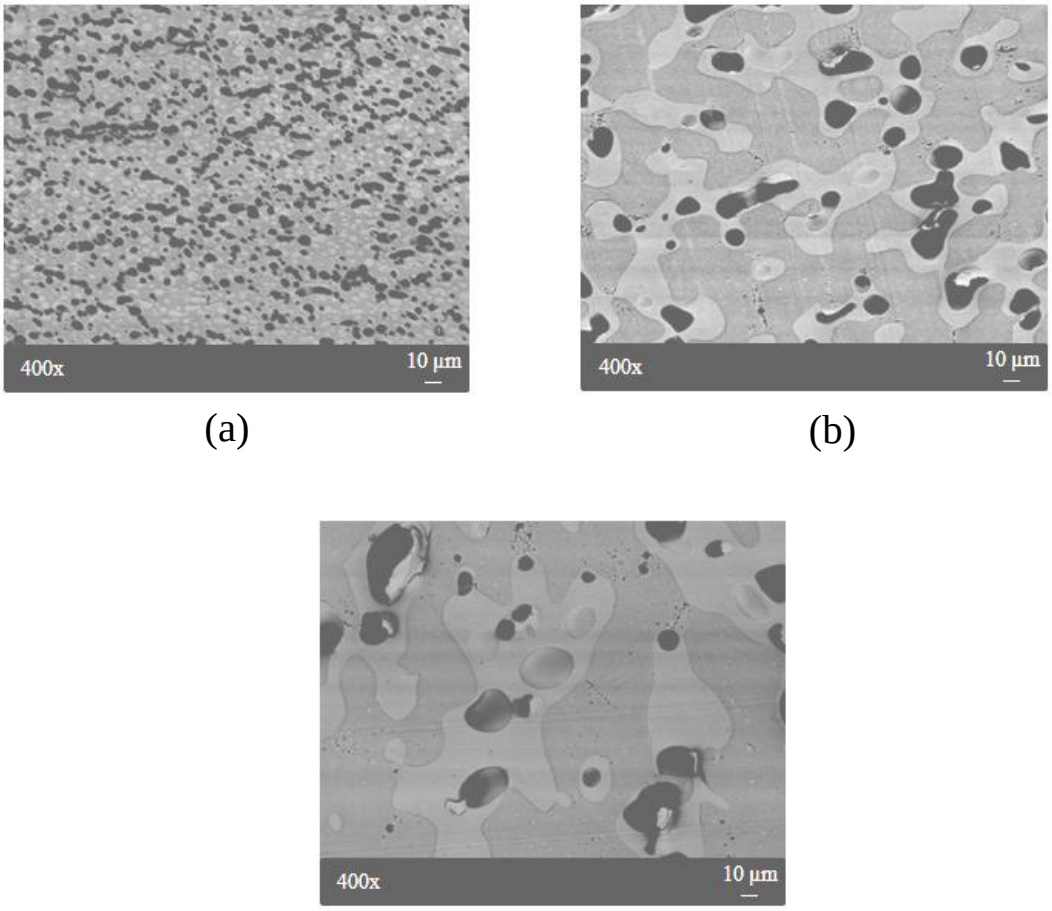

Fig. 7.6. Micrographs of foamed PP60n blends prepared under different shearing and thermal history: a) non annealed; b) annealed at 200 ^{o}C; and c) annealed at 200 ^{o}C and subsequently sheared at 0.01 s^{-1} for 20 min. Samples were foamed using temperature-induced foaming.

Again the trend is in agreement with the initial morphology of unfoamed TPOs: the finer the dispersed phase morphology, the finer the resulting cellular structure. The corresponding cell densities also vary from $2.5 \times 10^{9}/cm^{3}$ in the non-annealed blend to $1.6 \times 10^{7}/cm^{3}$ in the annealed sample and $6.0 \times 10^{6}/cm^{3}$ in the sheared blend. We note that the most significant phase

coarsening occurred during static annealing of the blends and the shear applied was not large enough to make a significant contribution to the overall coalescence.

Aside from the fact that in heterogeneous systems the nucleation rate is highly controlled by the dispersion of the nucleating sites (here the elastomer phase), the final cellular morphology is also influenced by cell coalescence. Indeed the smaller cell size in the compatibilized blends (Figs. 7.3b and c) can be partly attributed to the delayed bubble growth due to the high resistance of the PP phase, which hinders the expansion of the elastomer phase at the interface. This point is examined in more details in the next section where the rheological properties of the TPOs are also examined.

B. Pressure-induced foaming

As mentioned before, the gas pressure samples were firstly heated to 200 ^{o}C for 20 min and then cooled down to 155 ^{o}C. Such a thermal history causes the crystals of polypropylene to melt and hence the role of rheological properties of the melt components in controlling the foaming behavior becomes more evident. On the other hand this procedure can cause quiescent coalescence in the microstructure of the TPOs. Fig. 7.7 presents the morphologies of TPOs with different levels of compatibilizer after the annealing mentioned above. The specific interfacial areas were measured to be 0.05, 0.2 and 0.4 μm^{-1} for PP60n, PP60m and PP60h, respectively. Compared to the images for the non-annealed samples shown in Fig. 7.2, the dispersed phase morphology has become evidently coarser (e.g. in the case of non-compatibilized blend the interfacial area has decreased by almost 6 times). Such a significant level of static coalescence can be attributed to the high concentration of the dispersed phase in the blends used in this work (40 wt%).

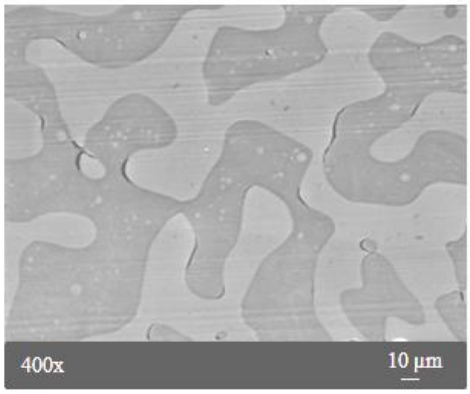

(a)

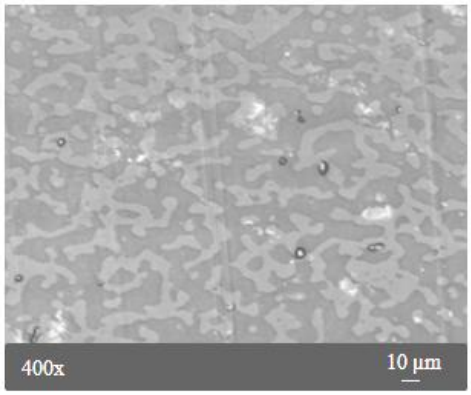

(b)

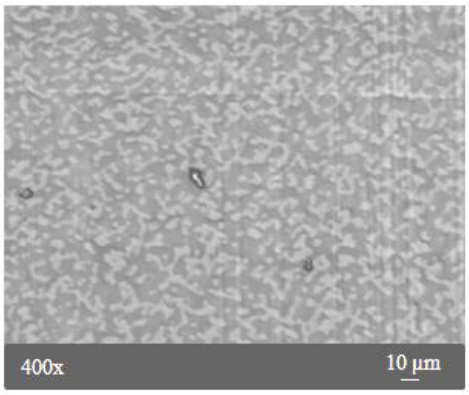

(c)

Fig. 7.7. Morphology of the unfoamed TPOs with different levels of compatibilizer: a) PP60n; b) PP60m; c) PP60h. The samples were firstly heated at 200 oC and annealed at 155 ^{o}C for 1 h.

The resulting morphology of the TPO foams is shown in Fig. 7.8. The foam produced for the non-compatibilized blend (Fig. 7.8a) exhibits very large bubbles. Such a foaming behavior is in clear contrast with what was observed in the previous section for the PP60n foam made through the temperature-induced foaming (Fig. 7.3a).

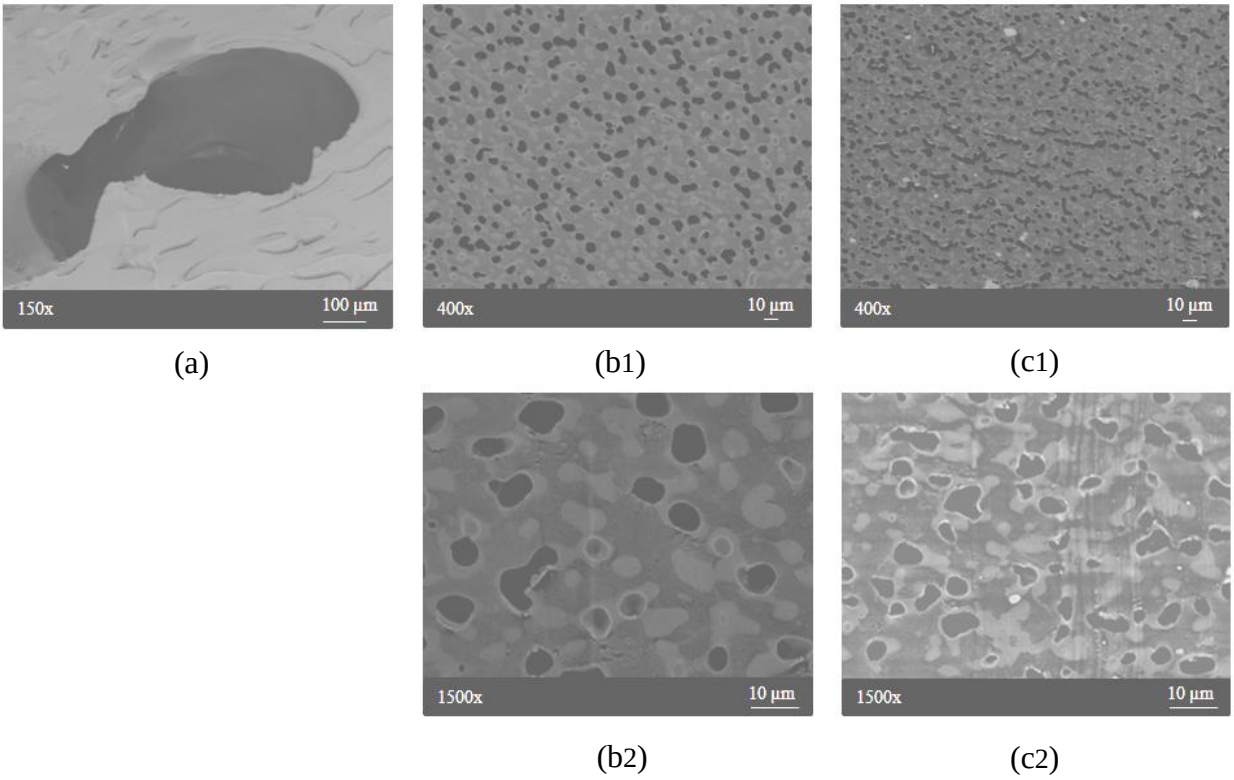

(a) (b1) (c1)

(b2) (c2)

Fig. 7.8. Micrographs at different scales of TPO foams with different levels of compatibilizer foamed by pressure-induced foaming: a) PP60n; (b1,b2) PP60m; (c1,c2) PP60h.

Two important factors should be considered to explain the differences in the cellular morphology of these samples. It should be first noted that in the second process (foaming by pressure release) the crystalline structure of the PP phase is molten prior to the free expansion step, and hence the PP matrix is no longer capable of controlling the growth stage of the nucleated bubbles. An estimation using the Avrami equation showed that the mass fraction of crystallinity at the temperature of foaming (155°C) was less than 1 wt%. It is worth noting that foaming of the neat polypropylene through the pressure release process also resulted in the formation of very coarse bubbles.

Fig. 7.8 also presents the morphology of the foams made from the compatibilized TPOs. The foaming morphology of the compatibilized blends significantly differs from the non-compatibilized sample. The corresponding cell diameters and cell densities were measured to be respectively 9 µm and $3.6x10^8/cm^3$ for PP60m and 7 µm and $9.9x10^8/cm^3$ for the PP60h blend. Considering the initial morphology of the different blends before foaming (Fig. 7.7) the improved melt foamability of the compatibilized blends can be again attributed to the significantly increased interfacial area in these systems, as compared to the non-compatibilized sample. It is worth noting that similar to what was observed in the previous section, the bubbles in these foams are also located in the dispersed phase. In fact even in the absence of a crystalline structure in the polypropylene matrix, the foaming behavior of the TPOs is controlled by heterogeneous nucleation. These observations are in agreement with the recent work of Kim et al. [14] who also found a direct relationship between the morphology of unfoamed blends and the final cellular structure in similar TPOs. Although their study did not report the respective location of the different phases, the variations of cell density and size of the rubber particles revealed that the foaming behavior could be explained by the heterogeneous nucleation theory. We also recall that beside the interfacial nucleation mechanism the facilitated nucleation and growth in the EC phase can be also attributed to the higher levels of CO_2 solubility in the EC phase as reported in Table 7.1.

As mentioned earlier the foaming behavior of these systems is also controlled by the rheological properties of the blends and blend components. In fact beside its effect on the blend microstructure, reactive compatibilization can also influence the foaming behavior through a change of the melt viscoelasticity. In this context the rheological behavior of the materials in

dynamic shear and transient extension was investigated. The dynamic rheological behavior of the different TPOs is illustrated in Fig. 7.9.

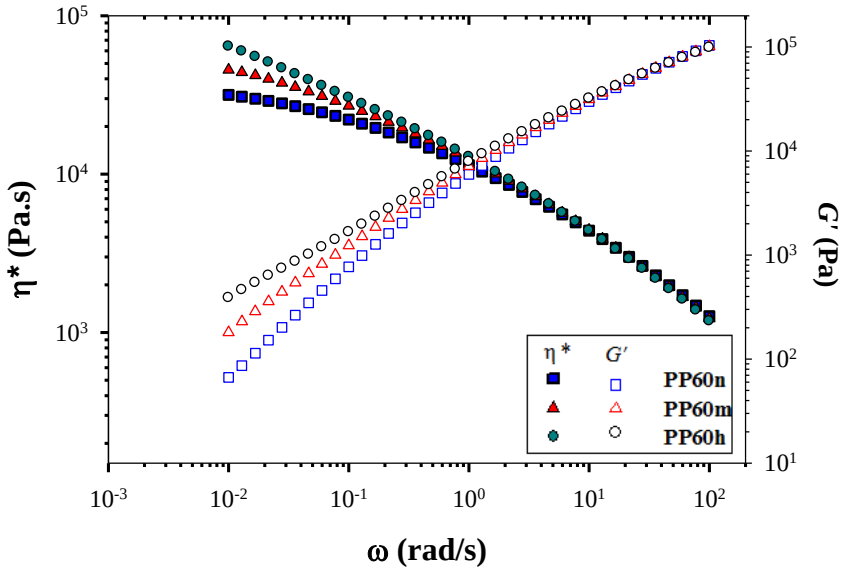

Fig. 7.9. Variations of the storage modulus and complex viscosities with frequency for TPOs with different levels of compatibilizer measured at 155 °C.

At high frequencies all TPOs present similar values for the complex viscosity and storage modulus, whereas the compatibilized blends feature an enhanced level of viscoelasticity at low frequencies. This behavior is similar to what was observed in our previous work [29] for 70/30 PP/EC blends. The complex viscosity for the non-compatibilized blend at low frequencies is less shear-thinning and is smaller than that of the compatibilized samples (e.g. the complex viscosity for PP60n at 0.01 rad/s is less than a half of that for the PP60h blend). Also the storage modulus of the non-compatibilized blend exhibits a different behavior at low frequencies. It is worth noting, however, that the variation of the low frequency values of the storage modulus for all

blends deviate from the liquid-like behavior, where in the terminal zone the storage modulus of liquid emulsions should vary on log-log plots as ω^2. The slopes of the storage modulus at low frequencies were found to be 1.1, 0.8, 0.6 for the PP60n, PP60m and PP60h blends, respectively. We believe that this is due to the relatively high concentration of the elastomer used in these TPOs, which results in the formation of a semi-continuous morphology as seen in Fig. 7.7. The enhanced values for the complex viscosity and storage modulus in the compatibilized blend are also in agreement with the morphological observations reported in Fig. 7.7, and explained by the formation of highly extended networks of compatibilized rubber domains with very long relaxation times. This can be better understood by examining the variation of loss tangent versus frequency(Fig. 7.10).

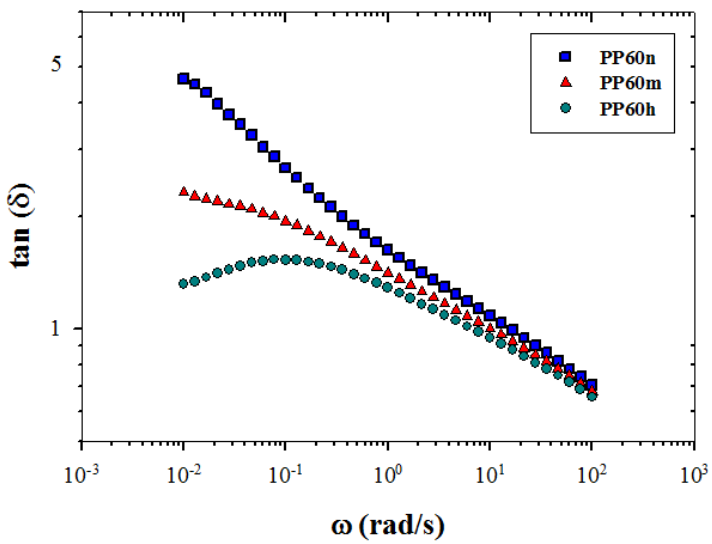

Fig. 7.10 .Variations of the loss tangent with frequency for TPOs with different levels of compatibilizer. Measurements were performed at 155 ^{o}C.

In the PP60n blend the loss tangent values increases more steeply as the frequency decreases. In the PP60h blend the loss tangent shows a decreasing trend with decreasing frequency. This is

clearly an indication of a permanent elasticity due to the presence of a developed gel-like structure in the system [43].

Although dynamic shear measurements provide important information they would not directly represent the rheological response of the melt during elongation, which is indeed the actual type of deformation occurring during expansion of nucleated bubbles. Fig. 7.11 presents the transient elongational viscosities of the neat materials and the blends measured at three different strain rates and at 155 ^{o}C (as mentioned in Section II, the samples were firstly molten at 185 ^{o}C and cooled down to 155 ^{o}C). The solid line shows 3 times the transient shear viscosity predicted by linear viscoelasticity using a generalized Maxwell model. The transient elongational viscosity of the neat polypropylene shows almost the same behavior as the predictions of linear viscoelasticity. This is expected from the linear structure of the PP used in this study. In contrast the elongational viscosity of the EC elastomer slightly deviates from the linear viscoelasticity and shows an upturn at longer times, implying a small level of strain hardening. This behavior can be possibly attributed to the presence of sparse long chain branches, which are incorporated into the molecular structure during metallocene-catalyzed polymerization. This has also been reported in a previous study of Bin Wadud and Baird [44].

As illustrated in Fig. 7.11b, the transient elongational viscositiy of the PP60n blend also deviates from the linear viscoelasticity and shows small terminal upturns, especially at low strain rates. This nonlinear behavior is due to the presence of the elastomer phase in the system, which was shown to be slightly strain-hardening in Fig. 7.11a. In addition the strain-hardening behavior of the blend can be partly attributed to the interfacial forces created during the deformation of the rubber domains in uniaxial elongation. Such an interfacial strain hardening is more pronounced in the compatibilized systems, especially at lower strain rates where the contribution of the

interface in the stress growth viscosity becomes comparable to the contribution of the neat components.

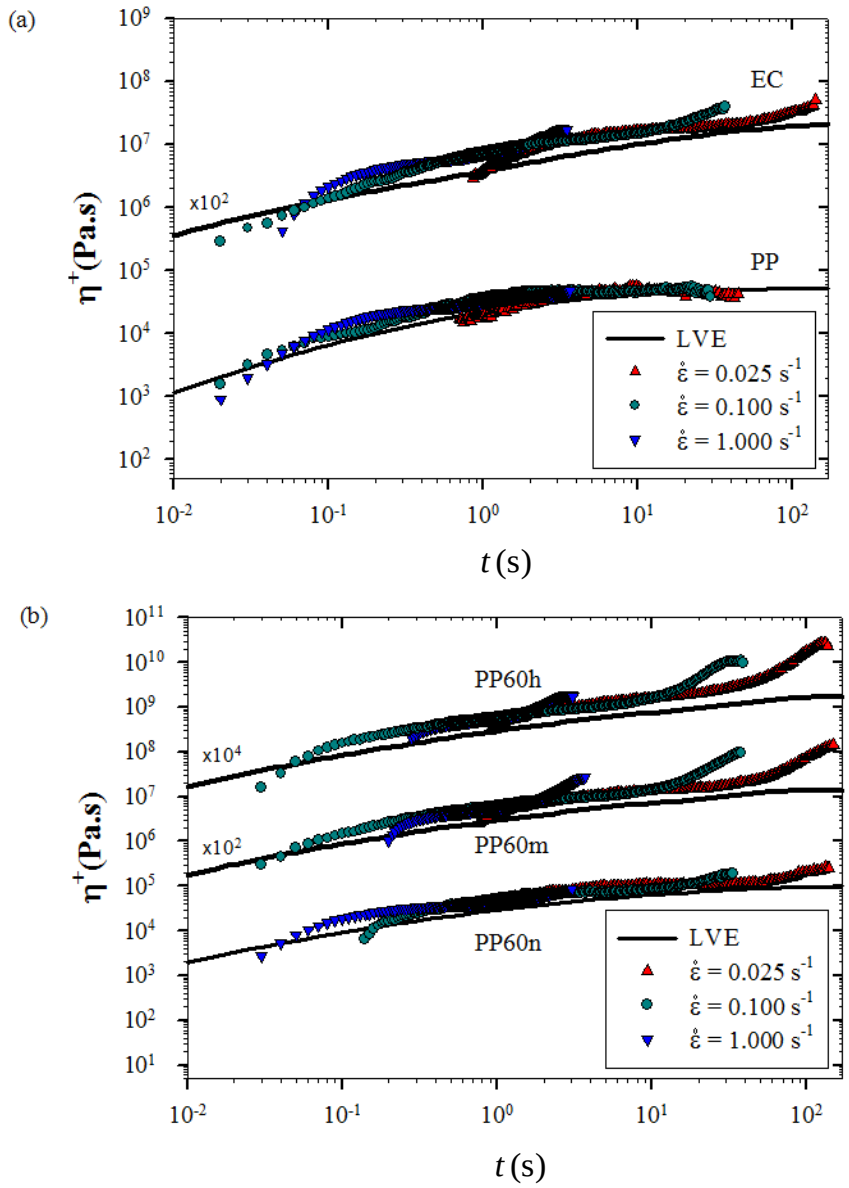

Fig. 7.11. Transient elongational viscosities of the neat materials (a) and the blends with different levels of compatibilizer (b) measured at 155 °C. Data have been multiplied by shown factors for clarity reasons.

It was shown by Venerus et al. [45] that the deformation rate at the gas-liquid interface decreases quite rapidly at the early stage of bubble growth, and consequently the diffusion-induced bubble expansion is mainly controlled by the rheological properties at low strain rates. The ratio of the transient elongational viscosities over the predicted values obtained from the linear viscoelasticity at 100 s and at a strain rate of 0.025 s^{-1} were found to be about 2, 5 and 10 for the PP60n, PP60m and PP60h blends, respectively; the corresponding values of the transient elongational viscosity at this point are approximately 200, 800 and 1800 kPa.s. These differences can further explain the distinct behavior observed in the foaming of the compatibilized blends compared to the non-compatibilized sample (Fig. 7.8). We recall that the foaming behavior of these systems is influenced by both the rheological behavior as well as the morphology. Obviously, further studies are still required to better understand the role of different contributing factors in the development of cellular morphology of TPO foams.

IV. Conclusions

In this study the foaming behavior of thermoplastic olefin blends prepared with different levels of reactive compatibilizer was investigated. Microscopic observations revealed that the bubbles are located in the dispersed elastomer domains. This can be attributed to the higher levels of gas solubility in the elastomer phase compared to the PP matrix. Morphological observations also revealed that the final cellular morphology is a strong function of the initial blend microstructure. It was found that among the two different foaming conditions used in this study, only the temperature-induced foaming resulted in the formation of a fine cellular morphology for the non-compatibilized sample. In pressure-induced foaming the free expansion of the molten non-compatibilized blend resulted in very coarse bubbles, mainly due to the

uncontrolled cell growth. The foaming of the compatibilized blends, however, provided fine cell structured foams (with cell diameters less than 10 μm) using both batch foaming processes. The significant differences observed among the foaming behavior of the non-compatibilized sample and its compatibilized counterparts were attributed to the microstructural features of the different TPOs as well as the enhanced melt viscoelastic properties caused by the addition of the reactive compatibilizer.

Acknowledgements

The authors are grateful to Dr. N. Virgilio, Mrs. W. Leelapornpisit and Mrs. M. Hamdine for advice and technical assistance in morphological and rheological measurements. This work was supported by a grant of NSERC.

References

1. Martini, J. E. "The production and analysis of microcellular foam." M.S. Thesis, Dept. of Mechanical Engineering, Massachusetts Institute of Technology (1981).

2. Baldwin, D. F., Park, C. B. and Suh, N. P. An extrusion system for the processing of microcellular polymer sheets: Shaping and cell growth control. *Polymer Engineering & Science*, 1996: **36:** 1425-1435.

3. Kumar, V. and Suh, N. P. A process for making microcellular thermoplastic parts. *Polymer Engineering & Science*, 1990: **30:** 1323-1329.

4. Park, C. B., Behravesh, A. H. and Venter, R. D. Low density microcellular foam processing in extrusion using CO2. *Polymer Engineering & Science*, 1998: **38:** 1812-1823.

5. Xu, X., Park, C. B., Xu, D. and Pop-Iliev, R. Effects of die geometry on cell nucleation of PS foams blown with CO2. *Polymer Engineering & Science*, 2003: **43:** 1378-1390.

6. Doroudiani, S., Park, C. B. and Kortschot, M. T. Effect of the crystallinity and morphology on the microcellular foam structure of semicrystalline polymers. *Polymer Engineering & Science*, 1996: **36:** 2645-2662.

7. Naguib, H. E., Park, C. B., Panzer, U. and Reichelt, N. Strategies for achieving ultra low-density polypropylene foams. *Polymer Engineering & Science*, 2002: **42:** 1481-1492.

8. Stafford, C. M., Russell, T. P. and McCarthy, T. J. Expansion of Polystyrene Using Supercritical Carbon Dioxide: Effects of Molecular Weight, Polydispersity, and Low Molecular Weight Components. *Macromolecules*, 1999: **32:** 7610-7616.

9. Ramesh, N. S., Rasmussen, D. H. and Campbell, G. A. The heterogeneous nucleation of microcellular foams assisted by the survival of microvoids in polymers containing low glass transition particles. Part I: Mathematical modeling and numerical simulation. *Polymer Engineering & Science*, 1994a: **34:** 1685-1697.

10. Ramesh, N. S., Rasmussen, D. H. and Campbell, G. A. The heterogeneous nucleation of microcellular foams assisted by the survival of microvoids in polymers containing low glass-transition particles. 2. Experimental results and discussion *Polym. Eng. Sci.*, 1994b: **34:** 1698-1706.

11. Blander, M. and Katz, J. L. Bubble nucleation in liquids. *AlChE J.*, 1975: **21:** 833-848.

12. Fletcher, N. H. Size Effect in Heterogeneous Nucleation. *The Journal of Chemical Physics*, 1958: **29:** 572-576.

13. Doroudiani, S., Park, C. B. and Kortschot, M. T. Processing and characterization of microcellular foamed high-density polythylene/isotactic polypropylene blends. *Polymer Engineering & Science*, 1998: **38:** 1205-1215.

14. Kim, S. G., Leung, S. N., Park, C. B. and Sain, M. The effect of dispersed elastomer particle size on heterogeneous nucleation of TPO with N2 foaming. *Chem. Eng. Sci.*, 2011: **66:** 3675-3686.

15. Park, C. B., Lee, P. C., Wang, J. and Padareva, V. Strategies for achieving microcellular LDPE foams in extrusion. *Cell. Polym.*, 2006: **25:** 1-18.

16. Sahagún, C. Z., González-Núñez, R. and Rodrigue, D. Morphology of Extruded PP/HDPE Foam Blends. *Journal of Cellular Plastics*, 2006: **42:** 469-485.

17. Spitael, P., Macosko, C. W. and McClurg, R. B. Block Copolymer Micelles for Nucleation of Microcellular Thermoplastic Foams. *Macromolecules*, 2004: **37:** 6874-6882.

18. Zhai, W., Wang, H., Yu, J., Dong, J. and He, J. Foaming behavior of polypropylene/polystyrene blends enhanced by improved interfacial compatibility. *J. Polym. Sci., Part B: Polym. Phys.*, 2008: **46:** 1641-1651.

19. Ruckdäschel, H., Gutmann, P., Altstädt, V., Schmalz, H. and Müller, A. Foaming of Microstructured and Nanostructured Polymer Blends in Complex Macromolecular Systems I. Müller, A. H. E. and Schmidt, H.-W., Springer Berlin / Heidelberg.**227:** 199-252 (2010).

20. Yokoyama, H. and Sugiyama, K. Nanocellular Structures in Block Copolymers with CO2-philic Blocks Using CO2 as a Blowing Agent: Crossover from Micro- to Nanocellular Structures with Depressurization Temperature. *Macromolecules*, 2005: **38:** 10516-10522.

21. Otsuka, T., Taki, K. and Ohshima, M. Nanocellular Foams of PS/PMMA Polymer Blends. *Macromolecular Materials and Engineering*, 2008: **293:** 78-82.

22. Park, C. B. and Cheung, L. K. A study of cell nucleation in the extrusion of polypropylene foams. *Polymer Engineering & Science*, 1997: **37:** 1-10.

23. Van Nuffel, C. T. E., Pham, H. T., Namhata, S. and Eiffler, J. Blend of branched and linear carbonate polymer resins. United States Patent The Dow Chemical Company **5804673**

24. Spitael, P. and Macosko, C. W. Strain hardening in polypropylenes and its role in extrusion foaming. *Polym. Eng. Sci.*, 2004: **44:** 2090-2100.

25. Stange, J. and Münstedt, H. Effect of Long-chain Branching on the Foaming of Polypropylene with Azodicarbonamide. *Journal of Cellular Plastics*, 2006: **42:** 445-467.

26. Santoni, A., Guo, M. C., Heuzey, M. C. and Carreau, P. J. Surface defects of TPO injected foam parts for automotive applications. *Int. Polym. Proc.*, 2007: **22:** 204-212.

27. Guo, M.-C., Santoni, A., Heuzey, M.-C. and Carreau, P. J. Occurrence of Surface Defects in TPO Injected Foam Parts. *Journal of Cellular Plastics*, 2007: **43:** 273-296.

28. Nemoto, T., Takagi, J. and Ohshima, M. Nanoscale Cellular Foams from a Poly(propylene)-Rubber Blend. *Macromolecular Materials and Engineering*, 2008: **293:** 991-998.

29. Maani, A., Blais, B., Heuzey, M. C. and Carreau, P. J. Rheological and morphological properties of reactively compatibilized thermoplastic olefin (TPO) blends. *J. Rheol.*, 2012: **56:** 625-647.

30. Dekmezian, A. H., Soares, J. B. P., Jiang, P., Garcia-Franco, C. A., Weng, W., Fruitwala, H., Sun, T. and Sarzotti, D. M. Characterization and Modeling of Metallocene-Based Branch−Block Copolymers. *Macromolecules*, 2002: **35:** 9586-9594.

31. Kokko, E., Malmberg, A., Lehmus, P., Löfgren, B. and Seppälä, J. V. Influence of the catalyst and polymerization conditions on the long-chain branching of metallocene-catalyzed polyethenes. *J. Polym. Sci., Part A: Polym. Chem.*, 2000: **38:** 376-388.

32. Lohse, D. J., Milner, S. T., Fetters, L. J., Xenidou, M., Hadjichristidis, N., Mendelson, R. A., García-Franco, C. A. and Lyon, M. K. Well-Defined, Model Long Chain Branched Polyethylene. 2. Melt Rheological Behavior. *Macromolecules*, 2002: **35:** 3066-3075.

33. Dreisbach, F. and Lösch, H. Magnetic Suspension Balance For Simultaneous Measurement of a Sample and the Density of the Measuring Fluid. *J. Therm. Anal. Calorim.*, 2000: **62:** 515-521.

34. Saltykov, S. A. "The determination of the size distribution of particles in an opaque material from a measurement of the size distribution of their section" Stereology. Elias, H. New York, Springer-Verlag**:** 163-173 (1967).

35. Russ, J. C. Practical Sterelogy New York, NY, Plenum Press (1986).

36. Galloway, J. A., Montminy, M. D. and Macosko, C. W. Image analysis for interfacial area and cocontinuity detection in polymer blends. *Polymer*, 2002: **43:** 4715-4722.

37. Park, C. B., Baldwin, D. F. and Suh, N. P. Effect of the pressure drop rate on cell nucleation in continuous processing of microcellular polymers. *Polymer Engineering & Science*, 1995: **35:** 432-440.

38. Collias, D. I., Baird, D. G. and Borggreve, R. J. M. Impact toughening of polycarbonate by microcellular foaming. *Polymer,* 1994: **35:** 3978-3983.

39. Waldman, F. A. "The processing of microcellular foam." M.S. Thesis, Dept. of Mechanical Engineering, Massachusetts Institute of Technology (1980).

40. Maani, A., Heuzey, M.-C. and Carreau, P. Coalescence in thermoplastic olefin (TPO) blends under shear flow. *Rheol. Acta,* 2011: **50:** 881-895.

41. Fortelný, I. and Živný, A. Coalescence in molten quiescent polymer blends. *Polymer,* 1995: **36:** 4113-4118.

42. Sondergaard, K. and Lyngaae-Jorgensen, J. Rheo-Physics of Multiphase Polymer Systems: Characterization by Rheo-Optical Techniques Lancaster, Pa, Technomic Pub. Co. (1995).

43. Schiessel, H. and Blumen, A. Mesoscopic Pictures of the Sol-Gel Transition: Ladder Models and Fractal Networks. *Macromolecules,* 1995: **28:** 4013-4019.

44. Bin Wadud, S. E. and Baird, D. G. Shear and extensional rheology of sparsely branched metallocene-catalyzed polyethylenes. *J. Rheol.,* 2000: **44:** 1151-1167.

45. Venerus, D. C., Yala, N. and Bernstein, B. Analysis of diffusion-induced bubble growth in viscoelastic liquids. *J. Non-Newtonian Fluid Mech.,* 1998: **75:** 55-75.

CHAPTER 8

GENERAL DISCUSSION

As for the other properties of immiscible polymer blends, the foaming behavior is a function of the blend microstructure developed during melt processing. Consequently, the foamability of thermoplastic olefin blends can be improved by controlling the coalescence phenomenon, which plays an important role in the morphology development. In this regard, the first part of this study was devoted at investigating the coalescence behavior of these blends. A rheological approach was introduced to evaluate the intensity of flow induced coalescence during shearing. Thermoplastic olefin blends studied were composed of polypropylene and metallocene catalyzed ethylene copolymers (EC) with different melt viscosities. To quantify the coalescence efficacy in different blends a phenomenological transient rheological model (LPL model) was used.

The capability of the LPL model in predicting the transient morphological states showed that the rheological methods can be thought as a strong tool in studies concerning flow induced coalescence in molten polymer blends; this can be understood by considering the difficulties faced in direct visualization of colliding drops in the molten systems. The conventional criterion for coalescence intensity (i.e. the final to initial droplet size ratio) was found to be a poor indicator of coalescence. The advantage of the transient phenomenological LPL model used in this study was the capability of this model in simulating the transient behavior of the blends so as to account for increased coalescence intensity and indirectly for increasing frequency collision with volume fraction of the dispersed phase. The results showed that the blends with lower levels of viscosity ratio are more prone to phase coalescence under shear flow. This was attributed to the increased interfacial mobility in the blends containing low viscosity drops. In fact lower

viscosity ratio decreases the hydrodynamic forces resisting the relative motion of the droplets, reduces the drainage time and eventually results in a facilitated coalescence. We recall however that the approach followed in this section is limited to relatively low shear rates. Implication of high strain rates can cause sample ejection out of the gap or other types of melt instabilities. In addition the transient model used in this study can only describe the viscoelastic effects due to the interface deformation. Highly viscoelastic polymer blends can show non Newtonian behaviors such as overshoot in the startup of shear which may interfere the prediction of the model.

In the second phase of this study an attempt was made to control the extent of phase coalescence via a compatibilization approach. Preliminary experiments with different types of olefinic copolymers showed that premade compatibilizers are inefficient in coalescence suppression. This was primarily due to the high possibility of micelle formation in such a system with low level of interfacial tension. As such a reactive compatibilization technique was necessary; an aminated polypropylene was firstly synthesized in a solution reaction through which amine groups are placed onto the maleic anhydride grafted polypropylene chains. The reaction between the amine groups of the functionalized polypropylene and maleic anhydride groups of the maleic anhydride grafted elastomer resulted in the formation of copolymers at the interface.

Dynamic rheological measurements revealed that reactive blending causes significant enhancement in the blend viscoelasticity at low frequencies, which could not be described by the emulsion model of Palierne. To account for the low frequency plateau a modified version of the Palierne model and a viscoelastic Zener model with two fractional elements were also employed wherein an equilibrium modulus was incorporated. Although the latter models described better the low frequency data, it failed at predicting the variation of tan δ at low frequencies; while the

models predicted a monotonically decreasing trend of loss tangent for the compatibilized blends the experimental data appeared to level off. A generalized viscoelastic Zener model with three fractional elements was found to be capable of describing the viscoelastic behavior of the blends over the whole frequency range. The power-law decay of the storage modulus along with the sharp viscosity upturn at low frequencies suggested that the compatibilized blends feature the structure of materials in sol-gel transitions. This was confirmed by atomic force microscopy technique which showed that in the compatibilized blends the dispersed elastomeric domains are formed in network like structures. In fact in these blends the copolymer on the surface of each particle favors the formation of a percolated structure. Stress growth experiments showed the impact of network structures on the transient rheological and morphological behavior of the blends. The LPL model failed in predicting the transient viscosity of the compatibilized blends. This was due to the fact that the extra stresses arising from the formation of networks of the compatibilizer molecules are not accounted for in the model. Generalized Zener model could only predict an initial portion of the transient data where deformations remained in the range of linear viscoelasticity. An enhanced level of stress growth viscosity developed at very long times along with the retarded stress relaxation behavior was also attributed to the presence of interconnected structures as observed by atomic force microscopy. It should be noted that preliminary experiments showed that scanning electron microscopy is unable to reflect the true morphology of the compatibilized elastomeric domains; this was found to be due the inefficiency of solvent extraction technique in dissolving the elastomeric domains with crosslinked compatibilizer. While AFM micrographs showed an interconnected structure, SEM images represented a droplet matrix morphology wherein only isolated domains were detected. This further highlights the capability of rheological methods in characterizing the microstructure of

such systems. It should be mentioned that at this stage the compatibilization technique proposed here is of interest only for laboratory studies; the solution reaction involved in this method makes it practically limited both due to economic and environmental issues. Moreover possible failures in the reaction control can cause extensive crosslinking reactions and undesirable processability. Further study is still needed to address these issues and to develop an industrially viable process.

The last part of this research aimed at correlating the foamability of the TPOs to the initial phase morphology and controlling the foaming behavior through reactive compatibilization .A new microscopic method based on the Back scattered Electron Imaging (BEI) technique was used to determine the respective locations of the 3 phases in the TPO foams: bubbles, elastomeric domains and the polypropylene matrix. The results revealed that in all of the TPO foams the bubbles are preferentially located in the elastomeric domains. This was attributed to diminished thermodynamic energy required for cell nucleation at the interface as well as the larger solubility of CO_2 in the elastomeric phase, which provides larger amount of gas molecules for cell nucleation and growth. In fact the significant synergistic effect of blending on the foaming behavior is due to the heterogeneous nucleation mechanism introduced by the presence of the dispersed rubbery domains. Microcellular foams with cell sizes as small as 3 µm and cell densities larger than 7.5×10^9 could be produced using compatibilized TPO foams. The variation of the cell size in TPO foams with different levels of compatibilizer was in agreement with the trend observed in the initial morphology of the blends. To further investigate the role of initial blend microstructure on the final cellular morphology, the phase morphology of the non compatibilized TPO was varied by phase coalescence induced either by quiescent annealing or gentle shear flow. The advantage of this technique compared to the methods used in other studies (e.g. varying the phase morphology with viscosity ratio or phase concentrations) is that the bulk

properties of the blend constituents remains unchanged. The results obtained by pressure induced foaming showed a significant effect of compatibilization on the foaming behavior of molten TPOs; while foaming of the non compatibilized blends resulted in the formation of very coarse cellular morphology, compatibilized TPOs rendered foams with cell sizes less than 10 µm. Extensional rheological measurements showed a pronounced strain-hardening behavior in the compatibilized blends especially at low strain rates. The enhanced elongational viscosity in the compatibilized TPOs compared to the non treated sample was attributed to the larger interfacial area and the presence of network structure formed during reactive blending. The enhanced melt foamability of the compatibilized TPOs was found to be the result of finer initial morphology as well as the improved viscoelastic properties. We stress again that the reactive compatibilization technique used in this study is accompanied by the practical limitations mentioned before and should be further developed for industrial use. The improvement achieved via this technique can, however, increase the motivation of future works on the development of commercialized reactive processes.

CHAPTER 9

CONCLUSIONS AND RECOMMENDATIONS

9.1 Conclusions

In this dissertation, the foaming behavior of thermoplastic olefin blends and its dependency on the morphological and rheological properties was investigated. As an important phenomenon in the phase morphology evolution of TPOs, the flow induced coalescence was firstly investigated using a rheological approach. It was shown that a modified version of the Lee and Park model is capable of predicting the extent of phase coalescence in conjunction with the transient stress growth viscosity data. Considering the limitations encountered in direct visualization of coalescence in polymer melts and also inefficiency of the classical coalescence models in predicting the coalescence rate in the concentrated polymer blends, the rheological technique used in this study can be thought as a practical method to assess the coalescence intensity. The efficiency of this technique was evaluated by investigating shear induced coalescence in TPOs with different concentrations of the dispersed phase. It was shown that the final to initial droplet size ratio is a poor indicator of coalescence and should be used only when the initial droplet sizes are in the same range; considering that this condition is difficult to meet experimentally the situation was simulated using LPL model while assuming a same initial droplet size for the blends with different concentrations. It was shown that this approach can provide a better understanding of the variation of coalescence intensity as a function of phase concentration. The results of shearing TPOs with different levels of viscosity ratio revealed that droplet coalescence was favored as the viscosity of the droplets decreased. This was found to be

due to the smaller drainage time as a result of increased interfacial mobility in droplets with low viscosity ratio.

In the second part of this thesis reactive compatibilization was employed and its influence on the rheological and morphological properties of the blends was investigated. Compatibilization was performed during a reactive melt blending where the reaction between aminated PP and maleic anhydride grafted EC chains resulted in the formation of compatibilizer copolymer at the interface. Linear viscoelastic measurements showed that the compatibilized blends feature the characteristics of materials in the sol-gel transition, with a power-law behavior for the dynamic moduli at low frequencies. The Palierne emulsion model failed in predicting the low frequency behavior of the compatibilized blends. It was shown that applying a modified version of the Palierne model and also a viscoelastic Zener model with two fractional elements resulted in better predictions of the storage modulus; however, the latter models could not predict the real trend of the loss tangent at low frequencies. A generalized Zener model with three fractional elements was shown to be capable of describing the linear viscoelastic data over the whole frequency range. The LPL model predicted very well the transient rheological and morphological behavior of the non-compatibilized blend, but failed in predicting the transient response of the compatibilized blends. The rheological properties of the reactively compatibilized blends, including gel-like behavior, enhanced viscosity at low shear rate, transient viscosity developed at very long times and retarded stress relaxation, suggest that these blends feature an interconnected structure linked by the compatibilizer copolymer, as confirmed by atomic force microscopy.

Finally the last part of this dissertation aimed at investigating the influence of coalescence and reactive compatibilization on the final cellular morphology of TPO foams. Foaming was assisted by a batch setup pressurized with carbon dioxide as blowing agent. A microscopic

characterization method based on the Back Scattering Electron Imaging (BEI) technique was employed and was shown to be powerful in positioning the respective locations of bubbles, elastomeric dispersed phase and polypropylene matrix. It was found that all the bubbles are preferentially located in the elastomeric phase. This was attributed to the higher solubility of gas molecules in the elastomeric phase as measured by sorption experiments. It was also shown that the finer initial morphology in the compatibilized blends resulted in the finer cellular morphology. A similar observation was also observed in the foaming behavior of the TPOs for which the morphology had been varied through static annealing and shear induced phase coalescence. All these results suggested a heterogeneous cell nucleation mechanism assisted by the presence of a rubbery phase dispersed in the polypropylene matrix. Reactive compatibilization resulted in significant improvement in the melt foamability of the TPOs. While free expansion of the non compatibilized blend resulted in the formation of very coarse bubbles, compatibilized TPO foams featured a fine cellular morphology with cell sizes less than 10 µm. The sever extent of cell coalescence in the non compatibilized TPO was attributed to the inadequate level of melt strength in this blend. The transient rheological measurements in uniaxial extension showed that the compatibilized blends feature a profound strain hardening behavior especially at low strain rates. This was attributed to the presence of interconnected compatibilizer molecules that cover the interface and bring about gel like behavior into the system. Dynamic viscoelastic characterization of the compatibilized blends also showed significant deviations from the typical behavior of binary emulsions at low frequencies; The result of this part suggested that the improved foaming behavior of the compatibilized blends should be described by the increased nucleation rate as a result of a finer initial morphology as well as the controlled cell coalescence due to the enhanced viscoelastic properties.

9.2 Original contributions

In the first part of this study it was demonstrated that the transient rheological models can be employed to describe the coalescence behavior of thermoplastic olefin blends during gentle shearing. To obtain a true measure of coalescence in different TPOs a new rheological approach was also introduced in which the impact of initial morphological state of the blends on the coalescence was accounted for. To control the extent of phase coalescence, in the second part of this thesis, a new, original compatibilization technique was developed. The microstructure of the reactively compatibilized blends was analyzed using rheological and microscopic techniques. It was shown that the rheological constitutive equations with fractional order time derivatives are capable of describing the viscoelastic properties of the reactively compatibilized TPOs. Examining the foaming behavior of TPOs, in the last part of this research revealed that in these systems the elastomeric domains act as nucleating sites and the bubbles are formed inside the rubbery domains. Reactive compatibilization was shown to be an effective technique to improve the foaming behavior of TPOs via the formation of finer initial morphologies and also modifying the blends viscoelastic properties.

9.3 Recommendations

The following issues remained to be explored and are the objects of recommendation for future studies:

1- In view of the importance of transient rheological behavior of the blends in controlling the cellular morphology, further studies on the role of phase morphology on the development of stress growth in elongational flow is recommended. It is also suggested to evaluate the capability of the transient rheological models (such as LPL model) in predicting the phase morphology evolution under uniaxial extension. It is also interesting to study the role of interfacial

modification and reactive compatibilization on the deformation and morphology evolution under elongational flow. This study is of great industrial interest since the flow in mixing devices features intensive elongational stresses.

2- To improve the capability of the LPL model in predicting the morphology evolution of viscoelastic polymer blends, it is suggested that the contribution of the neat components in the stress growth viscosity be described using linear viscoelastic models such as Generalized Maxwell model or non linear equations e.g. Leonov model. Such a modification becomes more important in modeling the extensional stress growth viscosity where transient data in short periods are commonly encountered and for which non Newtonian behaviors are dominant.

3- Although in an academic sense batch foaming is a useful process to correlate the material characteristics to the foaming behavior, the melt foamability of the TPOs in other processing methods used in foam industries should be also evaluated. In this respect it is suggested to investigate the role of rheological and morphological properties in the foaming behavior of TPOs in extrusion and injection foaming processes. The efficiency of reactive compatibilization in controlling the foaming behavior in these processes should be also investigated.

4- It is highly recommended to further investigate the nucleation and growth phenomena using direct visualization techniques. This can enable us to achieve a deeper insight on the initial stage of cell formation where bubble coalescence is not an issue. Moreover the strain rate experienced by the cell wall at different stages of cell growth can be directly evaluated by this technique. The latter is quite crucial to tailor the foaming behavior to the rheological properties of different compatbilized and non compatibilized systems. The resolution and the frame rate of the imaging device might be however the limiting issues.

5- Another important aspect that should be investigated in studies concerning TPO formulation for foaming is the mechanical strength of the produced foams. It has been widely accepted that the shape, size and size distribution of the dispersed phase particles has a pronounced effect on the mechanical properties of rubber toughened blends. Aside from the impact of reactive compatibilization on the blend morphology, reactive modification of the interface results in an improved compatibility and interfacial adhesion, which is of crucial influence on the blend toughness. On the other hand the specific strength of the cellular material is a strong function of the cells morphology; as such compatibilization can also improve the mechanical properties via controlling the final cellular morphology. The interrelationship of these parameters should be investigated in future studies.

6- Considering the recent advancements in gas pressurized rheological measurements and in view of the importance of viscoelastic properties in the final cellular morphology, a detailed study on the rheological properties of the gas plasticized TPOs is recommended. It has been shown in the literature that the presence of gas molecules can influence the interfacial tension and the phase morphology development of the gas laden polymer blends. Combination of the rheological approach used in this study with high pressurized rheometry techniques can provide an understanding of the phase morphology behavior of polymer blends in the presence of gas molecules.

7-Considering the improvement achieved by reactive compatibilization technique it is recommended to validate the findings of this study in other systems with the potential for reactive modifications; an example of these systems is the blend of polyethylene and polyamide which can be reactively modified using maleic anhydride grafted polyethylene. Considering that different grades of maleated polyethylene are commercially available, the influence of the

functionality of the reactive compatibilizer and consequently the structure of the copolymer formed can be more systematically investigated.

References

Asthana, H. and Jayaraman, K. "Rheology of Reactively Compatibilized Polymer Blends with Varying Extent of Interfacial Reaction." Macromolecules **32**, 3412-3419 (1999).

Baldwin, D. F., Park, C. B. and Suh, N. P. "An extrusion system for the processing of microcellular polymer sheets: Shaping and cell growth control." Polymer Engineering & Science **36**, 1425-1435 (1996).

Batchelor, G. K. "The stress system in a suspension of force-free particles." Journal of Fluid Mechanics **41**, 545-570 (1970).

Batchelor, G. K. and Green, J. T. "Hydrodynamic interaction of two small freely-moving spheres in a linear flow field." Journal of Fluid Mechanics **56**, 375-400 (1972).

Beck Tan, N. C., Tai, S. K. and Briber, R. M. "Morphology control and interfacial reinforcement in reactive polystyrene/amorphous polyamide blends." Polymer **37**, 3509-3519 (1996).

Bensason, S., Stepanov, E. V., Chum, S., Hiltner, A. and Baer, E. "Deformation of elastomeric ethylene-octene copolymers." Macromolecules **30**, 2436-2444 (1997).

Bentley, B. J. and Leal, L. G. "An experimental investigation of drop deformation and breakup in steady, two-dimensional linear flows." J . Fluid Mech. **167**, 241-283 (1986).

Bhadane, P. A., Tsou, A. H., Cheng, J. and Favis, B. D. "Morphology development and interfacial erosion in reactive polymer blending." Macromolecules **41**, 7549-7559 (2008).

Bin Wadud, S. E. and Baird, D. G. "Shear and extensional rheology of sparsely branched metallocene-catalyzed polyethylenes." Journal of Rheology **44**, 1151-1167 (2000).

Blander, M. and Katz, J. L. "Bubble nucleation in liquids." AIChE Journal **21**, 833-848 (1975).

Brown, B. S. "Reactive compatibilization of polymer blends" Polymer Blends Handbook. Utracki, L. A., Editor. Netherlands, Kluwer Academic Publishers**:** 339-415 (2003).

Carreau, P. J., Bousmina, M. and Ajji, A. (1994). "Rheological properties of blends: Facts and challenges". Progress in Pacific Polymer Science. New York, Springer-Verlag. **3:** 25-40.

Chakraborty, P., Ganguly, A., Mitra, S. and Bhowmick, A. K. "Influence of phase modifiers on morphology and properties of thermoplastic elastomers prepared from ethylene propylene diene rubber and isotactic polypropylene." Polymer Engineering and Science **48**, 477-489 (2008).

Chambon, F. and Winter, H. H. "Linear viscoelasticity at the gel Point of a crosslinking PDMS with Imbalanced stoichiometry." Journal of Rheology **31**, 683-697 (1987).

Chesters, A. K. "Modelling of coalescence processes in fluid-liquid dispersions. A review of current understanding." Chemical Engineering Research and Design **69**, 259-227 (1991).

Choi, S. J. and Schowalter, W. R. "Rheological properties of nondilute suspensions of deformable particles." Physics of Fluids **18**, 420-427 (1975).

Cigana, P., Favis, B. D. and Jerome, R. "Diblock copolymers as emulsifying agents in polymer blends: Influence of molecular weight, architecture, and chemical composition." Journal of Polymer Science Part B: Polymer Physics **34**, 1691-1700 (1996).

Collias, D. I., Baird, D. G. and Borggreve, R. J. M. "Impact toughening of polycarbonate by microcellular foaming." Polymer **35**, 3978-3983 (1994).

Colton, J. S. and Suh, N. P. "Nucleation of microcellular thermoplastic foam with additives: Part I: Theoretical considerations." Polymer Engineering and Science **27**, 485-492 (1987).

Crist, B. and Nesarikar, A. R. "Coarsening in Polyethylene-Copolymer Blends." Macromolecules **28**, 890-896 (1995).

Datta, S. and Lohse, D. J. "Graft polymers of functionalized ethylene-alpha-olefin copolymer with polypropylene, methods of preparation, and use in polypropylene compositions." United States Patent Exxon Chemical Patents Inc. **4,999,403**

Davis, R. H., Schonberg, J. A. and Rallison, J. M. "The lubrication force between two viscous drops." Physics of Fluids A (Fluid Dynamics) **1**, 77-81 (1989).

de Bruijn, R. A. "Deformation and breakup of drops in simple shear flows." Ph.D. Thesis, Eindhoven University of Technology (1989).

Dekmezian, A. H., Soares, J. B. P., Jiang, P., Garcia-Franco, C. A., Weng, W., Fruitwala, H., Sun, T. and Sarzotti, D. M. "Characterization and Modeling of Metallocene-Based Branch−Block Copolymers." Macromolecules **35**, 9586-9594 (2002).

DeLeo, C., Walsh, K. and Velankar, S. "Effect of compatibilizer concentration and weight fraction on model immiscible blends with interfacial crosslinking." Journal of Rheology **55**, 713-731 (2011).

DeLeo, C. L. and Velankar, S. S. "Morphology and rheology of compatibilized polymer blends: Diblock compatibilizers vs crosslinked reactive compatibilizers." Journal of Rheology **52**, 1385-1404 (2008).

Dias, P., Lin, Y. J., Poon, B., Chen, H. Y., Hiltner, A. and Baer, E. "Adhesion of statistical and blocky ethylene-octene copolymers to polypropylene." Polymer **49**, 2937-2946 (2008).

Doerpinghaus, P. J. and Baird, D. G. "Separating the effects of sparse long-chain branching on rheology from those due to molecular weight in polyethylenes." Journal of Rheology **47**, 717-736 (2003).

Doi, M. Physics of complex and super molecular fluids. Safran, S. S. and Clark, M. New York, Wiley(1987).

Doi, M. and Ohta, T. "Dynamics and rheology of complex interfaces. I." Journal of Chemical Physics **95**, 1242-1248 (1991).

Doroudiani, S., Park, C. B. and Kortschot, M. T. "Effect of the crystallinity and morphology on the microcellular foam structure of semicrystalline polymers." Polymer Engineering & Science **36**, 2645-2662 (1996).

Doroudiani, S., Park, C. B. and Kortschot, M. T. "Processing and characterization of microcellular foamed high-density polythylene/isotactic polypropylene blends." Polymer Engineering & Science **38**, 1205-1215 (1998).

Dreisbach, F. and Lösch, H. "Magnetic Suspension Balance For Simultaneous Measurement of a Sample and the Density of the Measuring Fluid." Journal of Thermal Analysis and Calorimetry **62**, 515-521 (2000).

Einstein, A. "Eine neue Bestimmung der Moleküldimensionen." Annalen der Physik **324**, 289-306 (1906).

Elemans, P. H. M., Janssen, J. M. H. and Meijer, H. E. H. "The measurement of interfacial tension in polymer/polymer systems: The breaking thread method." Journal of Rheology **34**, 1311-1325 (1990).

Fletcher, N. H. "Size Effect in Heterogeneous Nucleation." The Journal of Chemical Physics **29**, 572-576 (1958).

Fortelný, I. and Kovář, J. "Theory of coalescence in immiscible polymer blends." Polymer Composites **9**, 119-124 (1988).

Fortelný, I. and Živný, A. "Coalescence in molten quiescent polymer blends." Polymer **36**, 4113-4118 (1995).

Friedrich, C. and Heymann, L. "Extension of a model for crosslinking polymer at the gel point." Journal of Rheology **32**, 235-241 (1988).

Friedrich, C., Schiessel, H. and Blumen, A. "Constitutive behavior modeling and fractional derivatives" Rheology Series. Siginer, D. A., De Kee, D. and Chhabra, R. P., Editors. Netherlands, Elsevier **8:** 429-466 (1999).

Frohlich, H. and Sack, R. "Theory of the rheological propertiesof dispersions." Proceedings of the Royal Society of London, Series A: Mathematical and Physical Sciences **185** (1946).

Galloway, J. A., Montminy, M. D. and Macosko, C. W. "Image analysis for interfacial area and cocontinuity detection in polymer blends." Polymer **43**, 4715-4722 (2002).

Grace, H. P. "Dispersion phenomena in high viscosity immiscible fluid systems and application of static mixers as dispersion devices in such systems." Chemical Engineering Communications **14**, 225-277 (1982).

Graebling, D., Muller, R. and Palierne, J. F. "Linear viscoelastic behavior of some incompatible polymer blends in the melt. Interpretation of data with a model of emulsion of viscoelastic liquids." Macromolecules **26**, 320-329 (1993).

Gramespacher, H. and Meissner, J. "Interfacial tension between polymer melts measured by shear oscillations of their blends." Journal of Rheology **36**, 1127-1141 (1992).

Grmela, M. and Ait-Kadi, A. "Comments on the Doi-Ohta theory of blends." Journal of Non-Newtonian Fluid Mechanics **55**, 191-195 (1994).

Guenther, G. K. and Baird, D. G. "An evaluation of the Doi-Ohta theory for an immiscible polymer blend." Journal of Rheology **40**, 1-20 (1996).

Guidoa, S., Simeonea, M. and Greco, F. "Effects of matrix viscoelasticity on drop deformation in dilute polymer blends under slow shear flow." Polymer **44**, 467-471 (2003).

Guo, M.-C., Santoni, A., Heuzey, M.-C. and Carreau, P. J. "Occurrence of Surface Defects in TPO Injected Foam Parts." Journal of Cellular Plastics **43**, 273-296 (2007).

Hale, W., Keskkula, H. and Paul, D. R. "Compatibilization of PBT/ABS blends by methyl methacrylate glycidyl methacrylate ethyl acrylate terpolymers." Polymer **40**, 365-377 (1999).

Hassan, A., Othman, N., Wahit, M. U., Wei, L. J., Rahmat, A. R. and Mohd Ishak, Z. A. "Maleic anhydride polyethylene octene elastomer toughened polyamide 6/polypropylene nanocomposites: mechanical and morphological properties." Macromolecular Symposia **239**, 182-191 (2006).

Hemelrijck, E. V., Puyvelde, P. V., Velankar, S., Macosko, C. W. and Moldenaers, P. "Interfacial elasticity and coalescence suppression in compatibilized polymer blends." Journal of Rheology **48**, 143-158 (2004).

Hobbie, E. K. and Migler, K. B. "Vorticity Elongation in Polymeric Emulsions." Physical Review Letters **82**, 5393-5396 (1999).

Horak, Z., Hlavata, D., Fortelny, I. and Lednicky, F. "Effect of styrene-butadiene triblock copolymer structure on its compatibilization efficiency in PS/PB and PS/PP blends." Polymer Engineering and Science **42**, 2042-2047 (2002).

Huang, J. J., Keskkula, H. and Paul, D. R. "Elastomer particle morphology in ternary blends of maleated and non-maleated ethylene-based elastomers with polyamides: Role of elastomer phase miscibility." Polymer **47**, 624-638 (2006).

Huitric, J., Moan, M., Carreau, P. J. and Dufaure, N. "Effect of reactive compatibilization on droplet coalescence in shear flow." Journal of Non-Newtonian Fluid Mechanics **145**, 139-149 (2007).

Huo, Y., Groeninckx, G. and Moldenaers, P. "Rheology and morphology of polystyrene/polypropylene blends with in situ compatibilization." Rheologica Acta **46**, 507-520 (2007).

Jacobs, U., Fahrlander, M., Winterhalter, J. and Friedrich, C. "Analysis of Palierne's emulsion model in the case of viscoelastic interfacial properties." Journal of Rheology **43**, 1495-1509 (1999).

Jancar, J., DiAnselmo, A., DiBenedetto, A. T. and Kucera, J. "Failure mechanics in elastomer toughened polypropylene." Polymer **34**, 1684-1694 (1993).

Janssen, J. M. H. and Meijer, H. E. H. "Dynamics of liquid-liquid mixing: A 2-zone model." Polymer Engineering and Science **35**, 1766-1780 (1995).

Jiang, W., Liu, C. H., Wang, Z. G., An, L. J., Liang, H. J., Jiang, B. Z., Wang, X. H. and Zhang, H. X. "Brittle-tough transition in PP/EPDM blends: Effects of interparticle distance and temperature." Polymer **39**, 3285-3288 (1998).

Jiang, W., Tjong, S. C. and Li, R. K. Y. "Brittle-tough transition in PP/EPDM blends: effects of interparticle distance and tensile deformation speed." Polymer **41**, 3479-3482 (2000).

Kaufman, L., Cozewith, C., Gadkari, A. C., Dharmarajan, N. R. and Ellul, M. D. "Thermoplastic olefin compositions." United States Patent Exxon Chemical Patents Inc. **6,245,856**

Keskkula, H., Schwarz, M. and Paul, D. R. "Examination of failure in rubber toughened polystyrene." Polymer **27**, 211-216 (1986).

Kim, S. G., Leung, S. N., Park, C. B. and Sain, M. "The effect of dispersed elastomer particle size on heterogeneous nucleation of TPO with N2 foaming." Chemical Engineering Science **66**, 3675-3686 (2011).

Kim, Y. S., Chung, C. I., Lai, S. Y. and Hyun, K. S. "Melt rheological and thermodynamic properties of polyethylene homopolymers and poly(ethylene/-olefin) copolymers with respect to molecular composition and structure." Journal of Applied Polymer Science **59**, 125-137 (1996).

Kokko, E., Malmberg, A., Lehmus, P., Löfgren, B. and Seppälä, J. V. "Influence of the catalyst and polymerization conditions on the long-chain branching of metallocene-catalyzed polyethenes." Journal of Polymer Science Part A: Polymer Chemistry **38**, 376-388 (2000).

Kontopoulou, M., Wang, W., Gopakumar, T. G. and Cheung, C. "Effect of composition and comonomer type on the rheology, morphology and properties of ethylene--olefin copolymer/polypropylene blends." Polymer **44**, 7495-7504 (2003).

Kumar, V. and Suh, N. P. "A process for making microcellular thermoplastic parts." Polymer Engineering & Science **30**, 1323-1329 (1990).

Lacroix, C., Aressy, M. and Carreau, P. J. "Linear viscoelastic behavior of molten polymer blends: A comparative study of the Palierne and Lee and Park models." Rheologica Acta **36**, 416-416 (1997).

Lacroix, C., Grmela, M. and Carreau, P. J. "Relationships between rheology and morphology for immiscible molten blends of polypropylene and ethylene copolymers under shear flow." Journal of Rheology **42**, 41-62 (1998).

Lacroix, C., Grmela, M. and Carreau, P. J. "Morphological evolution of immiscible polymer blends in simple shear and elongational flows." Journal of Non-Newtonian Fluid Mechanics **86**, 37-59 (1999).

Lacroix, C., Grmela, M. and Carreau, P. J. "Morphological evolution of immiscible polymer blends in simple shear and elongational flows." Conference on Mechanics of Non-Linear Materials, 13-16 May 1998, Netherlands, Elsevier (1999).

Larson, R. G. "Constitutive relationships for polymeric materials with power-law distributions of relaxation times." Rheologica Acta **24**, 327-334 (1985).

Lee, H. M. and Park, O. O. "Rheology and dynamics of immiscible polymer blends." Journal of Rheology **38**, 1405-1425 (1994).

Lee, S. T., Ed. (2004). Foam Extrusion: Principles and Practice. Florida, CRC Press.

Li, J. and Favis, B. D. "Strategies to measure and optimize the migration of the interfacial modifier to the interface in immiscible polymer blends." Polymer **43**, 4935-4945 (2002).

Liang, H., Favis, B. D., Yu, Y. S. and Eisenberg, A. "Correlation between the Interfacial Tension and Dispersed Phase Morphology in Interfacially Modified Blends of LLDPE and PVC." Macromolecules **32**, 1637-1642 (1999).

Lin, B., Mighri, F., Huneault, M. A. and Sundararaj, U. "Parallel Breakup of Polymer Drops under Simple Shear." Macromolecular Rapid Communications **24**, 783-788 (2003a).

Lin, B., Mighri, F., Huneault, M. A. and Sundararaj, U. "Effect of premade compatibilizer and reactive polymers on polystyrene drop deformation and breakup in simple shear." Macromolecules **38**, 5609-5616 (2005).

Lin, B., Sundararaj, U., Mighri, F. and Huneault, M. A. "Erosion and breakup of polymer drops under simple shear in high viscosity ratio systems." Polymer Engineering & Science **43**, 891-904 (2003b).

Lindt, J. T. and Ghosh, A. K. "Fluid mechanics of the formation of polymer blends. Part I: Formation of lamellar structures." Polymer Engineering & Science **32**, 1802-1813 (1992).

Lohse, D. J., Milner, S. T., Fetters, L. J., Xenidou, M., Hadjichristidis, N., Mendelson, R. A., García-Franco, C. A. and Lyon, M. K. "Well-Defined, Model Long Chain Branched Polyethylene. 2. Melt Rheological Behavior." Macromolecules **35**, 3066-3075 (2002).

Lyu, S.-P., Bates, F. S. and Macosko, C. W. "Coalescence in polymer blends during shearing." AIChE Journal **46**, 229-238 (2000).

Lyu, S., Bates, F. S. and Macosko, C. W. "Modeling of coalescence in polymer blends." AIChE Journal **48**, 7-14 (2002).

Lyu, S., Bates, F. S. and Macosko, C. W. "Modeling of coalescence in polymer blends." AIChE Journal **48**, 7-14 (2002a).

Lyu, S., Jones, T. D., Bates, F. S. and Macosko, C. W. "Role of block copolymers on suppression of droplet coalescence." Macromolecules **35**, 7845-7855 (2002).

Lyu, S., Jones, T. D., Bates, F. S. and Macosko, C. W. "Role of block copolymers on suppression of droplet coalescence." Macromolecules **35**, 7845-7855 (2002b).

Maani, A., Blais, B., Heuzey, M. C. and Carreau, P. J. "Rheological and morphological properties of reactively compatibilized thermoplastic olefin (TPO) blends." Journal of Rheology **56**, 625-647 (2012).

Maani, A., Heuzey, M.-C. and Carreau, P. "Coalescence in thermoplastic olefin (TPO) blends under shear flow." Rheologica Acta, 1-15 (2010).

Maani, A., Heuzey, M.-C. and Carreau, P. "Coalescence in thermoplastic olefin (TPO) blends under shear flow." Rheologica Acta **50**, 881-895 (2011).

Macosko, C. W., Guégan, P., Khandpur, A. K., Nakayama, A., Marechal, P. and Inoue, T. "Compatibilizers for Melt Blending: Premade Block Copolymers†." Macromolecules **29**, 5590-5598 (1996).

Majumdar, B., Keskkula, H. and Paul, D. R. "Mechanical behaviour and morphology of toughened aliphatic polyamides." Polymer **35**, 1399-1408 (1994).

Majumdar, B. and Paul, D. R. "Reactive compatibilization" Polymer Blends. Paul, D. R. and Bucknall, C. B., Editors. New York, Academic Press. **1:** 539-579 (1978).

Martin, P., Carreau, P. J., Favis, B. D. and Jerome, R. "Investigating the morphology/rheology interrelationships in immiscible polymer blends." Journal of Rheology **44**, 569-583 (2000).

Martini, J. E. "The production and analysis of microcellular foam." M.S. Thesis, Dept. of Mechanical Engineering, Massachusetts Institute of Technology (1981).

McNally, T., McShane, P., Nally, G. M., Murphy, W. R., Cook, M. and Miller, A. "Rheology, phase morphology, mechanical, impact and thermal properties of polypropylene/metallocene catalysed ethylene 1-octene copolymer blends." Polymer **43**, 3785-3793 (2002).

Mighri, F., Ajji, A. and Carreau, P. J. "Influence of elastic properties on drop deformation in elongational flow." Journal of Rheology **41**, 1183-1201 (1997).

Mighri, F., Carreau, P. J. and Ajji, A. "Influence of elastic properties on drop deformation and breakup in shear flow." Journal of Rheology **42**, 1477-1490 (1998).

Mighri, F. and Huneault, M. A. "Dispersion visualization of model fluids in a transparent Couette flow cell." Journal of Rheology **45**, 783-797 (2001).

Migler, K. B. "Droplet vorticity alignment in model polymer blends." Journal of Rheology **44**, 277-290 (2000).

Milner, S. T. and Xi, H. W. "How copolymers promote mixing of immiscible homopolymers." Journal of Rheology **40**, 663-687 (1996).

Minale, M., Mewis, J. and Moldenaers, P. "Study of the morphological hysteresis in immiscible polymer blends." AIChE Journal **44**, 943-950 (1998).

Minale, M., Moldenaers, P. and Mewis, J. "Effect of shear history on the morphology of immiscible polymer blends." Macromolecules **30**, 5470-5475 (1997).

Naguib, H. E., Park, C. B., Panzer, U. and Reichelt, N. "Strategies for achieving ultra low-density polypropylene foams." Polymer Engineering & Science **42**, 1481-1492 (2002).

Nemoto, T., Takagi, J. and Ohshima, M. "Nanoscale Cellular Foams from a Poly(propylene)-Rubber Blend." Macromolecular Materials and Engineering **293**, 991-998 (2008).

Nemoto, T., Takagi, J. and Ohshima, M. "Nanocellular foams-cell structure difference between immiscible and miscible PEEK/PEI polymer blends." Polymer Engineering and Science **50**, 2408-2416 (2010).

Nitta, K. H., Okamoto, K. and Yamaguchi, M. "Mechanical properties of binary blends of polypropylene with ethylene-olefin copolymer." Polymer **39**, 53-58 (1998).

Noolandi, J. and Hong, K. M. "Interfacial properties of immiscible homopolymer blends in the presence of block copolymers." Macromolecules **15**, 482-492 (1982).

Oldroyd, J. G. "The elastic and viscous properties of emulsions and suspensions." Proceedings of the Royal Society of London, Series A: Mathematical and Physical Sciences **218**, 122-132 (1953).

Oldroyd, J. G. "The effect of interfacial stabilizing films on the elastic and viscous properties of emulsions." Proceedings of the Royal Society of London, Series A: Mathematical and Physical Sciences **232**, 567-577 (1955).

Onuki, A. "Viscosity enhancement by domains in phase-separating fluids near the critical point: Proposal of critical rheology." Physical Review A **35**, 5149-5155 (1987).

Otsuka, T., Taki, K. and Ohshima, M. "Nanocellular Foams of PS/PMMA Polymer Blends." Macromolecular Materials and Engineering **293**, 78-82 (2008).

Palierne, J. F. "Linear rheology of viscoelastic emulsions with interfacial tension." Rheologica Acta **29**, 204-214 (1990).

Park, C. B., Baldwin, D. F. and Suh, N. P. "Effect of the pressure drop rate on cell nucleation in continuous processing of microcellular polymers." Polymer Engineering & Science **35**, 432-440 (1995).

Park, C. B., Behravesh, A. H. and Venter, R. D. "Low density microcellular foam processing in extrusion using CO2." Polymer Engineering & Science **38**, 1812-1823 (1998).

Park, C. B. and Cheung, L. K. "A study of cell nucleation in the extrusion of polypropylene foams." Polymer Engineering & Science **37**, 1-10 (1997).

Park, C. B., Lee, P. C., Wang, J. and Padareva, V. "Strategies for achieving microcellular LDPE foams in extrusion." Cell Polym. **25**, 1-18 (2006).

Park, C. C., Baldessari, F. and Leal, L. G. "Study of molecular weight effects on coalescence: Interface slip layer." Journal of Rheology **47**, 911-942 (2003).

Patham, B. and Jayaraman, K. "Creep recovery of random ethylene-octene copolymer melts with varying comonomer content." Journal of Rheology **49**, 989-999 (2005).

Paul, D. R. and Newman, S. Polymer Blends New York, ACADEMIC PRESS, INC. (1978).

Peón, J., Vega, J. F., Del Amo, B. and Martínez-Salazar, J. "Phase morphology and melt viscoelastic properties in blends of ethylene/vinyl acetate copolymer and metallocene-catalysed linear polyethylene." Polymer **44**, 2911-2918 (2003).

Polios, I. S., Soliman, M., Lee, C., Gido, S. P., Schmidt-Rohr, K. and Winter, H. H. "Late Stages of Phase Separation in a Binary Polymer Blend Studied by Rheology, Optical and Electron Microscopy, and Solid State NMR." Macromolecules **30**, 4470-4480 (1997).

Ramesh, N. S., Rasmussen, D. H. and Campbell, G. A. "The heterogeneous nucleation of microcellular foams assisted by the survival of microvoids in polymers containing low glass transition particles. Part I: Mathematical modeling and numerical simulation." Polymer Engineering & Science **34**, 1685-1697 (1994a).

Ramesh, N. S., Rasmussen, D. H. and Campbell, G. A. "The heterogeneous nucleation of microcellular foams assisted by the survival of microvoids in polymers containing low glass-transition particles. 2. Experimental results and discussion " Polymer Engineering and Science **34**, 1698-1706 (1994b).

Riemann, R. E., Cantow, H. J. and Friedrich, C. "Interpretation of a New Interface-Governed Relaxation Process in Compatibilized Polymer Blends." Macromolecules **30**, 5476-5484 (1997).

Ruckdäschel, H., Gutmann, P., Altstädt, V., Schmalz, H. and Müller, A. "Foaming of Microstructured and Nanostructured Polymer Blends" Complex Macromolecular Systems I. Müller, A. H. E. and Schmidt, H.-W., Editors. Springer Berlin / Heidelberg. **227:** 199-252 (2010).

Rumscheidt, F. D. and Mason, S. G. "Particle motions in sheared suspensions XII. Deformation and burst of fluid drops in shear and hyperbolic flow." J. Colloid Sci. **16**, 238-261 (1961).

Russ, J. C. Practical Sterelogy New York, NY, Plenum Press (1986).

Sahagún, C. Z., González-Núñez, R. and Rodrigue, D. "Morphology of Extruded PP/HDPE Foam Blends." Journal of Cellular Plastics **42**, 469-485 (2006).

Sailer, C. and Handge, U. A. "Melt viscosity, elasticity, and morphology of reactively compatibilized polyamide 6/styrene−acrylonitrile blends in shear and elongation." Macromolecules **40**, 2019-2028 (2007).

Sailer, C. and Handge, U. A. "Reactive blending of polyamide 6 and styrene−acrylonitrile copolymer: Influence of blend composition and compatibilizer concentration on morphology and rheology." Macromolecules **41**, 4258-4267 (2008).

Saltykov, S. A. The determination of the size distribution of particles in an opaque material from a measurement of the size distribution of their section Stereology. Elias, H. New York, Springer-Verlag**:** 163-173 (1967).

Santoni, A., Guo, M. C., Heuzey, M. C. and Carreau, P. J. "Surface defects of TPO injected foam parts for automotive applications." Int. Polym. Process. **22**, 204-212 (2007).

Scanlan, J. C. and Winter, H. H. "Composition dependence of the viscoelasticity of end-linked poly(dimethylsiloxane) at the gel point." Macromolecules **24**, 47-54 (1991).

Schiessel, H. and Blumen, A. "Mesoscopic Pictures of the Sol-Gel Transition: Ladder Models and Fractal Networks." Macromolecules **28**, 4013-4019 (1995).

Schiessel, H., Metzler, R., Blumen, A. and Nonnemacher, T. F. "Generalized viscoelastic models: their fractional equations with solutions." Journal of Physics A: Mathematical and General **28**, 6567-6584 (1995).

Schnell, M., Ziegler, V. and Wolf, B. A. "Evolution of viscosities and morphology for the two-phase system polyethylene oxide/poly(dimethylsiloxane)." Rheologica Acta **47**, 469-476 (2008).

Schowalter, W. R., Chaffey, C. E. and Brenner, H. "Rheological behavior of dilute-emulsion." Journal of Colloid and Interface Science **26**, 152-160 (1968).

Shahbikian, S., Carreau, P. J., Heuzey, M.-C., Ellul, M. D., Nadella, H. P., Cheng, J. and Shirodkar, P. "Rheology/morphology relationship of plasticized and nonplasticized thermoplastic elastomers based on ethylene–propylene–diene–terpolymer and polypropylene." Polymer Engineering & Science **51**, 2314-2327 (2011).

Smith, P. A., Cross, B. J., Gendron, R. and Daigneault, L. E. "Polystyrene/acrylic blends and their application in foam production. Part one: R22/142b blowing agent." Proceedings of the 1998 56th Annual Technical Conference, ANTEC. , Atlanta, GA, USA (1998).

Smoluchowski, V. "Versuch einer mathematischen Theorie der Koagulationskinetik kolloidaler Lösungen." Z. Phys. Chem. **92**, 129-168 (1917).

Sondergaard, K. and Lyngaae-Jorgensen, J. Rheo-Physics of Multiphase Polymer Systems: Characterization by Rheo-Optical Techniques Lancaster, Pa, Technomic Pub. Co. (1995).

Spitael, P. and Macosko, C. W. "Strain hardening in polypropylenes and its role in extrusion foaming." Polymer Engineering and Science **44**, 2090-2100 (2004).

Spitael, P., Macosko, C. W. and McClurg, R. B. "Block Copolymer Micelles for Nucleation of Microcellular Thermoplastic Foams." Macromolecules **37**, 6874-6882 (2004).

Stafford, C. M., Russell, T. P. and McCarthy, T. J. "Expansion of Polystyrene Using Supercritical Carbon Dioxide: Effects of Molecular Weight, Polydispersity, and Low Molecular Weight Components." Macromolecules **32**, 7610-7616 (1999).

Stange, J. and Münstedt, H. "Effect of Long-chain Branching on the Foaming of Polypropylene with Azodicarbonamide." Journal of Cellular Plastics **42**, 445-467 (2006).

Sundararaj, U. and Macosko, C. W. "Drop breakup and coalescence in polymer blends: The effects of concentration and compatibilization." Macromolecules **28**, 2647-2657 (1995).

Tan, N. C. B., Tai, S. K. and Briber, R. M. "Morphology control and interfacial reinforcement in reactive polystyrene/amorphous polyamide blends." Polymer **37**, 3509-3519 (1996).

Taylor, G. I. "The viscosity of a fluid containing small drops of another fluid." Proceedings of the Royal Society of London, Series A: Mathematical and Physical Sciences **138**, 41-48 (1932).

Taylor, G. I. "The formation of emulsions in definable fields of flow." Proc. R. Sot. London Ser. A **146**, 501-523 (1934).

Tejeda, E. H., Sahagún, C. Z., González-Núñez, R. and Rodrigue, D. "Morphology and Mechanical Properties of Foamed Polyethylene-Polypropylene Blends." Journal of Cellular Plastics **41**, 417-435 (2005).

The Freedonia Group Inc, "World thermoplastic elastomers" Cleveland, OH, The Freedonia Group Inc. (2005).

Van Der Wal, A., Verheul, A. J. J. and Gaymans, R. J. "Polypropylene-rubber blends: 4. The effect of the rubber particle size on the fracture behaviour at low and high test speed." Polymer **40**, 6057-6065 (1999).

Van Hemelrijck, E., Van Puyvelde, P., Velankar, S., Macosko, C. W. and Moldenaers, P. "Interfacial elasticity and coalescence suppression in compatibilized polymer blends." J. Rheol. **48**, 143-158 (2004).

Van Nuffel, C. T. E., Pham, H. T., Namhata, S. and Eiffler, J. Blend of branched and linear carbonate polymer resins. United States Patent The Dow Chemical Company **5804673.**

Venerus, D. C., Yala, N. and Bernstein, B. "Analysis of diffusion-induced bubble growth in viscoelastic liquids." Journal of Non-Newtonian Fluid Mechanics **75**, 55-75 (1998).

Vinckier, I., Moldenaers, P. and Mewis, J. "Relationship between rheology and morphology of model blends in steady shear flow." Journal of Rheology **40**, 613-631 (1996).

Vinckier, I., Moldenaers, P., Terracciano, A. M. and Grizzuti, N. "Droplet size evolution during coalescence in semiconcentrated model blends." AIChE Journal **44**, 951-958 (1998).

Waldman, F. A. "The processing of microcellular foam." M.S. Thesis, Dept. of Mechanical Engineering, Massachusetts Institute of Technology (1980).

Wallheinke, K., Pötschke, P., Macosko, C. W. and Stutz, H. "Coalescence in blends of thermoplastic polyurethane with polyolefins." Polymer Engineering & Science **39**, 1022-1034 (1999).

Wang, H., Zinchenko, A. Z. and Davis, R. H. "Collision rate of small drops in linear flow fields." Journal of Fluid Mechanics **265**, 161-188 (1994).

Winter, H. H. and Chambon, F. "Analysis of linear viscoelasticity of a crosslinking polymer at the gel point." Journal of Rheology **30**, 367-382 (1986).

Wu, S. "Phase structure and adhesion in polymer blends: A criterion for rubber toughening." Polymer **26**, 1855-1863 (1985).

Xing, P., Bousmina, M., Rodrigue, D. and Kamal, M. R. "Critical experimental comparison between five techniques for the determination of interfacial tension in polymer blends: model system of polystyrene/polyamide-6." Macromolecules **33**, 8020-8034 (2000).

Xu, X., Park, C. B., Xu, D. and Pop-Iliev, R. "Effects of die geometry on cell nucleation of PS foams blown with CO2." Polymer Engineering & Science **43**, 1378-1390 (2003).

Yang, H., Park, C. C., Hu, Y. T. and Leal, L. G. "The coalescene of two equal-sized drops in a two-dimensional linear flow." Physics of Fluids **13**, 1087-1106 (2001).

Yiantsios, S. G. and Davis, R. H. "On the buoyancy-driven motion of a drop towards a rigid surface or a deformable interface." Journal of Fluid Mechanics **217**, 547-573 (1990).

Yokoyama, H. and Sugiyama, K. "Nanocellular Structures in Block Copolymers with CO2-philic Blocks Using CO2 as a Blowing Agent: Crossover from Micro- to Nanocellular Structures with Depressurization Temperature." Macromolecules **38**, 10516-10522 (2005).

Yee, M., Calvão, P. and Demarquette, N. "Rheological behavior of poly(methyl methacrylate)/polystyrene (PMMA/PS) blends with the addition of PMMA- *ran* -PS." Rheol. Acta **46**, 653-664 (2007).

Yokoyama, Y. and Ricco, T. "Toughening of polypropylene by different elastomeric systems." Polymer **39**, 3675-3681 (1998).

Yoon, Y., Borrell, M., Park, C. C. and Leal, L. G. "Viscosity ratio effects on the coalescence of two equal-sized drops in a two-dimensional linear flow." Journal of Fluid Mechanics **525**, 355-379 (2005).

Yu, T. C. "Metallocene plastomer modification of polypropylenes." Polymer Engineering and Science **41**, 656-671 (2001).

Yu, W., Zhou, C. and Bousmina, M. "Theory of morphology evolution in mixtures of viscoelastic immiscible components." Journal of Rheology **49**, 215-236 (2005).

Yuan, Z. and Favis, B. D. "Coarsening of immiscible co-continuous blends during quiescent annealing." AIChE Journal **51**, 271-280 (2005).

Zhai, W., Wang, H., Yu, J., Dong, J. and He, J. "Foaming behavior of polypropylene/polystyrene blends enhanced by improved interfacial compatibility." Journal of Polymer Science Part B: Polymer Physics **46**, 1641-1651 (2008).